THESIS

FIELD, FLUID INCLUSION AND ISOTOPE CHEMISTRY EVIDENCE OF FLUIDS CIRCULATING AROUND THE HARRISON PASS PLUTON DURING INTRUSION: A FLUID MODEL FOR CARLIN-TYPE DEPOSITS

Submitted by

Charles Oliver Justin Musekamp

Department of Geosciences

In partial fulfillment of the requirements

For the Degree of Master of Science

Colorado State University

Fort Collins, Colorado

Spring 2012

Master's Committee:

Advisor: John Ridley

Sally Sutton
Christopher Myrick

ABSTRACT

FIELD, FLUID INCLUSION AND ISOTOPE CHEMISTRY EVIDENCE OF FLUIDS CIRCULATING AROUND THE HARRISON PASS PLUTON DURING INTRUSION: A FLUID MODEL FOR CARLIN-TYPE DEPOSITS

The ~60 km, northwest, southeast striking Carlin trend of Northeastern Nevada is host to approximately 40 Carlin-type gold deposits including a number of world class gold deposits. The ~36 Ma Harrison Pass pluton, located in the Ruby Mountains East Humboldt Range in Northeastern Nevada was emplaced along the Carlin trend during back arc-style magmatism between 40 and 32.4 Ma. This timing of plutonic magmatism was also contemporaneous with the regional hydrothermal event responsible for the ~42 to 33 Ma Carlin-type gold mineralization, but an acceptable explanation for the origin and source of fluids responsible for transporting gold remains outstanding. Through a multi-component field and geochemical study of the Harrison Pass pluton, magmatic-meteoric fluid mixing, after Muntean et al. (2011), is supported to explain the composition and origin of fluids responsible for deposition of gold in Carlin-type gold deposits along the Carlin trend.

Using fluid inclusion and $\delta^{18}O$ and $\delta^{13}C$ data combined with field relationships and petrology, a fluid history detailing fluid activity before intrusion, during

intrusion (Early Stage) and after intrusion (Late Stage) was constructed. Before intrusion, calcite veins within distal unaltered sedimentary siliciclastic and carbonate rocks were formed from connate waters. Fluids within these veins and wall rocks display typical $\delta^{18}O$ (~27‰) and $\delta^{13}C$ (~2.5‰) values of unaltered limestones. Type I (H_2O-NaCl-KCl), primary inclusions suggest that fluids are low salinity (~1% Mass% eq. NaCl) and were trapped at low temperatures (Tt~195-340°C). During intrusion and cooling of the Harrison Pass pluton, primitive, hot magmatic volatile phases were expelled and are interpreted to be responsible for the formation of miarolitic cavities, skarn, phyllic, and potassic alteration of wall rocks, and many quartz and calcite veins proximal to the pluton contact. Evidence for magmatically derived fluids around the pluton is provided by high homogenization temperatures of Type III (H_2O-CO_2-NaCl-KCl), CO_2-rich inclusions in miarolitic cavities, and vapor-rich Type II (H_2O-NaCl-KCl) inclusions in hydrogrossular and quartz within skarn wall rocks and quartz veins. Further corroboration is provided by near magmatic $\delta^{18}O$ and $\delta^{13}C$ values (~13 and -0.25‰) of skarn wall rocks and calcite-polymetallic sulfide veins. A later, cooler convecting meteoric phase (Late Stage) driven by the heat during and after intrusion is observed within thick, fault hosted, steeply dipping quartz veins and vugs crosscutting the Harrison Pass pluton and in skarn wall rocks.

It is interpreted, after Muntean et al. (2011), that Type II vapor-rich, primary inclusions found within Early Stage quartz veins, miarolitic cavities, and skarn wall rocks represent the vapor-rich magmatic phase in which Au and other base metals were transported. As the vapor-rich fluid rose through the crust, it would

have evolved and cooled and may be represented by the less vapor-rich, Early Stage, Type I inclusions within phyllically altered wall rocks and calcite-polymetallic sulfide veins. Further cooling and ascent of this fluid would have interacted with convecting meteoric waters at shallower depths. At this level, all fluids would have undergone some mixing, which is broadly supported by the wide range of recalculated $\delta^{18}O$ values in this study. As the magmatic phase becomes more diluted by circulating meteoric convection (Late Stage), low salinity (~3% Mass% eq. NaCl) and low temperature (Tt~200 to 480°C) secondary inclusions in skarn altered wall rocks in close proximity to the contact and major fault-hosted quartz veins/vugs crosscutting the Harrison Pass pluton are trapped. Infiltration of meteoric fluids around the contact is supported by mixed meteoric-connate $\delta^{18}O$ and $\delta^{13}C$ signatures in skarn wall rocks and calcite veins. It is speculated that mixed magmatic-meteoric fluids were then transported and focused along high angle faults along the flanks of the Harrison Pass pluton where a mixture of further cooling, oxidation and fluid-rock reactions resulted in gold deposition with pyrite and arsenopyrite within sedimentary country rocks along the Carlin trend.

ACKNOWLEDGEMENTS

I would like to thank the Society of Economic Geologists and the Colorado State University Geosciences Department for funding this project. I would also like to thank my advisors, Dr. John Ridley, Dr. Sally Sutton and Dr. Christopher Myrick, and field assistant Ryan Murphy, for their generous support, guidance, and advice during this project. I would especially like to thank my wife Allison, my friends, and my family for their continued encouragement and support during this endeavor.

TABLE OF CONTENTS

LIST OF FIGURES

Figure 5.2: Fluid history diagrams of the HPP and model for the source of fluids responsible for Carlin type gold deposits

LIST OF TABLES

1. INTRODUCTION

Carlin-type or sediment-hosted, disseminated gold deposits of the Great Basin have dominated gold production in the United States for several decades. However, the origin of and the driving force for circulation of the hydrothermal fluids responsible for these deposits are poorly understood. Meteoric and magmatic origins, with variants of each, have been proposed for the sources of gold and hydrothermal fluids in these deposits, and have been described by Sillitoe and Bonham (1990), Ilchik and Barton (1997) and Hofstra and Cline (2000). Recent debate, however, has been centered on the spatial and temporal association of gold and other base metals with distinct phases of plutonic as well as volcanic magmatism, which has narrowed to two contrasting genetic models for the origin of these ore forming fluids.

(1) Ore fluids were predominantly of magmatic origin derived from felsic magmas that crystallized at depth (10 to 15 km), which provided the ore components and thermal energy to drive fluid migration beyond the emplacement of the intruded plutons (Henry and Ressel, 2000; Ressel and Henry, 2006; Sillitoe and Bonham, 1990).

(2) Ore fluids were of meteoric origin that had convected, due to a magmatic heat source, to 10 to 15 km depth through sedimentary and meta-sedimentary rocks below the deposits. At this depth, fluids scavenged gold and other base metals,

and deposited them along high angle faults along trends in Northeastern Nevada (Emsbo et al., 2003; 2006).

This study tests the meteoric origin of fluids as proposed by Emsbo et al., (2003; 2006) through extensive field mapping, fluid inclusion and carbon and oxygen stable isotope analyses.

What is known about Carlin-type deposits is that the hydrothermal event influential in the formation of these deposits occurred in the mid-Eocene (42 to 37 Ma), and was of regional extent (~60,000 km^2) extending down to 10 km or greater in the northern Great Basin (Emsbo et al., 2006; Hofstra et al., 1999; Ressel et al., 2000; Arehart et al., 2003; Cline et al., 2005). Major ore deposits are concentrated along lineaments or “trends” including the Carlin trend, and the formation of these deposits are temporally associated with Eocene inboard arc-related magmatism that “swept” NE to SW through much of the Northern Great basin and western Utah, as a result of rollback or delamination of the shallow-dipping Farallon slab (Emsbo et al., 2006; Ilchik and Barton, 1997; Henry and Boden, 1998; Hofstra et al., 1999; Hofstra and Cline, 2000; Cline et al., 2005). This “sweep” is sometimes referred to as the Tuscarora Magmatic Belt or the Sierra-Wasatch Magmatic Zone and was generally manifested as dykes, calc-alkaline rocks of intermediate composition, and minor high-level stocks (Ressel and Henry, 2006). Recently, new aeromagnetic data and field evidence have suggested that these magmatic features are an extension of a suite of major buried felsic plutons that are present a few kilometers below current exposure (Ressel and Henry, 2006). These plutons were emplaced in the same linear

orientation as the Carlin trend, and geochronological and geochemical evidence suggests a spatial and temporal relationship with the formation of Carlin-type deposits. In order to test the proposed meteoric origin model, this study focuses on the Harrison Pass pluton (HPP), which is the only exposed ‘Carlin-aged’ pluton within the broad areal extent of known Carlin-type gold mineralization that is of the right size and depth of emplacement to be an analog for the geophysically imaged plutonic intrusions at depth. Thus, a full multi-element characterization of fluids circulating around the HPP during and after intrusion can help determine the chemistry and origin of fluids responsible for Carlin-type deposits.

As described in more detail in the following chapter, the HPP is a ~36 Ma complex multi-phase granodiorite to monzogranite, high-K, calc-alkaline intrusion in the central Ruby Mountains that intruded into the transitional zone of the Ruby Mountains Core complex (Burton, 1997). The pluton crops out ~80 km southeast of the major Carlin-type deposits along the Carlin trend, however it is in proximity to some smaller Carlin-type deposits in the region. The HPP was emplaced ~6 to 12 km (1600 to 3200 bars) at depth, and was tilted approximately 30° to the east during Basin and Range extension. This study tests the proposition that during intrusion, heat from the HPP was used to drive circulation of heated meteoric waters, which circulated down to 10 to 12 km depths, scavenged gold and other base metals, and were subsequently focused and precipitated along high angle faults along the Carlin trend.

This study uses a multidisciplinary approach of field mapping, petrographic observations, fluid inclusion analysis, and stable carbon and oxygen isotope studies to characterize the distribution, geometry and chemistry of migrating fluids around the HPP during and after intrusion. Field mapping was conducted *within* the HPP and *on* and *away* from the pluton-wall rock contact to observe and record the interrelation, distribution, and orientation of all vein types; distribution and relations of visible hydrothermal alteration; and faulted and brecciated zones. Samples collected include quartz, calcite and poly-metallic sulfide veins and adjacent wall rock, and hydrothermally altered granodiorite host rocks and metasedimentary wall rocks. Detailed petrographic observations and analyses were conducted on selected samples. Fluid inclusion analyses were conducted on quartz/calcite veins, miarolitic cavities, and altered wall rocks *within* the HPP and *on* and *away* from the contact to determine fluid chemistry at the time during and after the HPP intrusion. Fluid inclusions were analyzed petrographically and microthermometrically. Stable carbon and oxygen isotope studies were conducted on calcite veins to geochemically trace the origin of fluids around the HPP during and after intrusion.

Using the geochemical data from the HPP, it is possible to determine the chemistry and origin of fluids around the HPP during and after intrusion. It is also possible to reconstruct a fluid history around the HPP based on field observations and geochemical data. Also, by comparing the geochemical data obtained from the HPP with fluid characteristics from other Carlin-type deposit studies it is possible to note similarities or dissimilarities, which will help

determine a potential source and origin of fluids responsible for Carlin-type gold deposits.

2. REGIONAL GEOLOGY

2.1 TECTONIC HISTORY OF THE GREAT BASIN

The Great Basin is the largest section of the vast Basin and Range region, and extends for >2500 km from the Pacific Northwest to central Mexico (Dickinson, 2006). The basin is primarily located in Nevada, but also extends into western Utah and the eastern edge of California. Field studies of the HPP and surrounding areas took place in the Ruby Mountains-East Humboldt Range (RMEHR), which is situated in the eastern Great Basin in northeastern Nevada (Figure 2.1).

The area that became the Great Basin first developed along the western flank of Precambrian Laurentia ~1470 to 1370 Ma, and evolved through diverse stages of Earth history (Dickinson, 2006). During the Late Devonian and Early Mississippian compressional tectonics commenced due to the Antler Orogeny, which resulted in regional-scale folding, metamorphism and deformation of Paleozoic rocks of the Great Basin (Dickinson, 2006). This tectonic event also formed the Roberts Mountain thrust, where lower Paleozoic volcanic and continental slope sedimentary rocks were displaced over stratigraphically higher Paleozoic, stable shelf carbonate rocks. Additional deformation was applied to this region in the Late Permian to Early Triassic time during the Sonoma Orogeny

and in the Late Cretaceous-early Cenozoic time during the Sevier Orogeny (Dickinson, 2006). The Sevier Orogeny thickened continental crust producing a gravitationally unstable crustal welt, which in turn collapsed and is believed to be one of the causes for the onset of Basin and Range extension (Dickinson, 2006). By the end of the Sevier orogeny, deformation and eastward thrusting of stable shelf carbonate rocks over the foreland was essentially complete.

The first phase of Tertiary Basin and Range extension occurred between 41 to 39 Ma based on age estimates of extensional basins located northeast of the RMEHR that have been dated from 39 to 35 Ma, and from extensional basins that were contemporaneous with voluminous magmatism dated from 40 to 33 Ma (MacCready et al., 1997). This magmatism was part of the Sierra-Wasatch magmatic zone, which was an extensive calc-alkaline magmatic arc which migrated NE to SW across most of Nevada and western Utah between 40 and 32.4 million years ago (Henry and Ressel, 2000). The HPP was emplaced during this period of voluminous magmatism in the Great Basin.

2.2 RUBY MOUNTAINS EAST HUMBOLDT RANGE

The RMEHR is a high standing, north-northeast trending system of horsts in the Late Cenozoic Basin and Range district of Northeastern Nevada comprised mostly of high-grade crystalline rocks and miogeoclinal sediments (Fricke et al., 1992). The RMEHR is underlain by one of the best-exposed Cordilleran metamorphic core complexes in North America. Core complexes are formed in highly extended terrains and are characterized by a footwall of igneous and high-

grade metamorphic rocks, separated from a low-grade to non-metamorphosed upper plate by a normal-sense fault/shear zone (Burton, 1997).

Thermochronological data together with U-Pb zircon emplacement ages suggest that the RMEHR core complex development began during or immediately prior to the emplacement of the ~36 Ma HPP (Burton, 1997). The RMEHR core complex contains numerous groups of Paleozoic through Tertiary rocks, and can be broadly divided into three groups after Wright and Snoke (1993) (Figure 2.2). 'Zones' in Figure 2.2 are discussed in section 2.4.2.

1) South of the HPP pluton, the *suprastructure* is comprised of weakly metamorphosed to unmetamorphosed Paleozoic sedimentary rocks as well as Tertiary plutonic and sedimentary rocks. Regional metamorphism of this zone is of greenschist facies or lower.

2) North of the HPP, the *infrastructure* is comprised of plutonic and metamorphic rocks mostly classified as migmatitic mylonitic to nonmylonitic rocks. Regional metamorphism of this zone is of upper amphibolite facies.

3) The *transitional zone* is situated between the suprastructure and the infrastructure and is where the HPP was emplaced. This region is comprised mostly of metamorphosed sedimentary rocks intruded by Mesozoic igneous rocks (Wright and Snoke, 1993).

South of the HPP, sedimentary and metasedimentary strata of Cambrian to Carboniferous age generally dip ~30˚ eastward and were titled after the emplacement of the HPP (Burton, 1997). Structurally, this sedimentary sequence

is overlain on the western edge of the range by the west-dipping, Mitchell Creek klippe containing Devonian-aged strata. Proceeding north from the Mitchell Creek klippe on the western side of the Ruby Range and structurally above the HPP are Paleozoic rocks and jasperoid breccias, which exist as isolated remnants of the west-dipping Mitchell Creek klippe (Wright and Snoke, 1993).

On the eastern side of the range, and just north of the HPP, a traverse northwards encounters an increase in Mesozoic plutonic and granitic bodies, which is essentially the transition into the infrastructure of the core complex (Wright and Snoke, 1993). The rest of the RMEHR is comprised mostly of a metamorphic-core complex intruded by Late Jurassic to Tertiary aged granitic rocks. A full description and complete analysis of the metamorphic core complex of the RMEHR has been compiled by Kistler et al. (1981).

2.3 TECTONIC AND STRUCTURAL INFLUENCES ON THE RUBY MOUNTAINS

The RMEHR was subjected to a complex structural history after the emplacement of the HPP including: (1) an early episode of ductile strain during the development of the Ruby Mountain Shear Zone (RMSZ), which was overprinted by (2) cataclasite zones, and (3) Basin and Range normal faulting.

The RMSZ is a ductile-to-brittle structure that is ~1.5 to 2 km thick and extends for more than 100 km along the western margin of the RMEHR (Burton, 1997). It strikes southwest, dips northwest (~225°, 30°), and is characterized by mylonitic textures that show a west-northwest lineation and top-to-the west-northwest

sense of shear (Burton, 1997). Subsequent younger, crosscutting cataclasitic fault zones, striking ~290 to 310° and dipping moderately west ~25 to 30° are discontinuously exposed along the western flank of the central Ruby Mountains (Burton, 1997). These are tabular structures, often with clasts of mylonite, and mainly consist of a basal zone of chlorite alteration, a middle zone of tan, hydrothermally altered cataclasite, and an upper zone of >25 m of brecciated, hydrothermal quartz (Burton, 1997). This thick hydrothermal quartz unit has been mapped in discontinuous exposures for 4 km along the western flank of the RMEHR by Wilden and Kistler (1969) and Hudec (1990).

The east and west flanks of the RMEHR are bounded by a system of north-northeast striking, west-dipping normal faults that have been active from ~15.5 Ma to Recent (Hudec, 1990). Seismic reflection data by Reese (1986) show kilometer-scale, steeply west-dipping (~60°) normal faults on the western flank of the range beneath the adjacent Huntington valley (Burton, 1997). Subsequent mapping from this seismic data, revealed that the location of some of these faults beneath the Huntington Valley corresponds to the position of the terminus of Quaternary terraces, suggesting some of these faults were active in the Quaternary (Burton, 1997). Also, thick, white, hydrothermal quartz veins commonly occupy these faults on the western flank of the RMEHR. Similar faults on the eastern side of the RMEHR strike north-northeast and dip east between 35° and 70°, but do not contain hydrothermal quartz (Burton, 1997).

2.4 HARRISON PASS AND THE HARRISON PASS PLUTON

2.4.1 Harrison Pass

The Harrison Pass region is situated in a topographic low in the central Ruby Mountains of northeastern Nevada, ranging in elevation from ~6200 ft in the valleys to ~8600 ft along the mountain ridges (Burton, 1997). Mountain peaks north and south of the Harrison Pass region reach heights upwards to approximately 10,000 ft. This area falls within the Humboldt National Forest and borders the Ruby Wildlife Nature Preserve to the east. Access to most the area is gained through U.S. Forest Service roads, which twist through the majority of the region.

2.4.2 Harrison Pass pluton

The HPP is a ~36 Ma multiphase composite granitoid intrusive body, which occupies an area of ~110 km^2 in the central Ruby Mountains (Burton, 1997). The pluton outcrops ~50 km southeast of Elko, NV and is host to a number of small Pb-Zn and W deposits along the contact.

The HPP intruded into the transition zone between the infrastructure and suprastructure of the metamorphic complex, and is positioned in the footwall of the RMSZ. It was emplaced into a 2.6 km thick succession of Paleozoic sedimentary rocks that had been previously deformed and metamorphosed in the Jurassic (Burton, 1997). Post emplacement, the HPP and the RMEHR were tilted 30° east-southeast during later Basin and Range extension (~33 to 26 Ma) exposing a 5 km thick structural cross section of the pluton (Burton, 1997).

Regional stratigraphic evidence suggests that a minimum depth of emplacement, estimated for the roof zone in the eastern edge of pluton, is ~6 km. However, if Mesozoic structural thickening started in the central Ruby Mountains, as documented by Hudec (1990), then a maximum depth of pluton emplacement permitted is ~12 km. Burton (1997) concluded that on the eastern side of the range the HPP was emplaced ~6 km, and on the western side the pluton may have been emplaced ~12 km. The eastern and western sides are approximately 12 km apart. Amphibole-plagioclase thermobarometry data from Burton (1997), suggested a range of depths from 12.1 to 14.8 km, however Burton (1997) ignored this data because of a small sample base and evidence of post-crystallization re-equilibration of minerals.

Age constraints on the HPP emplacement have also varied. The age of emplacement of the HPP was first determined by Wilden and Kistler (1967) who used K-Ar biotite ages to yield emplacement ages ranging from 30 to 37 Ma (recalculated using revised decay constants). Wright and Snoke (1993) used U-Pb zircon age determinations to estimate that the HPP was emplaced ~36 Ma. This age is determined to be the most reliable estimate because the closure of the U-Pb zircon system is close to magmatic temperatures of granitic rocks (Burton, 1997). In this study, an age of ~36 Ma and a depth from ~6 to 12 km (~1600 to 3200 bars) will be used for the HPP emplacement.

Contact metamorphism (0.5 to 1.5 km wide) encircles the pluton, is superimposed on the metamorphism of the Jurassic metamorphic core complex, and is most apparent along the eastern and southern margins of the pluton

(Burton, 1997). The contact between the country rocks and the intrusive HPP is very irregular and varies spatially from concordant to discordant. The geometry of the contact along the northern margin is steeply dipping north north-east (45°), the southern margin is moderately dipping south (25 to 35°), and the eastern margin shallowly dips east (20°) (Burton, 1997). Three distinct contact zones have been described by Burton (1997) and they include: Zone I: the concordant roof zone; Zone II: highly discordant wall rock contact zone; and Zone III: generally discordant contact zone (Figure 2.2).

Zone I: is located on the eastern-southeastern pluton margin and is a generally a concordant sharp contact between the granodiorite and leucogranite of the HPP, and carbonate roof rocks of the Ordovician Pogonip group (roof zone). Many dikes (1 cm to 10 m) intrude the country rocks along the granodiorite margin. Contact metamorphism decreases rapidly with distance from the contact, and has caused recrystallization of the wall rocks into layers of calc-silicate and coarse-grained calcite marble containing locally scattered porphyroblasts of vesuvianite.

Zone II: is restricted to the northeast quadrant and southern margin of the HPP where much of the contact is discordant. This zone is characterized by small amplitude wall rock folding (4 to 15 cm), abundant elongate/oblate host rock xenoliths (>10 m^2), and sharp contacts between the upper unit of the carbonate Ordovician Pogonip Group, the hornfelsic siliciclastic Upper Cambrian unit and the granodiorite of Harrison Pass. Folds are well developed in layered calcite-silicate rock within 500 to 900 m of the contact and are generally tight,

asymmetric to overturned, and verge away from the pluton-wall rock contact. Near Corral Creek and Water Canyon, numerous east-dipping leucogranite sills intrude the lower carbonate Pogonip group.

Zone III: occurs along the central and western part of the southern and northern flanks of the HPP, and is different from Zones I and II because it includes a monzogranite, with minor screens of granodiorite. In the southern region, which was highly traversed in this study, the contact is highly irregular and is cut by abundant normal faults. Wall rock contacts are with hornsfelic and siliciclastic units of the Upper and Middle Cambrian units. These units are characterized by irregular, lensoidal compositional layering and contain small amplitude folding as described in zone II. This unit also displays map-scale folds that are upright, open, have 100's of meters of amplitude and kilometer scale-wavelengths. In Pearl Creek, an antiform has an east-south-east trending hinge and an axial surface of ~2 km. Some units display penetrative deformation including microstructures (e.g. pressure-solution cleavage) and foliation. Also, numerous granodiorite and monzogranite apophyses of the HPP intrusion occur south of the zone III contact within hornfelsic siliciclastic and shaly limestone Cambrian units.

2.5 HARRISON PASS PLUTON MAGMATISM

Geochemical evidence from Barnes et al. (2001) confirms that the emplacement of the plutonic magma comprising the HPP was in two stages. The early stage is defined by the Toyn Creek (Ttc) and Corral Creek (Tcc) units and is considered

to be the “granodioritic stage” (Figure 2.2) (Barnes et al., 2001). This stage includes porphyritic and equigranular roof dikes (Trd) associated with both units, bulbous and elliptical mafic microgranular enclaves enclosed in the Toyn Creek unit, and a leucogranitic cap on top of both units. The second and later stage consists of sheets and dikes of the leucocratic two-mica monzogranitic unit (Tmg), two-mica monzogranite of the Green Mountain Creek unit (Tgm), and intermediate to mafic, quartz-diorite to quartz-monzonite dikes (Barnes et al., 2001). Alaskite and aplite dikes comprised of muscovite, quartz, and alkali feldspar ± garnet are ubiquitous and are the youngest phases of the HPP (Barnes et al., 2001).

2.5.1 Early Stage

Rocks of the early stage crop out primarily in the eastern half of the pluton, but can be found as scattered outcrops bounded by later stage granites in the western half of the pluton (Barnes et al., 2001). Rocks are mainly coarse to very coarse grained, except for the porphyritic, rhyodacite roof dikes.

The Toyn Creek unit crops out in the northeastern and central parts of the HPP and ranges from biotite ± hornblende tonalite through granodiorite. The unit also locally contains microgranular mafic enclaves consisting of biotite ± hornblende ± quartz ± alkali feldspar ± titanite. Some synplutonic tonalitic dikes are also present (Barnes et al., 2001). Flow-aligned alkali-feldspar phenocrysts and flattened mafic enclaves are also observed in this unit and define the direction of magmatic foliation. The biotite monzogranite of Corral Creek unit is

predominantly found in the southern region of the pluton and is similar in grain size and mineralogy to the Toyn Creek unit, although chemically distinct making field discrimination difficult. It is medium to coarse grained, and is commonly equigranular but varies to porphyritic. This unit also contains sparse miarolitic quartz cavities and mafic enclaves.

Roof dikes (Trd) intrude Ordovician metacarbonate rocks along the eastern and southeastern side of the HPP and range from porphyritic dacitic dikes to equigranular granodiorite dikes (Barnes et al., 2001). Other roof dikes include monzogranitic hornblende alaskite and aphanitic rhyolite. Some alaskite dikes display K-metasomatic alteration, where alteration intensity decreases sharply away from the alteration zone (Burton, 1997).

2.5.2 Late Stage

The late stage units are predominantly monzogranitic and crop out in the western half and northern parts of the pluton. The ‘two mica’ stage consists of steeply dipping two mica monzogranite dikes and shallow east-dipping leucocratic monzogranite sheets with local pegmatitic aplite intrusions (Barnes et al., 2001). The biotite monzogranite unit contains pod-like leucogranite bodies that contain sparse medium to coarse-grained biotite and hornblende (Barnes et al., 2001). The earliest and largest late-stage unit is the homogeneous, medium-to-coarse grained two-mica monzogranite unit of Green Mountain Creek, which primarily crops out in the northern part of the HPP. This unit contains sparse enclaves of foliated, micaceous clots and avocado-sized, massive quartz pods (Barnes et al.,

2001). Medium to fine grained, diorite to quartz monzonite dikes were also emplaced during late-stage activity in the west-central part of the pluton (Barnes et al., 2001).

2.5.3 Geochemistry

Geochemically, early and late stage units are not related, and can be distinguished by their chemical makeup. Later stage units contain a lower Mg-number, higher Rb, Y, and Nb contents, and a more highly “evolved” REE pattern, in terms of deeper Eu anomalies (Barnes et al., 2001). A $\delta^{18}O$ stable isotope analysis conducted by Barnes et al. (2001), concluded that the difference in $\delta^{18}O$ values between early and late stages is nominal, and both display magmatic values between ~+9 to 11‰. However some late stage samples display anomalously low values <+7.5‰, suggesting exchange with ^{18}O-depleted meteoric fluids (Barnes et al., 2001). Such exchange has been recorded north of the HPP in stratigraphically higher jasperoid breccias and in the Northern Ruby Mountains (Fricke et al., 1992). However, the timing and structural controls on this exchange are not known, and is a subject of continued studies in the Harrison Pass region (Barnes et al., 2001).

2.6 MINERALIZATION AROUND THE HARRISON PASS PLUTON

Skarn and replacement deposits are concentrated along the “contact zone” between the HPP and the surrounding country rock. These types of deposits are also located in metasedimentary enclaves within the interior of the HPP.

The Corral Creek district was first mined in 1925, and is host to replacement deposits in upper Cambrian limestone and interbedded siltstone near the southwest contact zone of the HPP (Lapointe et al., 1991). Most of the mines of the Corral Creek district have yielded Pb, Zn, Ag, Cu, and W found principally in galena, hemimorphite, malachite, azurite, scheelite, and iron oxides. These prospects and mines are adjacent to the later stage Tmg unit and the early stage Tcc unit of the HPP.

The mines of the Harrison Pass district can be found along the southeast contact zone of the HPP. These mines are host to large scheelite-bearing skarn bodies up to 20 feet wide and 300 feet long, and are found within the Ordovician Pogonip group. In addition to tungsten, these skarns locally contain beryllium, tin, molybdenum, cadmium, and bismuth (Tingley, 1981a). The most impressive mine of this district is the Star tungsten mine found along the eastern contact zone near Harrison Pass Creek. It contained multiple ore bodies, and was developed by more than 1,000 ft of adits, drifts, and shafts. Mines and prospects of this district are adjacent to the early stage Ttc and Tcc intrusive units of the HPP.

2.7 CARLIN-TYPE GOLD DEPOSITS

Carlin-type deposits are epigenetic, disseminated, gold-only deposits, typically hosted in silty to sandy, calcareous sedimentary rocks (Howard, 2003). Gold is sub-microscopic and is typically hosted within pyrite, arsenopyrite, and marcasite. These deposits were first discovered in the Great Basin in Nevada,

however similar deposits occur in China, Macedonia, and Malaysia. Carlin-type deposits are thought to have formed from regionally upwelling hydrothermal fluids at temperatures 150 – 225°C at depths of 500 – 2500 m (Ressel and Henry, 2006) or 1 – 6.5 km (Cline et al., 2005). Fluid inclusion data show that fluids of the main stage ore are typically low salinity (< 6 wt% eq. NaCl) with detectable CO_2 content (< 4 mol%) (Arehart, 1996). Alteration varies greatly between deposits, but is comprised mainly of mixtures of decarbonization, silicification, and argillization (kaolinite and illite) (Arehart et al., 1993b). Replacement can be localized or penetrative, but typically occurs as ~100 m stratabound blankets within silty calcareous rocks. These alteration patterns and mineralogy suggest a weakly acidic ore fluid was responsible for Carlin-type deposits (Woitsekhowskaya and Peters, 1998). Crosscutting relationships with pre-, syn-, and post-mineralization rocks combined with direct dating of hydrothermal minerals have determined that the majority of all Carlin-type deposits in the Great Basin are of Late Eocene age (Henry and Ressel, 2000). Structurally, the control of major Carlin-type Au deposits is evident on a regional scale, where most deposits are positioned along high angle faults in lineaments or trends. One particular trend that has been highly investigated and studied is the Carlin trend.

The Carlin trend is a northwest-striking lineament in Northeastern Nevada that is approximately sixty kilometers long and eight kilometers wide, and contains several major world class Carlin-type gold deposits (Figure 2.3). Mineral deposits along the Carlin trend are spatially associated, and have been tied

chronologically to late Eocene calc-alkaline intrusions that were emplaced during voluminous magmatism that swept southward across Nevada and much of Utah 40 to 32.4 Ma (Henry and Ressel, 2000). The HPP was emplaced during this magmatic event and lies along strike of the Carlin trend.

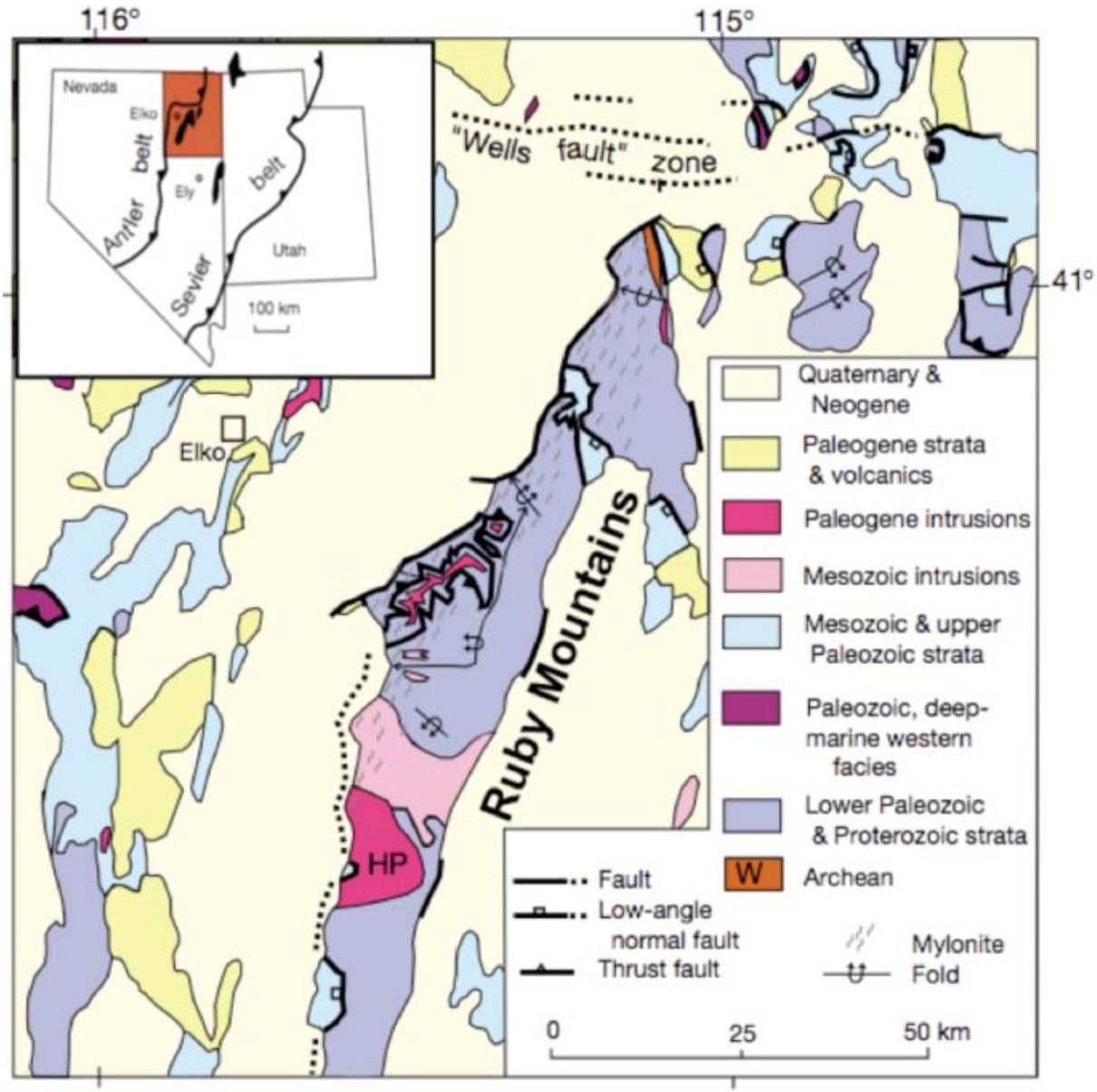

Figure 2.1: Location of the study area in northeastern Nevada (inset) and simplified geology of the Ruby Mountain East Humboldt Range core complex and surrounding areas in Northeastern Nevada. The Harrison Pass pluton (HP) is located ~50 km southeast of Elko, NV and was emplaced into the transitional zone between the suprastructure and infrastructure of the RMEHR core complex in the Southern Ruby Mountains. Map and inset has been modified after Howard (2003).

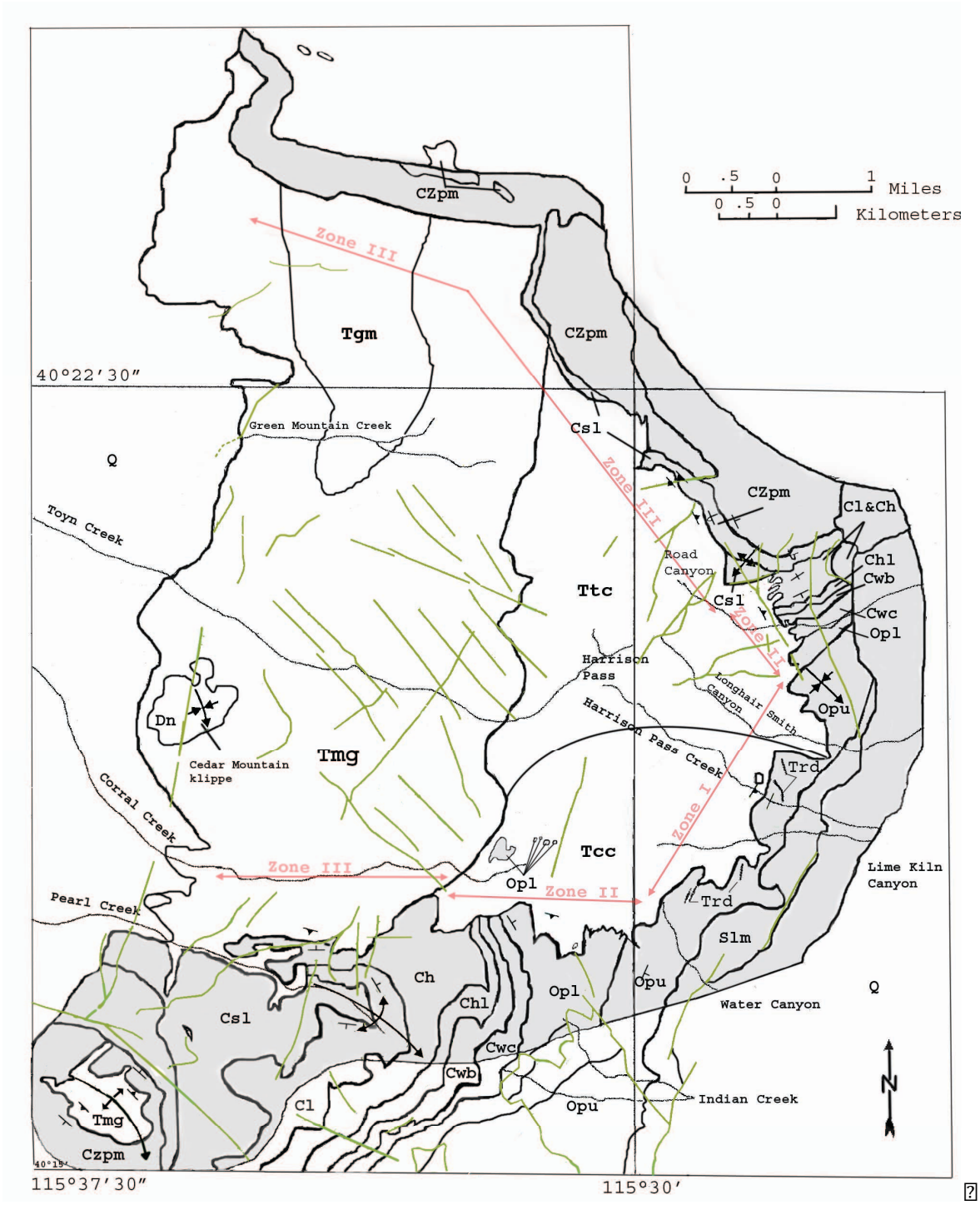

Figure 2.2: Simplified geologic map of the Harrison Pass pluton, and surrounding area illustrating three distinct contact zones after Burton (1997). The Tertiary contact metamorphic aureole outlined in grey is restricted within ~0.5 to 1.5 km of the pluton. Faults are shown by solid green lines after Burton (1997). Abbreviations for Paleogene intrusive rocks units of the Harrison Pass pluton and for the units of the metasedimentary wallrock sequence are given in Appendix 1.

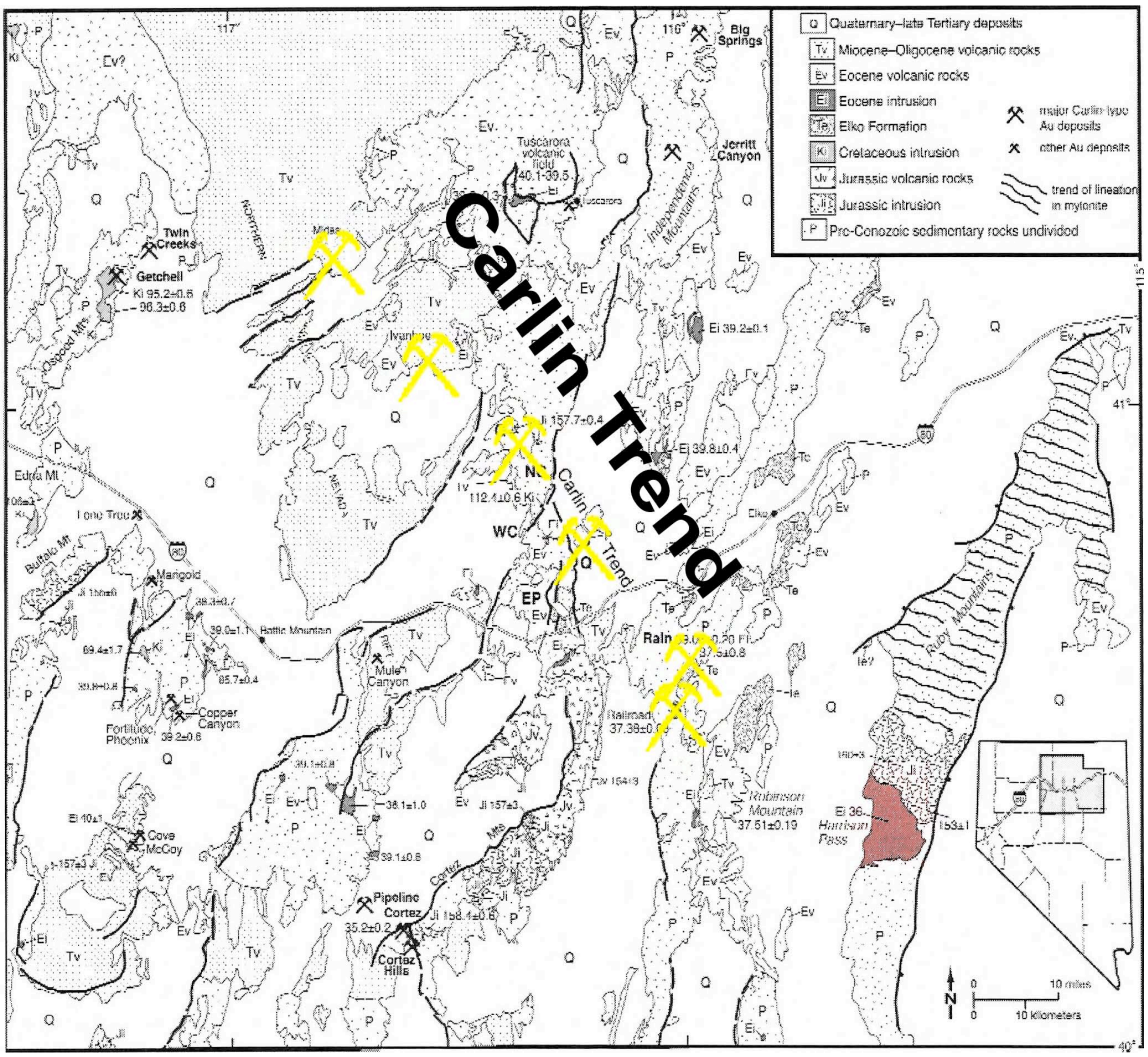

Figure 2.3: Geologic map of the surroundings of the Carlin trend, major known Carlin type gold deposits, and the HPP (red region), after Ressel and Henry, (2006).

3. METHODS

3.1 FIELD WORK

An 18-day field study of the HPP was conducted from July 10th, 2010 to July 28th, 2010. The author and his field assistant, Ryan Murphy, completed two E-W traverses: (1) one along the HPP contact and; (2) one approximately ~2 km south of the contact metamorphic aureole. The areas traversed were moderately accessible by a 4 X 4 vehicle, however back country hiking was necessary to access remote outcrops. Sampling was concentrated along the eastern and southern margins of the pluton contact as well as ~2 km south of the contact across the range of sedimentary host rocks and metamorphic grade exposed in the sections. Attention was specifically focused on zones of hydrothermal alteration, faulted and brecciated zones, veins of all types, and ore zones located in old mine workings and prospects. Sampling was not conducted on rocks near the flanks of the RMEHR because deformation and convecting hydrothermal fluids during Basin and Range extension may have had chemical and physical imprints.

A total of 121 samples were collected from the HPP and surrounding country rocks. Samples were carefully described in hand sample noting mineralogy, alteration facies, and textures/fabrics. 36 samples containing clear, non-milky quartz and calcite veins, well-defined quartz phenocrysts and vugs,

ore mineralization, and hydrothermal alteration were selected for further petrographic investigation (Table 3.1). Individual samples that display both wall rock alteration and quartz/calcite veining were separated out into two samples; a vein sample and a wall rock sample (“W”).

Maps prepared of this area were overlay maps based on earlier geological mapping by Burton (1997), and include the distribution of visible hydrothermal alteration and alteration zones around individual veins and faults. A Garmin Etrex GPS unit was utilized in conjunction with prepared maps to plot coordinates of samples collected and to assist in navigation of the areas traversed.

To gain a spatial understanding of physical and chemical differences around the HPP, observations will be subdivided into *within* the HPP and *on* and *away* from the contact. These words are italicized throughout to guide the reader. For clarity,

Within the HPP: observations and samples collected *within* the interior of the HPP intrusion.

On the contact: observations and samples collected *on* the contact are within 5 to 10 m of the intrusive HPP and the metasedimentary rocks it intruded into. This also includes metasedimentary enclaves *within* the HPP contact zone.

Away from pluton-wall rock contact: observations and samples collected in metasedimentary rocks *away* (~10 m to 2 km) from the pluton-wall rock contact.

3.2 PETROLOGY

Thirty-five ~120 μm thick doubly polished thin sections and one ~30 μm thick regular polished thin section were prepared by Mann Petrographics. Figure 3.1 displays localities of thin sections analyzed. Thin sections were examined in both transmitted and reflected light on a Leica DM2500 microscope. Petrographic examinations were conducted to determine mineralogy, textural fabrics, microstructures, paragenetical and crosscutting relationships, presence of fluid inclusion visibility, and alteration facies. Photographs were taken using an attached Leica Camera to document and record the aforementioned criteria. See Appendix 2 for detailed petrography descriptions.

3.3 FLUID INCLUSION PETROGRAPHY AND MEASUREMENT

Fluid inclusion studies were carried out using a detachable Linkam 600 heating-freezing stage attached to an Olympus BX50 petrographic microscope. The 35 doubly polished thin sections used for petrographic examinations were used for fluid inclusion petrographic analyses. Petrographic observations described the shape, size, the volume fraction vapor fill (fv), and fluid/solid phases of fluid inclusions mainly within quartz, calcite, and hydrogrossular. Primary, secondary, and pseudosecondary criteria discussed by Roedder (1984) were recorded to determine the origin of fluid inclusions and fluid inclusion assemblages within selected samples. From the 35 doubly polished thin sections, 24 were selected for further microthermometric analyses and were chosen based on fluid inclusion abundance, visibility, and size (>3 μm).

Heating and freezing of fluid inclusions were performed by conventional techniques described by Roedder (1984) and were used to determine the following microthermometric measurements in T (°C) as appropriate.

1) CO_2 melt (Tm_{CO_2})

2) Eutectic-First Ice Melt ($T_{eutectic}$)

3) Last ice melt (Tm_{ice})

4) Clathrate melt ($Tm_{clathrate}$)

5) Homogenization of CO_2 (Th_{CO_2})

6) Total Homogenization of vapor to a liquid phase (Th_{total})

Approximately 8 to 15 fluid inclusions were microthermometrically measured per sample. Measurements were conducted primarily on fluid inclusions within quartz and calcite grains in quartz/calcite veins and adjacent wall rock units, quartz vugs, and hydrothermally altered rocks. Fluid inclusions were classified into types based on their total homogenization temperatures, fv, and liquid/solid phases present. Types of fluid inclusions will be described in more detail in the following chapter. A detailed tabulation of each fluid inclusion measured can be seen in Appendix 3. Table 3.1 lists each sample microthermometrically analyzed. Note: miarolitic cavity samples contain both vapor-rich (samples ending in “a”) and CO_2-rich fluid inclusions.

3.4 COMPUTER ANALYSIS OF FLUID PROPERTIES

The software package *FLUIDS* of Bakker (2003) and its internal programs *CLATHRATE and BULK,* were used in conjunction with microthermometric measurements to determine salinity, density, and bulk composition of analyzed fluid inclusions. In *BULK*, empirical equations by Bodnar (1993) and Archer (1992) were used for calculating fluid inclusion properties for the H_2O-NaCl-KCl system. In *CLATHRATE*, empirical equations by Duan et al. (1992a,b) were used for the H_2O-CO_2-NaCl-KCl system. Fluid inclusion isochore plots for the H_2O-NaCl-KCl and the H_2O-CO_2-NaCl-KCl systems were calculated in the *ISOC* internal program using the empirical equations by Zhang and Frantz (1987).

3.5 CARBON AND OXYGEN STABLE ISOTOPE GEOCHEMISTRY

Ten samples were selected for carbon and oxygen isotope analyses; 5 *away* from the HPP contact metamorphic aureole and 5 *on* the HPP contact (Figure 3.1). Samples *on* the contact contain calcite veining and skarn alteration whereas samples *away* from contact contain calcite veining and unaltered wall rocks. Petrographic and microthermometric analyses of the selected samples were determined on 10 doubly polished thin sections using the same petrographic and microthermometric techniques described above (Table 3.1).

From each sample, >90 µg of fine, powdered, carbonate sample material was drilled from selected calcite veins and their adjacent wall rock using a diamond tipped rotary drill. Next, carbonate powder was weighed, separated into individual sample vials, and then sent to Dr. John Humphrey of the Colorado School of

Mines Stable Isotope Lab for carbon and oxygen isotope analyses. Four duplicates, (103.1 WR, 103.1 VN, 33.1 WR, 33.1 VN) were made for quality control.

Samples were quantitatively acidified *in vacuo* in an on-line autosampler with 100% orthophosphoric acid at 90°C (J. Humphrey, 2011, written communication). After cryogenic purification of the produced CO_2, the gas was analyzed simultaneously for stable carbon and oxygen isotopes in a Micromass Isoprime stable isotope ratio mass spectrometer using traditional dual-inlet techniques (J. Humphrey, 2011, written communication). The standard reference gas has been calibrated against a laboratory working $CaCO_3$ powder derived from the Colorado Yule Marble (CYM). $\delta^{13}C$ and $\delta^{18}O$ data are reported as a per mil difference from the Vienna PeeDee Belemnite (VPDB) international reference. Using the conversion equation provided in Sharp (2006), $\delta^{18}O$ data is also reported as a per mil difference from the Vienna Standard Mean Ocean Water (SMOW) international reference. Precision determined through repeated analyses of CYM and blind duplicate analysis of samples is 0.05‰ for carbon and 0.08‰ for oxygen. All data are corrected for the contribution of ^{17}O for carbon using the correction factors from Craig (1957) (J. Humphrey, 2011, written communication). Fractionation of CO_2 and calcite over a temperature range 273 to 4000 K at pressures 1 to 13 kilobars from Chacko et al. (1991) were used to determine fluid isotope compositions. Average pressure corrected fluid inclusion trapping temperatures (Tt) were used for each determination besides skarn and unaltered wall rocks. For skarn wall rocks *on* the contact a Tt of 587.50°C was used based

on average Tt values measured in hydrogrossular and quartz in a skarn wall rock (HPP-16W). For unaltered sedimentary wall rocks *away* from the contact a Tt of 365°C was used based on average Tt values of fluid inclusions in quartz in an unaltered wall rock (HPP-78W). See Appendix 4 for all carbon and oxygen stable isotope data and recalculations.

Table 3.1: List of petrographically analyzed samples. Samples that were used for fluid inclusion and stable isotope analysis are marked. Corresponding fluid inclusion type and setting are also listed.

Sample #	Fluid Inclusion Type	Setting
HPP-14	-	Quartz vein (within)
HPP-15†	Type I	Skarn WR (S)
HPP-16*†	Type II	Skarn WR (P)
HPP-18†	Type I	Type B Calcite vein (on)
HPP-21†	Type II	Quartz vein (on)
HPP-24†	Type III	MC (within)
HPP-24a†	Type II	MC (within)
HPP-26	-	Unaltered
HPP-28†	Type II	Quartz vein (within)
HPP-28V†	Type I	Vugs (within)
HPP-30a	-	Phyllic WR
HPP-33*†	Type I	Type B Calcite vein (on)
HPP-35	-	MC (within)
HPP-40†	Type II	Quartz vein (within)
HPP-40W†	Type I	Potassic WR
HPP-42*†	Type I	Type B Calcite vein (on)
HPP-43*†	Type II	Type B Calcite vein (on)
HPP-51	-	Quartz vein (away)
HPP-52†	Type I	Phyllic WR
HPP-56	-	Skarn WR (S)
HPP-57†	Type II	Quartz vein (on)
HPP-57W†	Type I	Skarn WR (S)
HPP-59	-	Skarn WR (S)
HPP-61*†	Type I	Type B Calcite vein (on)
HPP-71	-	Phyllic WR
HPP-74	-	MC (away)
HPP-78*†	Type I	Type A Calcite vein (away)
HPP-81†	Type I	Phyllic WR
HPP-84	-	Type B Calcite vein (on)
HPP-86	-	Quartz vein (on)
HPP-89†	Type II	Quartz vein (on)
HPP-98†	Type II	Quartz vein (on)
HPP-98W†	Type I	Phyllic WR
HPP-100*†	Type II	Type A Calcite vein (away)
HPP-103*†	Type I	Type A Calcite vein (away)
HPP-105*†	Type I	Type A Calcite vein (away)
HPP-107*†	Type I	Type A Calcite vein (away)
HPP-109	-	Type A Calcite vein (away)
HPP-111†	Type I	Potassic WR
HPP-113†	Type III	MC (away)
HPP-113a†	Type II	MC (away)
HPP-115†	Type II	Quartz vein (away)
HPP-115W†	Type I	Skarn WR (S)

† Denotes samples analyzed for fluid inclusion microthermometry

* Denotes samples analyzed for carbon and oxygen stable isotope analyses

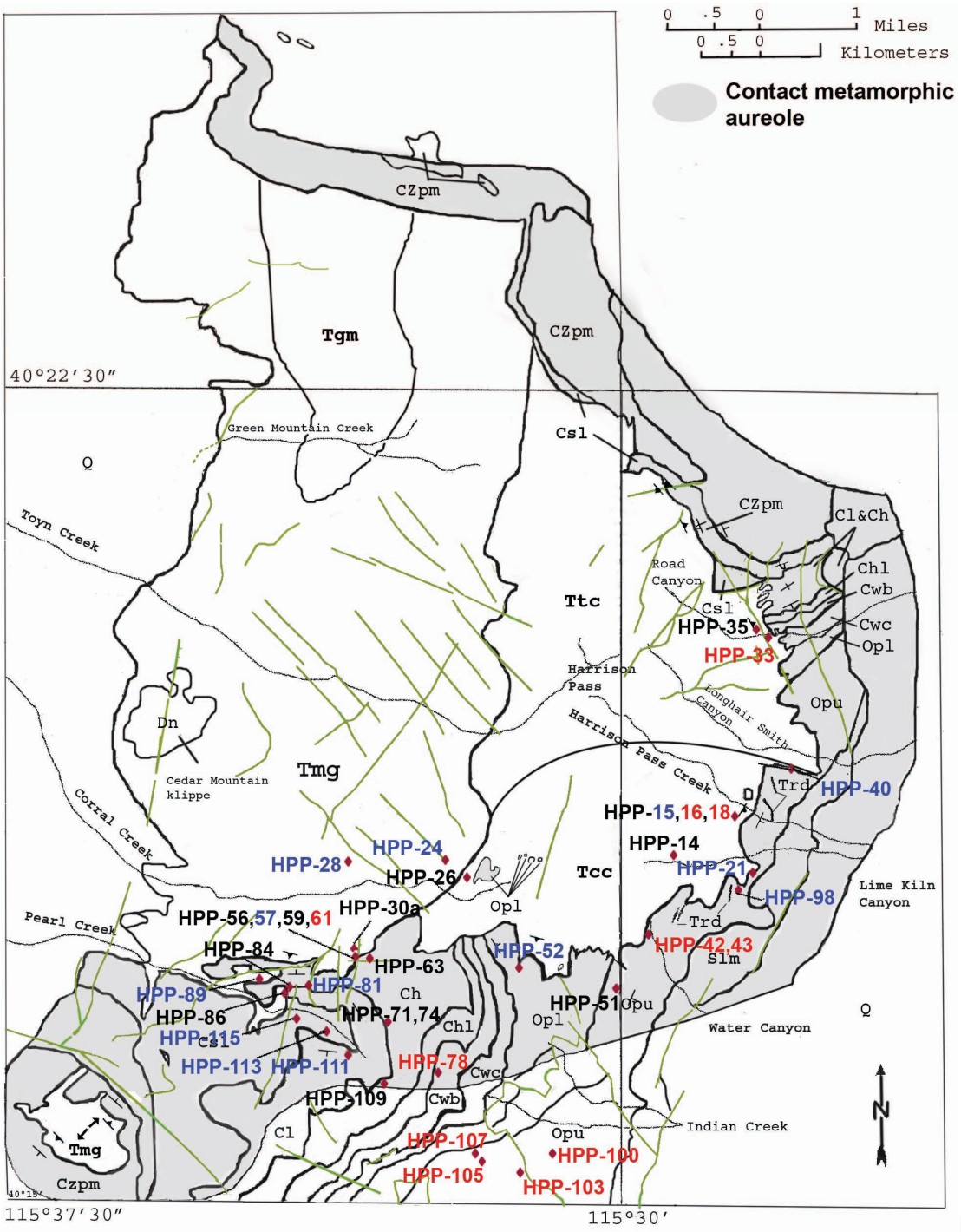

Figure 3.1: Map of the HPP and surrounding lithologies showing thin section sample locations, after Burton (1997). All samples were petrographically analyzed. 'Blue' colored samples indicate only fluid inclusion analysis whereas 'red' colored samples indicate both fluid inclusion and carbon and oxygen isotope analysis.

4. DATA OF HYDROTHERMAL ACTIVITY IN AND AROUND THE HPP

Two traverses, one along the eastern and southern margins of the HPP contact, and one approximately 2 km south of the southern contact were conducted to describe and map zones of hydrothermal alteration. Attention was specifically focused on veins of all types, faulted and brecciated zones, and ore zones within old mine workings and prospects to observe what types of fluids had migrated *within* the HPP and *on* and *away* from the contact during and after intrusion.

4.1 ALTERATION TYPES

Three types of alteration were mapped *on* and *away* from the HPP contact (Figure 4.1). Petrographical examinations were conducted on several samples containing alteration to confirm field observations. Below, are descriptions of the three types of alterations observed in the field with accompanying thin section descriptions. A full description of each thin section analyzed can be found in Appendix 2, and a list of samples and settings are shown in Table 3.1.

4.1.1 Skarn wall rock alteration

Skarn wall rock (WR) alteration is the most ubiquitous type of alteration observed *on* and *away* from the eastern and southern margins of the HPP contact. This alteration facies is predominately found at the contact between the early stage Ttc, Tcc and later stage Tmg units and the range of sedimentary host rocks

exposed in the eastern and southern sections. Skarn alteration was also observed in metasedimentary enclaves *within* the interior of the pluton. Old Pb, Zn, Ag, Cu, and W mine workings and prospects in skarns were mined until the 1960's, and provided the opportunity to examine skarn alteration and mineralogy in detail.

This type of alteration is typically pervasive and found adjacent to veins, fractures, and commonly is interlayered within metasedimentary carbonate wall rocks, but also occurs as alteration haloes around quartz/calcite veins. Alteration zones have varied thicknesses (~0.5 to 3 m), and are characterized mainly by diopside, tremolite, quartz, and calcite (Figure 4.2A). Minor minerals include biotite, sericite, hydrogrossular, pyrite, magnetite, sphalerite, and iron oxides. In hand sample, diopside is pale, greenish-brown, blocky, subhedral, and displays typical clinopyroxene cleavage. Tremolite is darker green, displays massive to fibrous habit, and has a vitreous to silky luster. Quartz and calcite are fine to coarse-grained, seriate, subhedral, and dispersed throughout the groundmass. Samples that display skarn wall rock alteration include: HPP-16, HPP-18, HPP-56, HPP-57W, HPP-59, HPP-61 and HPP-115W.

In thin section, skarn alteration is predominantly characterized by a calcite+quartz+tremolite+diopside+biotite mineral assemblage (Figure 4.2B). However, in most calcite vein samples *on* the contact (HPP-18, HPP-43, HPP-61) tremolite is absent from the wall rock. Quartz and calcite range from fine to coarse-grained, are mostly subhedral, and make up the majority of the calc-silicate groundmass. In some instances, calcite displays a bladed to crystalline

habit and can be as large as 2500 μm. Quartz grains are often highly fractured and brecciated, and display undulose extinction, which suggests a period of deformation and/or metamorphism. Tremolite occurs as euhedral, acicular aggregates, that can be as long as 500 μm. Typically, tremolite can be seen replacing and overprinting diopside near vein edges, presumably as the temperature lowered. Diopside is fine to coarse-grained, subhedral to euhedral, and often displays a blocky to columnar habit. In most cases, diopside grains have been highly fractured, and partially to fully replaced by tremolite±biotite±sericite. Biotite is found as subhedral masses disseminated throughout the groundmass and regularly has replaced plagioclase and diopside. Commonly, biotite has been partially replaced by chlorite.

Where skarn alteration is evident, a clear progression in mineralogy exists away from quartz veins towards the adjacent altered wall rock. Typically on the edge of the vein the mineral assemblage consists of tremolite±diopside±calcite±quartz±biotite (Figure 4.2A/B). Here, tremolite dominates as large, euhedral, acicular needles often fully replacing diopside and calcite. Progressing away from quartz veins, tremolite abundance dissipates, quartz and calcite are more fine-grained, and diopside becomes the dominant mineral. Here, diopside grains are coarse-grained, subhedral, highly fractured, and show minimal to partial tremolite replacement. Fine to coarse-sized quartz grains can also be observed away from veins where they are typically subhedral and highly fractured. Samples HPP-42, HPP-59 and HPP-115 display this spatial sequence of mineralogy.

Minor minerals include: hydrogrossular±sphalerite±epidote±pyrite±magnetite±sericite. Hydrogrossular is only apparent in sample HPP-16 within the skarn of Star Mine, and is characterized by subhedral, massive, and blocky grains that give the sample a pinkish tint (Figure 4.2C). Sphalerite is only prevalent as a vein crosscutting a calc-silicate wall rock in sample HPP-61, and as a minor constituent in sample HPP-33. Typically, sphalerite is coarse-grained, subhedral, and moderately brecciated (Figure 4.2D). Epidote is seen in sample HPP-42, as well-developed subhedral to euhedral brecciated masses within a calc-silicate mineral assemblage. Pyrite and magnetite grains are sparse, disseminated, and fine to medium-grained (2 to 1050 μm). Pyrite grains display a subhedral to euhedral cubic habit, and often have been partially to fully oxidized by hematite±goethite. In most instances, magnetite displays ilmenite exsolution and has been partially replaced by pyrite.

4.1.2 Phyllic wall rock alteration

This type of alteration is the second most abundant type of alteration observed, and is ubiquitously found altering granodiorite and monzogranite *on* and *away* from the eastern and southern margins of the HPP contact. This alteration style is typically pervasive throughout the original host rock and is found as massive host rock replacement. Recognition of phyllic alteration in the field included the addition of quartz, sericite and pyrite to the original granodiorite host rock (Figure 4.2E).

In thin section, phyllic alteration is characterized by mainly a quartz+sericite+pyrite±biotite±magnetite mineral assemblage (Figure 4.2F). Quartz is typically fine to coarse-grained, fractured, and hypidiomorphic. Sericite is found within veins and fracture fills, but also can be seen as massive aggregates partially to fully replacing plagioclase feldspar. Pyrite occurs as subhedral to euhedral cubes, and predominantly displays partial to full hematite oxidation. Also, pyrite twinning can be seen in some samples. Trace magnetites are subhedral to euhedral cubes that typically display ilmenite exsolution and have been partially to fully oxidized by hematite. In some instances, pyrite can be seen as inclusions within magnetite. Samples that display this type of alteration include: HPP-30a, HPP-52, HPP-71, HPP-81, and HPP-98W.

4.1.3 Potassic wall rock alteration

Potassic alteration (K-metasomatism) was the least abundant type of alteration observed around the HPP, and was only found altering granodiorite/monzogranite *on* (HPP-40W) and *away* (HPP-111) from the HPP contact. In map view, HPP-40W is located on the eastern edge of the HPP pluton-wall rock contact near rhyodacite roof dikes (Trd) in the ‘roof zone’ of the HPP. Alternatively, HPP-111 was found in an apophysis of the intrusion ~1.5 km south of the HPP in the Cl Fm. In the field, this type of alteration was not as evident or as intense as the other wall rock alterations described above, however the patchy addition of biotite+K-feldspar±sericite to granodiorite/monzogranite plutonic rocks is diagnostic of potassic alteration (Figure 4.2G).

In thin section, potassic alteration is characterized by the addition of dark brown, patchy, aggregates of subhedral biotite and subhedral, granular K-feldspar to the granodiorite wall rock (Figure 4.2H). Commonly, biotite has replaced plagioclase feldspar and, more rarely, quartz. Sparse pyrite is also observed as disseminated subhedral to euhedral cubes throughout the wall rock that have been partially to fully oxidized by hematite.

4.2 VEINS

Quartz and calcite veins and quartz miarolitic cavities were mapped (Figure 4.1) and petrographically described in detail. The following sections describe veins based on their type (quartz, calcite) and locality (within, on, away) from the HPP contact. See Appendix 2 for a comprehensive petrographic description of samples analyzed.

4.2.1 Fault-hosted quartz veins

Major hydrothermal quartz veins (HQV) (dotted red lines) *within* the HPP have been mapped in detail by Lapointe et al. (1991) (Figure 4.1). These northeast and northwest striking quartz veins are typically hosted in faults/joints *within* the central, western interior and flanks of the HPP. They crosscut both the early and late plutonic rocks of the HPP and adjacent metasedimentary wall rocks along the contact at nearly ~90°. Veins are thick (~4 to 8 m), and composed of a majority of extremely hard, milky white quartz that can continuously or irregularly be exposed for 100’s of meters along strike along a fault. Contacts are typically sharp with host granodiorite and metasedimentary wall rocks, and quartz habits

can vary from massive to comb and vuggy (Figure 4.3A). Comb and vuggy habits often display well-defined, euhedral quartz terminations growing inward from the edge of the vein or vug (Figure 4.3B). Hydrothermal or fault brecciation is also evident where these veins crosscut the range of metasedimentary rocks along the southern margin of the HPP, where highly angular pieces of adjacent metasedimentary wall rocks are included in the vein. Due to lack of field evidence, the origins of brecciation cannot be defined. However, Burton (1997) identified chlorite alteration within mafic minerals adjacent to one of these structures north of Toyn Creek, which suggest that these fault zones formed at moderately high temperatures.

A petrographic examination of a HQV (HPP-28) *within* the HPP, has confirmed these field observations and has revealed three generations of vein infill. 1) The oldest generation is 99% subhedral-euhedral, medium to coarse-grained, slightly brecciated and massive quartz±magnetite±pyrite; 2) The next generation is euhedral quartz, infilling vugs (HPP-28V) with crystals as long as 1300 μm; 3) The youngest generation are comb textured euhedral quartz veins, which crosscut earlier vuggy quartz. Quartz crystals can be as long 8250 μm, and in some instances Brazil twinning, which reflects a quartz lattice transformation, can be seen in some quartz crystals. The fact that these veins occupy crosscutting fault zones and contain open-filled quartz textures suggests that these veins formed from later, possibly shallow epithermal fluids.

4.2.2 Minor quartz veins

Minor quartz veins *within* the HPP and *on* and *away* from the contact are typically ~mm's to ~cm's across, clear to milky, and contacts with host wall rocks are sharp. Most quartz veins trend approximately north-south, striking between ~340 to 20° and are steeply dipping (almost vertical).

4.2.2.1 Minor quartz veins within the HPP

Most quartz veins observed *within* the HPP resemble the *major quartz veins* discussed above, however some were thinner (~mm's to ~cm's), contain clearer quartz, and are continuous for only a couple of meters. In hand sample, quartz is mainly subhedral, fine to coarse-grained, and equigranular. Contacts are sharp with megacrystic granodiorite and monzogranite wall rocks, which display no evidence of hydrothermal alteration.

In thin section, quartz veins are composed of mostly medium to coarse-grained, subhedral quartz with trace biotite±chlorite±plagioclase±iron oxides. Locally, some quartz displays minor undulose extinction suggesting a low strain deformation event. One sample that displays these characteristics is HPP-14, however microthermometric analyses were not carried out.

4.2.2.2 Minor quartz veins on the HPP contact

Quartz veins *on* the HPP contact are slightly larger (~mm's to <20 cm) than minor quartz veins *within* the interior the HPP. However, both vein types contain similar strike and dip measurements.

Quartz veins *on* the contact range in style from multiple sets of branching, to parallel and sheeted quartz veins (Figure 4.3 C/D). Chaotic branching of quartz veins occurs mostly within fractured and brecciated limestone and granodiorite where alteration is minimal whereas sheeted quartz veining typically occurs in skarn prospects and mines where alteration is apparent. Often, these veins crosscut or have been crosscut by ~mm to ~cm Type B calcite+quartz±pyrite veins (referenced below), which suggest multiple fluid flow events. Typically, contacts with adjacent granodiorite/monzogranite and metasedimentary wall rocks are sharp.

In thin section, quartz is fine to coarse-grained, subhedral, equigranular, and often displays undulose extinction. A calc-silicate zonation, as discussed in the section *4.1.1*, often occurs adjacent to quartz veins that are hosted in a skarn wall rock and mainly consists of a tremolite to diopside progression away from the vein. Quartz veins *on* the contact are the only type of veins that show this distinct mineral progression, which suggest that water used to create tremolite near the vein edge was primarily in the fluid responsible for the formation of quartz veins *on* the contact.

Also, subhedral, fine to coarse-grained calcite is sometimes present within the quartz vein and can be in abundance up to ~30 to 40%. Minor minerals include plagioclase±sericite±biotite.

4.2.2.3 Minor quartz veins away from the HPP contact

Quartz veins *away* from the HPP contact are not as widespread as those on the contact and were mapped as far as ~3 km away. Quartz veins are ~mm's to 2-3 cm's thick and are either roughly parallel with bedding (strike ~40 to 60°) or orthogonal to bedding (strike ~120 to 160°C). In hand sample, mineralogy typically consists of pure, clear to white, fine to medium-grained quartz with varying abundances of calcite. Minor minerals include biotite±chlorite±pyrite±iron oxides.

Contacts with host rocks are sharp, and typically no alteration is observed. However, in samples HPP-111 and HPP-115W potassic and skarn wall rock alteration was documented respectively within granodiorite and metasedimentary host rocks locally *away* from the HPP contact. In thin section, quartz is medium to coarse-grained, subhedral, equigranular, and displays minor undulose extinction. Typically, subhedral, fine to medium-grained calcite is intergrown with quartz. However, in sample HPP-111, coarse-grained, subhedral plagioclase is observed in the vein.

4.2.3 Calcite veins on the HPP contact

Calcite veins were only observed *on* (±5 to 10 m), and *away* from the HPP contact. No calcite veins were documented or observed *within* the early and late stage intrusive units of the HPP.

Two types of calcite veins were observed *on* the HPP contact. Type A consists of calcite veins that range in size from ~mm's to ~cm's and typically are oriented

parallel with bedding (strike of 40 to 60°) (Figure 4.3E). Contacts are generally razor sharp with metasedimentary host rocks, and no alteration is visible. In hand sample, these veins are composed of predominantly fine to coarse-grained, equigranular, brownish-white calcite with trace quartz.

Type B calcite veins occur mainly in prospects and mines around skarn zones, and typically trend NE-SW along the southern edge of the pluton and N-S along the eastern edge. These veins are frequently associated with adjacent wall rock hydrothermal alteration and contain quartz±biotite and commonly Pb-Zn-Fe sulfides (Figure 4.3F). These veins are sometimes massive and sugary, where bundles of calcite crystals have been recrystallized and appear intergrown together, which is most likely due to deformation during of after the HPP intrusion.

In hand sample, Type B calcite veins are crusty yellow and exude a pungent sulfur smell indicating the presence of sulfides. Vein size ranges from ~mm's to 40 to 50 cm's, and contacts with adjacent skarn wall rock range from sharp to slightly diffuse. Typically, multiple Type B calcite veins within a prospect/mine are oriented parallel, but can also splay in multiple directions adjoining other calcite veins. Type B calcite veins regularly crosscut Type A calcite veins, and are seldomly crosscut by later generation veins. However, in some instances minor quartz veins *on* the contact crosscut or have been crosscut by Type B calcite veins *on* the contact, inferring overlapping generations. Ore minerals identified in hand sample include galena, sphalerite, pyrite, and magnetite, which often form veins or pockets within Type B calcite veins. In sample HPP-61, a sphalerite

pocket is contained within a Type B calcite vein (Figure 4.2D). The pocket is composed of dominantly coarse-grained, subhedral, moderately brecciated, bronzy-yellow sphalerite.

In thin section, Type B veins are predominantly calcite, however varying amounts of diopside+quartz can also be found in and around the vein. Alteration around the vein is similar to the skarn alteration described earlier, however Type B calcite veins do not contain tremolite near the vein edge. Calcite is fine to coarse-grained (20 to 5000 μm), subhedral to euhedral, and can occur as bladed crystals or as large aggregate masses. Diopside occurs as pale green, subhedral columnar, fragmented blocks, that display typical ~90° pyroxene cleavage. Minor minerals include biotite±magnetite±pyrite±sericite. Pyrite is often disseminated throughout the veins as subhedral to euhedral cubes (3 to 45 μm), partially to fully oxidized to hematite. Magnetite is generally sparse, but in sample HPP-33 it is found as fine-grained, euhedral cubes with pyrite inclusions/lamellae, ilmenite exsolution, and oxidized rims of hematite. Pyrite inclusions/lamellae within magnetite grains are interpreted to represent magnetite replacement of pyrite. Fundamentally, this textural evidence suggests that sulfur was released and iron (Fe^{2+}) was partially oxidized during the mineral history. For example:
$2Fe^{2+} + 4H_2O + FeS_2 = Fe_3O_4 + 6H^+ + 2HS^-$ (Florindo et al., 2003).

4.2.4 Calcite veins away from the HPP contact

Calcite veins *away* from the HPP contact are the same as Type A calcite veins described above, and are found ubiquitously within Cambrian and Ordovician

metasedimentary rocks *away* from the HPP. These veins can either be parallel with bedding (strike 40 to 60°), or can crosscut at varying angles. Typically, these veins range from ~cm's to 15 to 20 cm across. However, on the southeastern side of the HPP, within the Ordovician Pogonip Fm. (Opu) sheeted calcite veins range from 30 to 50 cm across (Figure 4.3G). Contacts with adjacent metasedimentary rocks are sharp and show no sign of alteration. In hand sample, calcite veins are made up of mostly pure, medium to coarse-grained, brownish-white calcite.

In thin section, veins are comprised of mainly calcite with trace quartz±pyrite±iron oxides. Calcite is medium to coarse-grained, subhedral to euhedral, and occasionally locally brecciated. Quartz is typically medium to coarse-grained, subhedral, equigranular and displays slight undulose extinction. Pyrite grains are typically small (5 to 15 μm), disseminated, euhedral, and have been partially to fully oxidized to hematite.

4.3 MIAROLITIC CAVITIES

Miarolitic cavities were sampled in igneous rocks of the HPP to document the last crystallizing and coexisting volatile phases of the HPP (Figure 4.3H). Most miarolitic cavities were observed *within* the HPP (HPP-24, HPP-35), however some were observed in detached granodiorite bodies, *away* from the main plutonic intrusion (HPP-74, HPP-113). Cavities range in size, but on average are approximately less than 10 cm X 10 cm, and are crudely oblate or lobate in shape. These cavities typically contain pure, clear, coarse-grained, massive

quartz. Wall rock mineralogy consists of a typical granodiorite mineral assemblage, which includes: quartz+K-feldspar+plagioclase+biotite±pyrite± magnetite±sericite±iron oxides. Quartz in thin section is typically coarse-grained, subhedral, and equigranular. However, in sample HPP-35 quartz has been sheared and displays a ribbon-type texture indicative of a shearing/deformational event. Subhedral, partially oxidized grains of pyrite are disseminated in the wall rock around some cavities and in HPP-74 they reach up to 950 μm in size. Irregular, anhedral polygonal magnetite cones were also observed rimming and growing into some cavities (HPP-113, HPP-41).

The adjacent granodiorite wall rock can also display myrmekite textures of interfingering quartz+plagioclase+K-feldspar. Sericite veining is also common throughout the wall rock.

4.4 FLUID INCLUSION PETROGRAPHY AND MICROTHERMOMETRY

Fluid inclusion petrography and microthermometry techniques were utilized on trapped fluid inclusions in veins, wall rocks, and miarolitic cavities *within* the HPP and *on* and *away* from the contact to document the chemistry and origin of fluids. A total of 24 samples were investigated (Table 3.1), and >200 measurements were recorded over the whole sample suite.

Fluid inclusion petrography and microthermometry was focused on; 1) Primary (P) inclusions in quartz/calcite grains within quartz/calcite veins to provide an estimate of the migrating fluid chemistry that is responsible for vein formation; 2) Secondary (S) quartz/calcite inclusions in crosscutting trails within hydrothermally

altered wall rock to estimate migrating fluid chemistry responsible for wall rock metasomatism (Skarn WR (S), Phyllic WR, and Potassic WR); 3) Primary inclusions within quartz miarolitic cavities to estimate the chemistry of a magmatic fluid phase of the HPP for comparative analysis; 4) Primary inclusions in hydrogrossular and quartz (Skarn WR (P)), within skarn wall rocks to provide an estimate of chemistry during contact metamorphism; 5) Primary inclusions in unaltered wall rock adjacent to veins. *Category 5 inclusions were not included in the fluid inclusion data analysis because they do not provide the information on the chemistry of migrating and circulating fluids around HPP during intrusion.* See Appendix 3 for a list of all fluid inclusions measured, types, and microthermometric measurements.

Types of measurements made include:

1) CO_2 melt (Tm_{CO_2})

2) Eutectic-First Ice Melt ($T_{eutectic}$)

3) Last ice melt (Tm_{ice})

4) Clathrate melt ($Tm_{clathrate}$)

5) Homogenization of CO_2 (Th_{CO_2})

6) Total Homogenization of vapor to a liquid phase (Th_{total})

Not all phase changes were observed within every measured inclusion, and occasionally several microthermometric runs were needed in order to accurately determine the temperature of the phase change.

Fluid inclusion microthermometry does have limitations in determining the true $T_{eutectic}$ because the first ice-melt phase change is often extremely subtle and difficult to discern. The $T_{eutectic}$ is an invariant point and is solely used to estimate the composition of the end member components within the fluids (Shephard et al., 1985). Therefore, limitations in discerning the true $T_{eutectic}$ can affect the estimate of fluid composition. Hence, where anomalously high $T_{eutectic}$ temperatures (-10 to -14°C) are recorded, consideration of this limitation is taken into account.

4.5 FLUID INCLUSION TYPES

From the 24 samples analyzed, 3 types of fluid inclusions were identified from petrographic observations at room temperature (~25°C). Fluid inclusion types were divided by average and modal Th_{total} values, vapor volume fraction (fv), and composition. Fluid inclusion types observed within samples are shown in Table 3.1.

4.5.1 Type I

Type I inclusions (Figure 4.4 A/B) are characterized by a 2-phase, liquid-vapor (L-V) system, where the outer part of the inclusion is dominated by an aqueous liquid phase, and the inner part contains a small vapor gas phase giving most of the inclusions a fv between 0.20 and 0.30. Type I inclusions are the most common type found throughout the samples and exist as primary, pseudosecondary, and secondary inclusions in quartz and calcite host minerals *within* the HPP and *on* and *away* from the HPP contact. This type of inclusion is

found as secondary linear trails crosscutting grain boundaries, as isolated primary inclusions and as 3-D clusters. These inclusions are typically small ranging in size from ~3 to 10 μm, and can take on varying shapes including round, oblate, negative crystal, slightly irregular, and elongated. Some Type I inclusions contain an accidental solid phase, where a solid was incorporated into the inclusion during fluid inclusion formation.

Modes and ranges of microthermometric measurements provide additional insight into this inclusion type. Type I inclusions: $T_{eutectic}$~-21.5°C, Tm_{ice}~-0.5 to -6.5°C, homogenized to a liquid at Th_{total}~160°C, Ph_{total}~5.5 bar, and Mass% eq. NaCl~0.5 to 6.5%.

Given the theoretical $T_{eutectic}$ values for the H_2O-NaCl (-21.2°C), H_2O-KCl (-10.6°C), and H_2O-NaCl-KCl (-23.5°C) chemical systems (Shepherd et al., 1985), in comparison with the Type I $T_{eutectic}$ mode (~-21.5°C) and range (~-11 to -29°C), it is determined that Type I fluid inclusions are most likely a mixture between all three end member species: H_2O, NaCl, and KCl. Therefore, Type I inclusions are characterized by the H_2O-NaCl-KCl system.

4.5.2 Type II

Type II inclusions were the second most common inclusions observed, and are characterized by a 2-phase (L-V) system, where the outer part of the inclusions is occupied by an aqueous liquid phase, and the inner part is occupied by a medium-sized vapor bubble giving most inclusions a fv from 0.30 to 0.35. Hence, not a real clear fv distinction from Type I inclusions. These inclusions were only

found as primary and pseudosecondary inclusions in undeformed host quartz and hydrogrossular crystals *within* the HPP and *on* and locally *away* from the HPP contact (Figure 4.4C). These inclusions exist as single, isolated inclusions or as a fluid inclusion assemblage within pseudosecondary trails and 3D clusters. Fluid inclusion size averages between ~15 to 20 μm, however inclusions as large as 60 μm have been observed in hydrogrossular crystals (HPP-16). Inclusion shapes are typically round, oblate, and negative crystal, but some can be elongated. Also, Type II inclusions have been identified coexisting with less vapor-rich Type I inclusions.

Microthermometric analyses reveal that Type II inclusions contain similar $T_{eutectic}$ (~-21°C), Tm_{ice} (~-0.5 to -4.5°C), and Mass% eq. NaCl (~1 to 6%) values as Type I inclusions. However, Th_{total} and Ph_{total} are significantly higher; ~315°C, ~200 bars. Similar to that of Type I $T_{eutectic}$, Type II inclusions $T_{eutectic}$ mode (~21°C) and range (-10 to -30°C) are interpreted to be characterized by the same Type I H_2O-NaCl-KCl system. This type of inclusion was distinguished from Type I inclusions based on generally higher Th_{total} values (~180 to 450°C) and larger sized fluid inclusions and fv values.

4.5.3 Type III

Type III inclusions are the least abundant inclusions observed, and are characterized by a three phase (L-L-V) system at room temperature, in which the outer part of the inclusion is occupied by an aqueous liquid; inside this exists a smaller phase of carbonic liquid; and inside that a CO_2 gas bubble. These

inclusions only exist as primary fluid inclusions in quartz crystals in miarolitic cavities *within* the HPP and locally *away* from the HPP contact (Figure 4.4D). Usually, Type III fluid inclusions exist as large isolated primary fluid inclusions, however in some instances they have been observed in pseudosecondary trails. The fv value between the inner liquid and gas CO_2, and the outer aqueous liquid phase is less consistent than Type I and II inclusions and can range between 0.25 and 0.95. These inclusions are large and average ~24 µm but can be up to 30 µm across. Shapes are typically round and oblate, but some are elongated. Only in miarolitic cavities are Type II inclusions associated with Type III inclusions.

Microthermometric measurements are sparse due to a low Type III inclusion population. Measurements reveal that Type III inclusions have slightly lower, but not statistically significant $T_{eutectic}$ (~-24°C), and Mass% eq. NaCl (~0.5 to 6%) values, in which the Mass% eq. NaCl was calculated from $Tm_{clathrate}$ melting temperatures (~5.5 to 8.5°C). Comparatively, fluid inclusions homogenized to a liquid at intermediate temperatures (Th_{total}~240°C), however some homogenized at significantly higher temperatures (Th_{total}~480°C). Minimum trapped pressures (Ph_{total}) were the highest recorded in the study and were ~630 bars, but could be as high as ~2000 bars. Some mixtures of low melting point gases were also apparent as Tm_{CO_2} melted ~-57°C. Using observed Tm_{CO_2} and Th_{CO_2} temperatures and graphs from Ridley and Hagemann (1999), XCO_2 carbonic and XCH_4 methane phases were calculated and ranged respectively from 0.952 to 0.987 and 0.013 to 0.018. Similar to that of Type I and Type II inclusions, Type III

$T_{eutectic}$ values are ~-24°C and range between ~-13.5 to -26.50°C, which indicates a primary H_2O-NaCl-KCl system. However, the presence of a CO_2 carbonic phase will characterize Type III inclusions as part of the H_2O-CO_2-NaCl-KCl system.

4.6 ISOCHORES

Fluid inclusion microthermometry revealed that fluid inclusion chemistry is dominated by the H_2O-NaCl-KCl system in Type I and Type II inclusions whereas a less prevalent H_2O-CO_2-NaCl-KCl system in Type III inclusions is only observed in miarolitic cavities. These systems, in conjunction with microthermometric data, were utilized with the *FLUIDS* programs by Bakker (2003) to calculate fluid inclusion isochores for each sample (Figure 4.5), which provide minimum temperature (Th_{total}) and pressure corrected (Tt) estimates of trapped fluids. Minimum pressure estimates (Ph_{total}) were calculated based on minimum fluid inclusion homogenization temperatures and results for each sample are displayed in Appendix 3b.

Based on the main cluster of microthermometric data for a sample and type, each isochore plot displays a range of possible temperatures and pressures existing between *solid lines*. Outlier(s) are represented by *dotted lines*, which represent inclusions that were not consistent with the distribution of Th_{total} data for each sample. Isochores are categorically organized by type of inclusion, location around the HPP and fluid inclusion setting.

4.6.1 Type I and Type II isochores

The H_2O-NaCl-KCl system represents the fluid composition for the whole sample suite, besides miarolitic cavity samples HPP-24 and HPP-113, and is characterized by Type I and Type II fluid inclusions. Type I and II inclusion isochores are characterized respectively by 200°C>Th_{total} and 200°C<Th_{total}. It is evident that Type II inclusions display a shallower isochore slope than Type I inclusions, which is a function of lower density and higher minimum temperatures and pressures of entrapment (Shepherd et al., 1985). For both types, isochores display a moderately consistent and narrow distribution, which is interpreted to imply entrapment at near constant pressure and temperature conditions. However, sample HPP-21 displays three different sets of isochores, which may infer entrapment at different stages in the history of the rock, fluid inclusion recrystallization, post-entrapment deformation, or leakage during microthermometric analysis.

4.6.2 Type III isochores

The H_2O-CO_2-NaCl-KCl system is characterized by Type III inclusions, and was only observed within miarolitic cavities in samples HPP-24 and HPP-113 respectively *within* and *away* from the HPP contact (Figure 4.5). Both samples contain Type II and Type III fluid inclusions, which most likely reflects immiscible fluid phases between CO_2 and vapor within the miarolitic cavity as the HPP was crystallizing. Isochores for Type II and III inclusions in both miarolitic cavity samples intersect (if superposed on top of one another) further suggesting a

coeval temperature and pressure relationship between fluid types. Type II inclusions (HPP-24a, HPP-113a) contain similar Th_{total} estimates and likely represent a later magmatic vapor-rich exsolution phase as the HPP was crystallizing at depth. Type III inclusions display some of the highest Th_{total} values (~240 to 450°C) of all the inclusions, and likely represent CO_2-rich volatile fluids trapped in miarolitic cavities during the HPP intrusion.

4.6.3 Comparison between Types, Location and Setting

It is clear from the isochore plots that no significant variation exists within each fluid type in regards to locality around the HPP, suggesting that fluids were trapped at similar homogeneous trapping conditions. It is evident however, that different settings around the HPP contain distinct fluid types.

Type I: Type B calcite veins (on), Type A calcite veins (away), Skarn WR (S), Phyllic WR, Potassic WR, and Vugs (within). As mentioned above, Skarn WR (S) inclusions represent secondary inclusions in crosscutting trails trapped in quartz/calcite grains in skarn wall rocks, whereas Skarn WR (P) represents isolated, primary inclusions trapped in hydrogrossular/quartz in skarn wall rocks.

Type II: Skarn WR (P), Type B calcite veins (on)-HPP-43, and Type A calcite veins (away)-HPP-100, quartz veins (on), (away), and (within), and miarolitic cavities (on) and (away).

Type III: Miarolitic cavities (on) and (away).

Detailed comparisons between these different subgroups are presented in the following sections.

4.6.4 Pressure correction determination from fluid inclusions

In most fluid inclusion investigations, pressure is not determined from fluid inclusions because most fluid inclusions have trapped at pressures significantly higher than their vapor pressures (Roedder and Bodnar, 1980). Thus, minimum pressure estimates (Ph_{total}) calculated from minimum homogenization temperatures (Th_{total}) using the *FLUIDS* software does not reflect the true pressure trapping conditions. Normally, the pressure is estimated from geological reconstructions in order to provide the depth of cover at the time of trapping (Roedder and Bodnar, 1980). A geological reconstruction of the HPP through stratigraphic studies, plutonic textures, and contact metamorphic conditions by Burton (1997) provide strong evidence that the HPP was emplaced between ~6-12 km depth at pressures between ~1600 to 3200 bars. Therefore, it can be inferred that convecting hydrothermal and exsolved magmatic fluids at the time of the intrusion were presumably trapped at similar depths and pressure ranges. Given this independent estimate of pressure, a geobarometric pressure correction (Tt) was applied to Th_{total}, to constrain actual fluid inclusion trapping temperatures (Roedder and Bodnar, 1980). Tt ranges are displayed within fluid inclusion isochore plots in Figure 4.5 and in Table 4.2, and on average are pressure corrected from 90 to 275°C based on the range of HPP emplacement pressures at depth ~1600 to 3200 bars. Relative temperatures of fluid

entrapment as measured by (Th_{total}) will only be discussed in this chapter whereas pressure corrected temperatures will be considered in chapter 5.

4.7 REGIONAL MICROTHERMOMETRIC VARIATION AROUND THE HPP

More than 200 inclusions were measured in 24 samples *within* the HPP and *on* and *away* from the contact. Histograms, graphs and maps were prepared to illustrate the differences in Tm_{CO_2}, $T_{eutectic}$, $Tm_{clathrate}$, Th_{CO_2}, Th_{total}, and Mass% eq. NaCl of fluid inclusions *within* the HPP and *on* and *away* from the contact. The following sections provide microthermometric results and comparisons from varying perspectives, starting regionally and gradually narrowing down to more specific subgroups. Histograms of Type I, II, and III inclusions and fluid inclusion settings are displayed in Figure 4.6. Th_{total} versus Tm_{ice} and Th_{total} versus $Tm_{clathrate}$ plots are displayed in Figure 4.7. Table 4.1 displays each fluid setting's calculated mode. See Appendix 3C for microthermometric statistical data arranged from each perspective. Note: Tm_{ice} values are analyzed within the Mass% eq. NaCl sections because Tm_{ice} values are used to calculate Mass% eq. NaCl and therefore analogous in meaning.

4.7.1 Total results

$T_{eutectic}$ values for Type I, II, and III fluid inclusions all fall between a range of ~-10 to -30°C, and no distinct value of $T_{eutectic}$ is apparent for any fluid inclusion type. Type I inclusions are normally distributed between ~-16 to -22°C and the mode is -22°C. Type II inclusions are bimodal displaying two groups; one at higher temperatures (-10 to -16°C) and one at lower temperatures (-20 to -24°C). Type

III inclusions (only observed in miarolitic cavities) show a scattered distribution, and no clear $T_{eutectic}$ value is recognizable. A pure H_2O-KCl system has a $T_{eutectic}$ = -10.6°C and a H_2O-NaCl-KCl system has a $T_{eutectic}$ = -23.5°C. Other major cations common within multicomponent fluid systems include $MgCl_2$ and $CaCl_2$, which have respective eutectic temperatures of -33.6°C and -49.5°C. Since measured $T_{eutectic}$ values for all fluid inclusion types fall between -10 to -30°C, and no type displays a unique $T_{eutectic}$, it can be inferred that the major cation in Type I, II, and III fluid inclusions is KCl. Hence, H_2O-NaCl-KCl is the dominant chemical system *within* the HPP and *on* and *away* from the contact. Overall, it is clear that a bimodal distribution exists within all types, with a group at lower temperatures ~-20 to -26°C and another at higher temperatures ~-10 to -18°C. This difference is statistically insignificant suggesting a minor variation in the overall H_2O-NaCl-KCl system.

Mass% eq. NaCl values for all three types are low and are <10% Mass% eq. NaCl. Type I inclusions are broadly bimodal with two sets of data occurring between ~0.5 to 1.5%, and 3 to 6.5%. Type II inclusions are normally distributed around 4 to 4.5%. Type III inclusions are low salinity and are <6%. Corresponding Tm_{ice} values for Type I and II inclusions display a range between ~0 to -6.5°C, and display a similar distribution between 0 to 4.5% Mass% eq. NaCl. Type III inclusions Mass% eq. NaCl were calculated from $Tm_{clathrate}$ measurements and range from 5.5 to 8.5°C (Type III section). Overall, Mass% eq. NaCl for all fluid types around the HPP are low, and are consistent with low

salinity (~<10 wt % eq. NaCl) gold ore related fluid inclusions in many Carlin-type gold deposits (Arehart, 1996).

Th_{total} values for the three types of inclusions are clearly distinct. Type I inclusions <200°C and have a mode between ~150 to 160°C; Type II >200°C and are bimodal with one peak between ~230 to 240°C and another between ~310 to 340°C and; Type III >230°C and are bimodal with one group of data between ~230 to 290°C, and another >440°C. Type III inclusions display some of the highest minimum trapping temperatures recorded in this study (480 to 490°C), which fall near the average temperature window (500 to 800°C) of exsolved volatile phases from a typical crystallizing felsic magma (Kamenetsky et al., 2004). These differences in Th_{total} values between Type I, II, and III inclusions may be related to the difference between magmatic and convecting external fluids during and after intrusion.

The Th_{total} versus Tm_{ice} plot in Figure 4.7A displays the narrow range and distribution of Type I and Type II inclusions measured *within* the HPP and *on away* from the contact. The plot reveals that most Tm_{ice} data is between -5.5 and 0°C and Th_{total} ranges approximately between 125 to 425°C. This plot also confirms the distinct differences in Th_{total} between Type I and II fluid inclusions. The Th_{total} versus $Tm_{clathrate}$ plot in Figure 4.7A for Type III inclusions shows relatively close Th_{total} similarities to Type II inclusions suggesting a possible relationship between fluids.

4.7.2 Comparison of Type I, II, and III inclusions by location

Type I, II, and III fluid inclusions were spatially compared *within* the HPP and *on* and *away* from the contact to determine if different types of fluids existed and whether fluids differed chemically or thermally around the HPP.

$T_{eutectic}$ values for Type I, II, and III inclusions display no major differences *within* the HPP or *on* and *away* from the contact. However, Type III *on* and *away* inclusions do show a distinct statistical scatter. This is likely due to a low number of measurements recorded because of a limited sample population of Type III inclusions.

Mass% eq. NaCl ranges *on, away*, and *within* the contact for Type, I, II, and III inclusions are similar and no major differences exist. Type I inclusions *on and away* display a similar bimodal distribution with one group occurring between ~0 to 2% and another between ~2.5 to 6%. *Within* values are single peaked and occur between 3.5 to 4%. Type II inclusions *on* values display a normal distribution around 4%, and *away* and *within* values are bimodally distributed between 0 to 1.5% and 4 to 7%. Type III inclusions show slightly higher values (>4%) with one sample showing values between ~9 to 9.5%. Corresponding Tm_{ice} values for Type I and II inclusions and $Tm_{clathrate}$ values for Type III inclusions range respectively between 0 to -4.5°C and 5.5 to 8.5°C. Overall, salinity for all categories is low (<10%), and significant variation in salinity between locations is not evident.

Th_{total} values for Type I inclusions *on* the contact dominantly range between ~150 to 200°C. *Away* from the contact values are skewed right and a main peak occurs between ~120 to 130°C. *Within* the contact values display a plateau distribution between ~120 to 190°C (HPP-28V). Type II inclusions are significantly higher in temperature (~>200°C) than Type I inclusions. Type II *on* and *away* values are bimodally distributed between ~200 to 280°C and ~310 to 380°C, and *within* values cluster primarily around ~220 to 240°C, which were measured in a later stage crosscutting quartz vein (HPP-28). Type III inclusions display a distinct separation where it is clear that miarolitic cavities *away* from the contact contain much higher temperature fluid inclusions (>440°C) than inclusions in miarolitic cavities *within* the HPP. What is clear is that there is a marked difference between *on* and *away* Type I inclusions. Type II inclusions *on* the contact are bimodal and some *on* and *away* values appear indistinguishable. Type III inclusions are also bimodal showing the highest trapping temperatures >440°C in a miarolitic cavity *away* from the contact. However, the bimodal distribution is likely due to the low number of measurements recorded.

It is well known in a plutonic environment that the temperature and heat transfer decrease with increased distance away from the center of a pluton. Field evidence around the HPP confirms this. As the distance increases *away* from the HPP contact, the metacarbonate and siliciclastic marine country rocks become less metamorphosed, and less thermally and chemically influenced by the HPP intrusion. This relationship is broadly preserved within the Th_{total} values of Type I inclusions. It is clear that Type I *away* Th_{total} values measured in unaltered

shallow marine carbonates >2 km *away* from the HPP contact are lower than Type I, II, and III inclusions measured *within* the HPP and *on* and near the contact. This is suggested by the different modal distribution of all three fluid types. 1) *Within*: Type I: ~120 to 190°C, Type II: ~220 to 240°C, Type III: ~230 to 290°C; 2) *On:* Type I: ~150 to 200°C; Type II: ~200 to 280°C; 3) *Away:* Type I: ~120 to 130°C; Type II: ~310 to 380°C; Type III: ~440 to 490°C. Quantitatively, this relationship is difficult to express, however in the following section average Th_{total} temperatures around the HPP are displayed visually.

The Th_{total} vs. Tm_{ice} plot for Type I, II, and III inclusions by location in Figure 4.7A confirms the above distributions and ranges. It is evident that Type I and II inclusions contain Tm_{ice}~>-5°C and Type III inclusions have $Tm_{clathrate}$~5 to 9°C, which equates to an overall low Mass% eq. NaCl fluid for all three fluid types. These plots also illustrate the marked Th_{total} difference between Type I and Type II and III inclusions, and the temperature gradient between Type I *away* and the other fluid types. However, an overlap between Type I *on* and Type II and III inclusions is apparent, which may reflect the complexity and variation of fluids around the HPP during and after intrusion.

4.7.3 Settings of fluid inclusions

The data sorted by quartz/calcite veins, altered wall rocks, vugs, and miarolitic cavities *within* the HPP and *on* and *away* from the contact are compared to test whether fluid chemistry varies between different geological settings and locations. A comparison against other subgroups will also provide insight into the

origin and timing of fluids responsible for vein formation and wall rock alteration. Table 4.2 displays consolidated microthermometric measurements for each setting.

The Th_{total} vs. Tm_{ice} plot in Figure 4.7B displays the different fluids analyzed around the HPP. It is evident that there are clear individual clusters or bands of values suggesting distinct conditions of entrapment, however there are considerable overlaps between some clusters. Type II Th_{total} (~>200°C) individual clusters include: Skarn WR (P), quartz veins *on*, *away*, and *within* and Type A calcite veins *away* (HPP-100). Lower Type I Th_{total} (~<200°C) fluid inclusions display major overlap between Type B calcite veins *on*, quartz veins *on*, Vugs *within*, Skarn WR (S), Phyllic WR, and Potassic WR. However, it is apparent that some Type I fluid settings (Phyllic WR and Type B calcite veins *on*) contain some Th_{total} values near or slightly above this threshold. Type III inclusions in miarolitic cavities also display high Th_{total} values, possibly suggesting a similar fluid origin between Type II and Type III inclusions.

4.7.3.1 Quartz veins and vugs

Quartz veins were sampled *within* the HPP and *on* and *away* from the HPP contact. Quartz vugs (HPP-28V) are contained within a later stage crosscutting fault hosted quartz vein (HPP-28) and contain Type I inclusions. All quartz veins, including HPP-28, contain only Type II fluid inclusions.

$\mathbf{T_{eutectic}}$ values for quartz veins *within*, *on* and *away* display no major statistical differences. It is evident however that *on* values are bimodal between high (-10 to

-16°C) and low (-20 to -28°C) values suggesting a slight variation between H_2O-NaCl and H_2O-KCl systems. *Away* values occur at lower values (-22 to -30°C), and *within* values occur between -12 to -14°C and -18 to -20°C. *Vug* values display a narrow distribution at anomalously higher temperatures (-10 to -12°C). Overall, quartz veins *on*, *away*, *within* and quartz vugs display no major statistical differences in $T_{eutectic}$ values and range approximately from -10 to -30°C.

Mass% eq. NaCl of quartz veins *on* display the highest salinity values within the group, and are approximately bimodally distributed primarily between 2.5 to 3%, and 5 to 6.5%. Quartz veins *within* and *away* are lower salinity and range between 0 to 1.5%. Quartz vugs display one pronounced peak between 3.5 to 4%, and an outlier from 1 to 1.5%. Corresponding Tm_{ice} values for all subgroups occur between 0 and -4°C. However, Tm_{ice} *on* values are slightly lower (-2 to -4.5°C) than the other subgroups. Overall, quartz vein values are low salinity (~0 to 7%) and consistent differences between subgroups are not apparent.

Th_{total} values for quartz veins *on* show a bimodal distribution between ~180 to 260°C (HPP-40, HPP-89) and 280 to 450°C (HPP-21, HPP-57, HPP-98). Petrographically, the first group contains inclusions that do not appear as oblate or round as other primary inclusions in quartz veins, but instead are irregular and contain a halo of tiny inclusions suggesting reequilibration of the fluid inclusion after entrapment (Vityk and Bodnar, 1995). HPP-89 also displays abundant secondary trails that crosscut the Type II assemblage inferring a later stage fluid event, which could represent the reequilibration fluid event. Reequilibration of fluid inclusions after entrapment infers that fluid density within the inclusion is not

representative of the initial pressure and temperature conditions. Therefore, HPP-40 and HPP-89 are not included in further discussions.

Quartz veins *away* (HPP-115) overlap *on* values at the higher Th_{total} interval (280 to 450°C), suggesting a similar minimum temperature of entrapment. The later stage, fault hosted hydrothermal quartz vein *within* the HPP (HPP-28) displays a normal distribution between ~220 to 250°C. Quartz vugs (HPP-28V) measured within this later stage crosscutting quartz vein display a low temperature plateau distribution mainly between 140 to 190°C. Overall, quartz *on* and *away* values overlap at higher temperatures, whereas *within* and quartz Vug values overlap at lower homogenization temperatures. Comparatively, quartz veins *on* and *away* display similar temperatures to Skarn WR (P) (310 to 350°), and Type III miarolitic cavity values, which may suggest a synmagmatic origin of fluids. Later stage quartz veins *within* Th_{total} values (~220 to 250°C) are predominantly higher than the Th_{total} values for Type B Calcite veins *on* (~120 to 210°C), Type A Calcite veins *away* (~110 to 180°C), and Potassic WR (~150 to 170°), but only slightly higher than Skarn WR (S) (~180 to 200°C), and Phyllic WR (~180 to 200°C). These later, crosscutting fault-hosted quartz veins observed in faults *within* the HPP may have been formed from lower temperature, convecting fluids after intrusion, or during later Basin and Range extension. *Vug* values are some of the lowest Th_{total} values recorded within this study and since they were observed within the later stage hydrothermal crosscutting quartz veins, they are presumably the product of an open space precipitation of the same or later stage

SiO_2-rich fluid that was responsible for the fault-hosted hydrothermal crosscutting quartz vein (HPP-28).

4.7.3.2 Calcite veins

Calcite veins were sampled *on* and *away* from the HPP contact, and were separated into Type A (*away* from the contact) and Type B (*on* the contact) based on their mineralogical makeup (see section 4.2.3). Type A and B calcite veins generally contained Type I inclusions, however a few samples contained inclusions with higher homogenization temperatures and fv values.

$T_{eutectic}$ values for Type B calcite veins *on* and Type A calcite veins *away* show a narrow distribution approximately between -14 and -24°C, however some higher values occur between -10 to -12°C. It is evident that a major overlap occurs between *on* and *away* values, and the $T_{eutectic}$ ranges suggest a mix between H_2O-NaCl and H_2O-KCl systems.

Mass% eq. NaCl values of Type B calcite veins o*n* are skewed right with the highest peak occurring between 1 to 1.5%. Values for Type A calcite veins *away* are bimodal with two main peaks occurring between 0.5 to 1% and 5.5 to 6%. Corresponding Tm_{ice} Type B calcite vein *on* and Type A calcite vein *away* values range between 0 to 4°C. Type B values clearly display higher values between ~0 and -2°C whereas Type A values occur ~-2.5 to -4°C. Overall, both types of calcite veins are low salinity (0 to 6.5%), and some overlap is apparent at lower values. Higher Mass% eq. NaCl (4.5 to 6%) for some Type A calcite veins *away* may suggest a distant fluid with more dissolved salts.

Th_{total} values for Type B calcite veins *on* show a skewed right distribution with the highest peak occurring between ~130 to 140°C, and most of the values range between 120 to 210°C. Values for Type A calcite veins *away* also show a skewed right distribution with the highest peak occurring between 120 to 130°C, and most of the values range between 110 to 180°C. Some Type A calcite veins *away* values occur at higher temperatures above 320°C (HPP-100). It is clear that both calcite vein types overlap, which may reflect similarities in fluid chemistry and conditions of entrapment. Comparatively against other subgroups, Type B calcite veins *on* and Type A calcite veins *away* display low to intermediate homogenization temperatures and are similar to Quartz Vugs, Skarn WR (S), Phyllic WR, and Potassic WR. Overall, Type B calcite veins *on* and Type A calcite veins *away* contain only Type I inclusions, and primarily have Th_{total} values <200°C besides HPP-100 (away) and HPP-43 (on), which have Th_{total} values >200°C and thus contain Type II inclusions. However, HPP-43 has a Th_{total}~210°C which is near the Type I Th_{total} threshold.

4.7.3.3 Fluids responsible for wall rock metasomatism

Fluids within altered wall rocks were compared to understand if fluids responsible for the different types of wall rock metasomatism are thermally and/or chemically different. Secondary fluid inclusions were measured in skarn, phyllic, and potassic wall rocks and are designated by Skarn WR (S), Phyllic WR, and Potassic WR. These alteration types are characterized by only Type I inclusions. Primary fluid inclusions measured within hydrogrossular and quartz within skarn wall rocks are labeled Skarn WR (P) and contain only Type II inclusions.

$T_{eutectic}$ values for Skarn WR (S), Skarn WR (P), Phyllic WR, and Potassic WR alteration styles show no systematic relationship, and are statistically spread between -10 to -30°C. No distinct range is evident for these alteration styles other than Skarn WR (P), which displays an anomalously high $T_{eutectic}$ range between ~-10 to -16°C. Overall, the measured $T_{eutectic}$ averages and ranges compared to theoretical $T_{eutectic}$ values suggest that fluids responsible for wall rock alteration are primarily composed of H_2O-NaCl-KCl.

Mass% eq. NaCl values for all alteration types are ~<8.5%. Skarn WR (S) values range between approximately between 0.5 to 7.5%, however most values occur between 0.5 to 1.5%. Skarn WR (P) values show one main peak between 4 to 4.5%, and a less distinct one between 5 to 5.5%. Phyllic WR values range between 1.5 to 7%, however most values range between 3 to 7%. Potassic WR values display the highest Mass% eq. NaCl values, displaying a dominant peak between 8 to 8.5%, and slightly lesser ones <6%. Corresponding Tm_{ice} values for all groups range between ~-0.5 to -5.5°C, and no significant difference exist between subgroups besides Potassic WR alteration, which displays one main peak between -5 to -5.5°C. Overall, Mass% eq. NaCl variation between subgroups is statistically insignificant.

In comparison to quartz and calcite veins, Mass% eq. NaCl is similar besides the potassically altered wall rock in sample HPP-40W, which shows a slightly increased Mass% eq. NaCl values.

Th_{total} values are clearly divided between the varying subgroups. Skarn WR (S), Phyllic WR and Potassic WR values are generally <200°C, and Skarn WR (P)> 280°C. Skarn WR (S) and Phyllic WR alteration Th_{total} values range approximately between 180 to 200°C and Potassic WR alteration values display the lowest homogenization temperatures, which range between ~150 to 170°C. Skarn WR (P) values display the highest Th_{total} values, which range between ~310 to 350°C. Comparatively, Skarn WR (S), Phyllic WR and Potassic WR values occur at low to intermediate temperatures (~130 to 200°C), and span closely with those of quartz veins *within*, quartz vugs *within,* and Type B and A calcite veins *on* and *away*. Skarn WR (P) Th_{total} values occur at higher temperatures (~310 to 350°C), which are analogous to Th_{total} values of quartz veins *on* and *away*, and Type III inclusions in miarolitic cavities.

4.7.3.4 Miarolitic cavities

Miarolitic cavities were sampled because they can provide evidence of fluids derived in the magmatic environment, and thus can be a comparative benchmark for fluids derived from a different origin. In both miarolitic cavities found *within* (HPP-24) and locally *away* (HPP-113) from the contact in a granodiorite/monzogranite apophysis of the intrusion, two types of fluid inclusions were observed: Type II inclusions (H_2O-NaCl-KCl system), and Type III inclusions (H_2O-CO_2-NaCl-KCl system). The presence of both these types of inclusions within quartz miarolitic cavities suggest that during the final stages of the HPP crystallization CO_2-rich and water vapor-rich volatiles were exsolved, due to unmixing or immiscibility, and were subsequently trapped as separate

volatile rich fluid phases (Kamenetsky et al., 2004). It is hypothesized that volatile phases exsolved during the last stages of a crystallizing magma may carry a significant amount of ore related elements (e.g. Candela and Holland, 1984; Shinohara, 1994; Webster, 1997; Kamenetsky et al., 1999), and if buoyant may enter hydrothermal systems and be responsible for the formation of a number of hydrothermal related ore deposits including W-Sn, skarns and greisens, pegmatites, and Cu-Mo-Au porphyries (Kamenetsky et al., 2004). Since Type III inclusions are only found in miarolitic cavities only Tm_{CO_2} and Th_{CO_2} values will be discussed. Refer to section 4.5.3 for $T_{eutectic,}$ Th_{total}, $Th_{clathrate}$, and Mass% eq. NaCl data.

Tm_{CO_2} values for Type III inclusions narrowly range between -56.6 to -57.6°C. Using these values in conjunction with graphs from Ridley and Hagemann (1999) produced 0.98 XCO_2, 0.02 CH_4 and 0.95 XCO_2, 0.05 CH_4 for Type III inclusions in miarolitic cavities *within* and *away* respectively. The presence of a carbonic phase within primary fluid inclusions within quartz miarolitic cavities presumably represents trapped CO_2 volatiles released during the final crystallizing stages of the HPP.

Th_{CO_2} values for Type III *within* and Type III *away* range between 27.6 to 31°C. Type III *within* values show a statistical scatter between 28 to 31°C, however the main peak occurs between 30.4 to 30.6°C. Type III *away* values only display one main peak between 27.6 to 26.8°C. Corresponding calculated CO_2 phase densities are intermediate to low and range from ~0.60 to 0.80 g/cc.

4.8 REGIONAL TEMPERATURE VARIATION

As expected in an intrusive environment, the temperature at any time in the intrusion and cooling history will be higher within and near an intrusion and lower as distance increases away from the contact. However, convecting fluid circulation cells involving cool, surface derived fluids active during and after intrusion can also modify the geothermal gradient (e.g. Burnham, 1979; Cathles, 1977). Figure 4.8 displays a weak gradient of average homogenization temperatures broadly preserved *away* from the HPP contact. Discussed below are the Th_{total} averages in respect to locations *within* the HPP and *on* and *away* from the contact.

Within: The 90 to 200°C group is represented by Type I inclusions in quartz Vugs (HPP-28V). The 200 to 300°C group is represented by Type II primary fluids in a major, later stage, crosscutting, fault hosted quartz vein (HPP-28), and by Type II and III primary fluids in a miarolitic cavity (HPP-24).

On: All three temperature ranges exist along the contact. The 90 to 200°C is represented by primary Type I fluids in Type B calcite veins *on* and Type I secondary fluids in Skarn WR (S), Phyllic WR, and Potassic WR. The 200 to 300°C group is represented by one Type B calcite vein *on* (HPP-43) and two quartz vein *on* samples (HPP-40, HPP-89). The >300°C range exist on the eastern side of the contact and is only seen as primary Type II fluid inclusions within quartz veins *on* and in Skarn WR (P).

Away: The 90 to 150°C range dominates as Type I primary fluids in Type A calcite veins *away*. A >300°C anomaly does exist and may reflect proximity to a shallowly buried apophysis of the intrusion. In the contact metamorphosed aureole near the edge of the southern contact, the same temperature ranges discussed in the *on* section are still maintained in quartz veins, altered wall rocks, and miarolitic cavities.

It is clear that there was a wide range of homogenization temperatures *within* the HPP and *on* and *away* from the contact, which may be related to the complexity and variation of fluid types, and convection history around the intrusive center.

4.9 CARBON AND OXYGEN STABLE ISOTOPE GEOCHEMISTRY

$\delta^{18}O$ (‰ SMOW) and $\delta^{13}C$ (‰ VPDB) data for calcite veins, skarn, and unaltered wall rocks *on* and *away* from the HPP contact were recalculated in order to determine coexisting water and CO_2 compositions (Figure 4.9). Fields of regional fluids adapted from Hofstra and Cline (2000) are shown in order to geochemically fingerprint the origin of fluids circulating around the HPP during and after intrusion. Raw carbon and oxygen stable isotope data is displayed in Appendix 4.

Ten samples were selected for carbon and oxygen isotope analyses; 5 *away* from the HPP contact metamorphic aureole and 5 *on* the HPP contact. Samples were taken from calcite veins and their adjacent wall rocks: 5 Type B calcite veins *on*, 5 Type A calcite veins *away*, 5 Skarn WR *on*, and 4 unaltered wall rocks *away* (wall rock to HPP-107 was not sampled). Duplicate samples from each category are also displayed (Table 4.2). For each sample, a recalculation of

$\delta^{18}O$ and $\delta^{13}C$ was performed using fractionization factors between CO_2 and calcite over a temperature range of 273 to 4000 K and pressure range of 1 to 13 kb in order to correct for carbon and oxygen isotope fractionization between calcite and aqueous CO_2 (Chacko et al., 1991). Average pressure corrected (Tt) temperatures measured in each calcite vein were used for recalculations (see chapter 5). For skarn wall rocks *on* the contact a temperature ~587.50°C was used for recalculations, which is the Tt average of primary fluid inclusions in quartz/hydrogrossular in skarn wall rock sample HPP-16. For unaltered wall rocks *away* from the contact a Tt~ 365°C was used for recalculations, which is the average Tt of primary inclusions in the unaltered wall rock in sample HPP-78. Recalculated carbon and oxygen isotope data is displayed in Table 4.2.

4.9.1 Carbon and oxygen stable isotope data

Table 4.2 displays the recalculated $\delta^{18}O$ and $\delta^{13}C$ values for each sample and the corresponding theoretical fields (boxes) they are associated with (Figure 4.9). It is evident that the carbon and oxygen data display a large variation, especially in $\delta^{18}O$ values, which suggest a variety or mixture in fluid origins (meteoric, magmatic, connate). For clarity, meteoric waters are surface derived fluids, magmatic waters (carbonatite box) are primary juvenile fluids exsolved from a cooling magma during crystallization processes, and connate waters (Limestone (L.S.)/calcite in carbonaceous shale boxes) are interstitial pore fluids, likely in isotopic equilibrium with the surrounding rock. The *skarn* box has shifted right of the *carbonatite* box to slightly higher $\delta^{18}O$ values due to interaction between magmatic waters and unaltered limestones/calcite in carbonaceous shale. The

ore fluid region, after Hofstra and Cline (2000), represents the general range of carbon and isotope data measured in ore stage calcite veins in Carlin-type deposits. Note that the *ore fluid* region trends towards the *Mid-Tertiary Meteoric Water* box, which is interpreted by Hofstra and Cline (2000) to represent that ore stage fluids in calcite veins experienced mixing between *Mid-Tertiary Meteoric Water* and connate water in unaltered limestones. An interpretation of fluid origin(s) will be discussed in chapter 5.

4.9.1.1 Skarn wall rock on

Skarn WR *on* samples were taken from skarn wall rocks *on* the HPP contact and display a $\delta^{18}O$ average of 8.63‰ and a range from 2.30 to 14.66‰. $\delta^{13}C$ values average -0.75‰ and range from 1.36 to 3.45‰. Some of the $\delta^{18}O$ and $\delta^{13}C$ data linearly trends towards the *carbonatite* and *skarn* boxes, which may suggest a possible relationship with magmatic fluids. However, some data points fall within the *ore fluid* region inferring a possible linkage to fluids in Carlin-type ore deposits and/or meteoric water input.

4.9.1.2 Type B calcite veins on

Type B calcite veins *on* the contact contain a $\delta^{18}O$ average of 13.89‰ and values range widely between 1.09 to 25.85‰. $\delta^{13}C$ values average 0.60‰ and range between -2.17 to 2.16‰. The $\delta^{18}O$ and $\delta^{13}C$ data show some variability where it is clear that two samples are near the *carbonatite/skarn* boxes, two samples are within the *ore fluid* region, and two samples within the *L.S.* box. The variability in data may suggest a complex history of fluid mixing between end

member fluid components either between i) connate fluids in unaltered limestones and magmatic waters or ii) connate fluids in unaltered limestones and *Mid-Tertiary Meteoric Waters*.

4.9.1.3 Unaltered wall rock away

Unaltered shallow marine sedimentary wall rocks *away* from the HPP contact display one main group within the *L.S.* box that has an average $\delta^{18}O$ of 27.01‰ and range between 25.08 to 29.02‰. $\delta^{13}C$ values average 2.81‰ and range between 2.39 to 3.80‰. These values are typical of connate waters in unaltered limestones. Sample HPP-105 (not included in the above statistical data) clearly occurs away from the main data set near the *ore fluid box*, and contains a $\delta^{18}O$ of 6.23‰ and a $\delta^{13}C$ of 2.14‰ indicating fluid mixing with meteoric waters.

4.9.1.4 Type A calcite veins away

Figure 4.9 shows two scenarios of Type A calcite veins *away* data; i) Non-filled squares representing recalculated carbon and oxygen isotope values recalculated using Th_{total} values and; ii) Filled squares representing carbon and oxygen isotope values recalculated using Tt values. Since Type A calcite veins *away* occur >2 km *away* from the pluton-wall rock contact pressure corrected Tt values may not be applicable to this setting. The line connecting these two scenarios represents the range of carbon and oxygen isotope values each Type A calcite vein *away* sample could contain. Unaltered wall rocks *away* did not show appreciable change in recalculated $\delta^{18}O$ and $\delta^{13}C$ when using Th_{total} values; therefore only recalculated $\delta^{18}O$ and $\delta^{13}C$ for Tt values will be shown.

Ranges are shown in Table 4.2. Data reporting for Type A calcite veins *away* will refer to the average $\delta^{18}O$ and $\delta^{13}C$ between both scenarios.

Type A calcite veins *away* display: i) A group within the *L.S.* box (HPP-100, HPP-103, HPP-78), which yields a recalculated average $\delta^{18}O$ of 29.49‰ and range between 24.32 to 31.34‰, and a recalculated $\delta^{13}C$ average of 0.77‰ and range between -4.07 to 2.40‰. The variation in this group's $\delta^{18}O$ and $\delta^{13}C$ values are minimal and most values plot within the *L.S.* box indicating that fluids responsible for these calcite veins are of connate origin. ii) The second group (HPP-105, HPP-107), yields a recalculated $\delta^{18}O$ average of 6.94‰ and range from 3.12 to 10.66‰, and a recalculated $\delta^{13}C$ average of -1.32‰ and range from -3.99 to 1.13‰. This group displays a $\delta^{18}O$ and $\delta^{13}C$ range from the *carbonatite*/skarn boxes to the *ore fluid* region.

Table 4.1: Modes of fluid inclusion microthermometric data for types of inclusions and fluid inclusion settings

Subgroup	Type	Tm_{CO_2}	$T_{eutectic}$	Tm_{ice}	Tm_{clath}	Th_{CO_2}	Th_{total}	Tt (low)	Tt (high)	Tt (avg.)	Mass% eq. NaCl	Ph_{total} (bars)	Density (g/cc)	XCO_2	XCH_4	VCAR
Type I			-21.6	-0.8			158.2	245.6	380.3	312.9	1.0	5.4	0.92			
Type II			-21.0	-1.8			312.6	391.4	591.4	491.4	3.1	203.8	0.57			
Type III		-56.7	-23.8		8.1	30.4	238.8	447.5	652.5	550.0	4.1	628.6	0.80	0.99	0.01	94.00
Type I (on)			-21.6	-0.7			158.2	243.5	396.0	319.8	1.2	5.4	0.92			
Type I (away)			-19.2	-0.8			126.8	201.7	345.8	273.8	1.0	4.5	0.95			
Type I (within)			-19.2	-0.8			126.8	200.0	360.0	280.0	1.0	4.5	0.95			
Type II (on)			-21.0	-2.4			312.6	275.0	800.0	537.5	3.4	203.8	0.57			
Type II (away)			-23.5	-2.6			258.6	430.0	602.5	516.3	4.3	41.8	0.83			
Type II (within)			-10.8	-0.6			231.6	340.0	470.0	405.0	1.1	24.9	0.78			
Type III (within)		-56.7	-23.8		8.1	30.4	238.8	355.0	505.0	430.0	4.1	628.6	0.80	0.99	0.01	94.00
Type III (away)		-57.5	-13.6		7.6	27.6	465.0	540.0	800.0	670.0	6.0	1008.7	0.58	0.95	0.05	80.00
Quartz vein (on)	Type II		-21.0	-2.0			372.5	360.0	572.0	466.0	3.4	203.8	0.57			
Quartz vein (away)	Type II		-29.0	-0.8			340.0	510.0	705.0	607.5	1.4	101.0	0.68			
Quartz vein (within)	Type II		-10.8	-0.6			231.6	325.0	480.0	402.5	1.1	24.9	0.83			
Quartz vugs (within)	Type I		-11.0	-2.1			153.1	200.0	360.0	280.0	3.5	5.7	0.94			
Type B Calcite veins (on)	Type I		-21.6	-0.7			158.2	235.0	388.0	311.5	1.2	5.4	0.92			
Type A Calcite veins (away)	Type I		-19.2	-3.4			126.5	197.5	340.0	268.8	1.0	4.5	0.95			
Skarn WR (S)	Type I		-13.5	-0.6			185.0	253.3	401.7	327.5	1.0	9.6	0.91			
Skarn WR (P)	Type II		-14.6	-2.6			312.6	465.0	710.0	587.5	4.3	116.3	0.72			
Phyllic WR	Type I		-24.1	-1.5			178.8	261.7	426.7	344.2	2.6	7.9	0.92			
Potassic WR	Type I		-11.2	-5.2			168.5	205.0	350.0	277.5	8.1	6.4	0.96			
Miarolitic Cavity (within)	Type III	-56.7	-23.8		8.1	30.4	238.8	355.0	505.0	430.0	4.1	628.6	0.80	0.99	0.01	94.00
Miarolitic Cavity (away)	Type III	-57.5	-13.6		7.6	27.6	465.0	540.0	800.0	670.0	6.0	1008.7	0.58	0.95	0.05	80.00

Table 4.2: Carbon and oxygen stable isotope results. Note samples ending in ".1" are duplicate test samples

Sample	Type	Adjusted $\delta^{13}C$ (‰ VPDB)	Adjusted $\delta^{18}O$ (‰ SMOW)	Regional Fluid Box (fluid type)
HPP-78	Type A Calcite vein (away)	-4.07 to 0.32	29.36 to 31.34	Calcite in Carbonaceous shale to L.S. (connate)
HPP-100	Type A Calcite vein (away)	2.28 to 2.40	24.32 to 27.45	L.S. (connate)
HPP-103	Type A Calcite vein (away)	-0.88 to 1.86	27.78 to 30.01	L.S. (connate)
HPP-103.1	Type A Calcite vein (away)	-0.77 to 1.97	27.45 to 29.68	L.S. (connate)
HPP-105	Type A Calcite vein (away)	-2.89 to 1.13	3.12 to 5.13	Carbonatite (magmatic-connate) to Ore Fluid (mixture: meteoric-connate)
HPP-107	Type A Calcite vein (away)	-3.99 to 0.49	8.87 to 10.66	Carbonatite (magmatic-connate) to Ore Fluid (mixture: meteoric-connate)
HPP-18	Type B Calcite vein (on)	-2.17	13.97	Mixture (magmatic-connate)
HPP-33	Type B Calcite vein (on)	1.97	25.41	L.S. (connate)
HPP-33.1	Type B Calcite vein (on)	2.16	25.85	L.S. (connate)
HPP-42	Type B Calcite vein (on)	-0.90	11.59	Mixture (magmatic-connate or meteoric-connate)
HPP-43	Type B Calcite vein (on)	1.48	1.09	Ore Fluid (mixture: meteoric-connate)
HPP-61	Type B Calcite vein (on)	1.09	5.43	Ore Fluid (mixture: meteoric-connate)
HPP-78	Unaltered WR (away)	3.80	28.62	L.S. (connate)
HPP-100	Unaltered WR (away)	2.53	29.02	L.S. (connate)
HPP-103	Unaltered WR (away)	2.39	25.08	L.S. (connate)
HPP-103.1	Unaltered WR (away)	2.53	25.31	L.S. (connate)
HPP-105	Unaltered WR (away)	2.14	6.23	Ore Fluid (mixture: meteoric-connate)
HPP-16	Skarn WR (on)	-0.75	10.48	Mixture (magmatic-connate or meteoric-connate)
HPP-33	Skarn WR (on)	3.39	2.36	Ore Fluid (mixture: meteoric-connate)
HPP-33.1	Skarn WR (on)	3.45	2.30	Ore Fluid (mixture: meteoric-connate)
HPP-42	Skarn WR (on)	-0.56	8.61	Mixture (magmatic-connate or meteoric-connate)
HPP-43	Skarn WR (on)	1.79	14.66	Mixture (magmatic-connate or meteoric-connate)
HPP-61	Skarn WR (on)	0.84	13.36	Mixture (magmatic-connate or meteoric-connate)

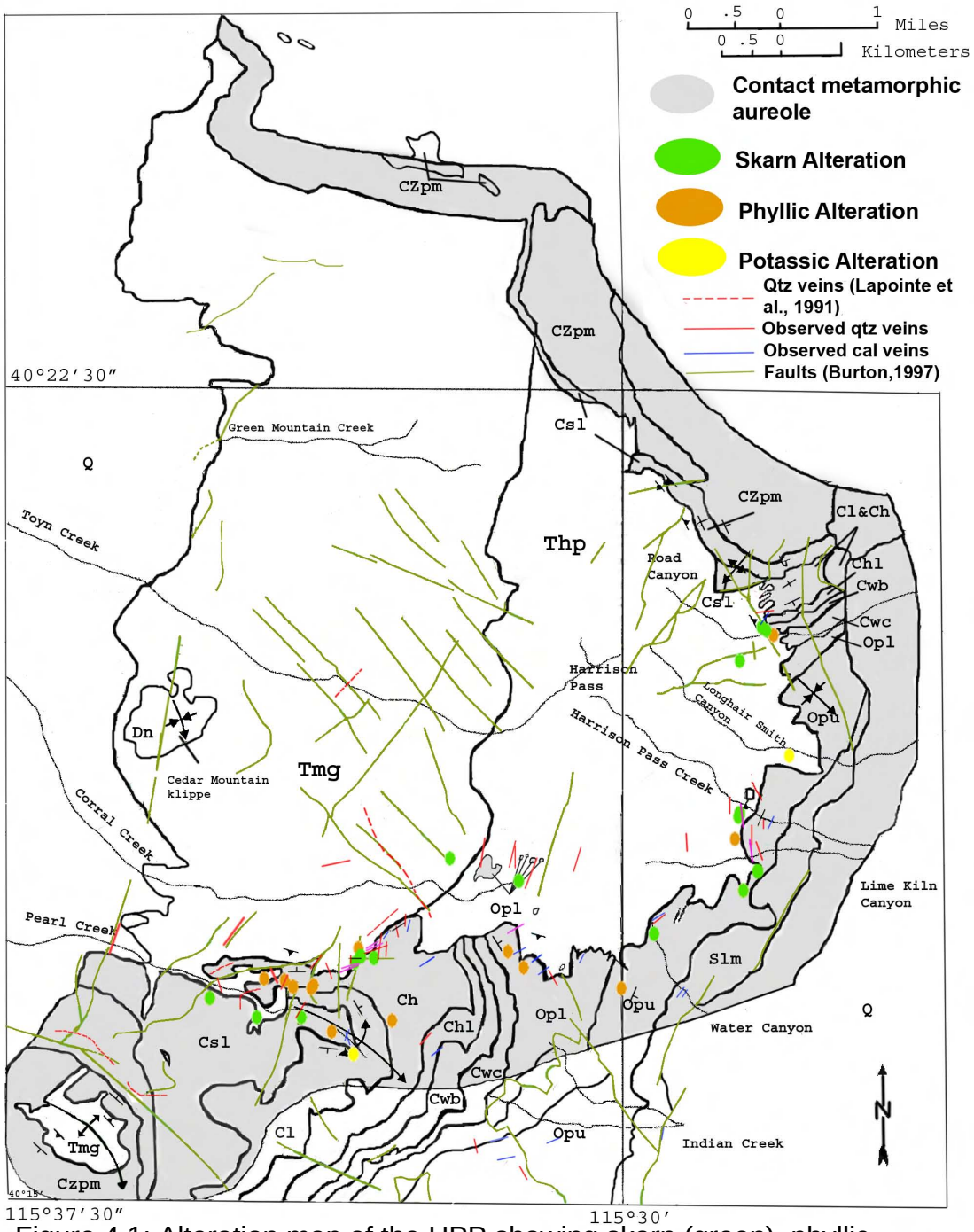

Figure 4.1: Alteration map of the HPP showing skarn (green), phyllic (orange) and potassic (yellow) alteration styles. Observed quartz/calcite veins and previously mapped quartz veins and faults are also displayed. Map adapted from Burton (1997).

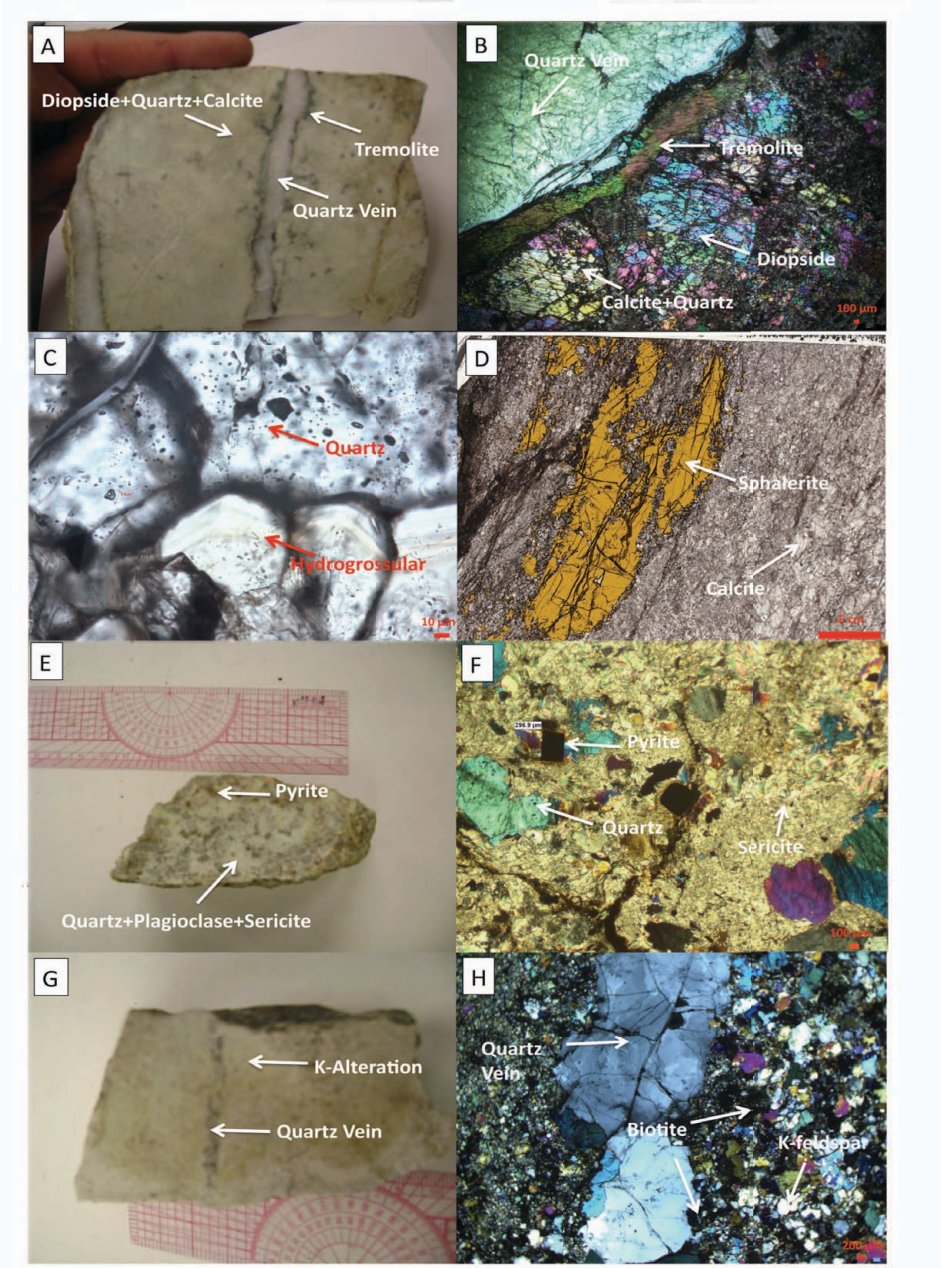

Figure 4.2: Photographs and photomicrographs showing A) Skarn alteration in HPP-59, displaying tremolite to diopside+calcite+quartz mineral progression away from a crosscutting quartz vein (finger for scale ~9.5 cm). B) Tremolite-diopside mineral progression in sample HPP-59. Notice the sharp contact between tremolite and diopside+quartz+calcite C) Euhedral hydrogrossular in HPP-16, a skarn altered WR, displaying characteristic chemical zoning. D) Coarse-grained sphalerite vein in HPP-61 crosscutting a calc-silicate wallrock. E) Phyllic alteration in HPP-52, a granodiorite *on* the HPP contact (15 cm ruler). F) Phyllic alteration in HPP-52, showing classic QSP mineralization. G) Potassic alteration in hand sample (HPP-40). H) Same sample (HPP-40), showing secondary potassic minerals, which includes patchy, dark brown biotite, and subhedral, granular, K-feldspar.

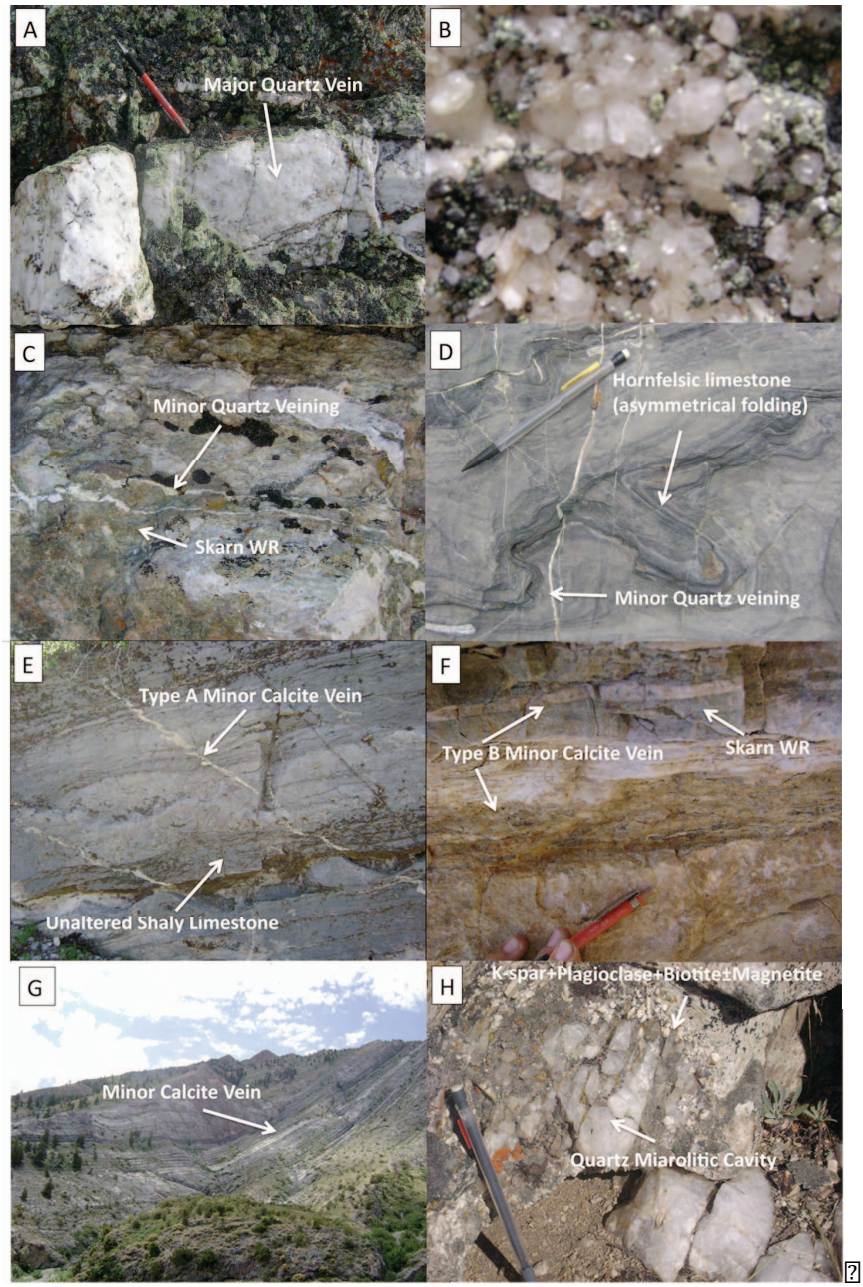

Figure 4.3: Photographs of A) Major, late stage, HQV (HPP-28) crosscutting granodiorite *within* the HPP (Pencil= 13.5 cm). B) Quartz vugs in sample HPP-28 *within* the HPP. C) Irregular, sub-parallel minor quartz veining crosscutting a skarn wall rock *on* the HPP contact within the Opu Fm (HPP-92). D) Minor quartz veining crosscutting hornfelsic limestone *away* from the HPP contact. E) Type A sigmoidal and sheeted minor calcite veining obtusely cutting limestone wall rock *away* from the HPP contact. F) Type B calcite veins *on* the contact crosscutting a skarn wall rock. G) Large (15 to 20 cm), sheeted, Type A minor calcite veins *away* from the contact within the Opu Fm. (HPP-107). H) Miarolitic quartz cavity in a granodiorite wall rock apophysis *away* from the contact (HPP-113). Magnetite cones+K-feldspar+plagioclase+ quartz were observed growing inwards towards the miarolitic cavity.

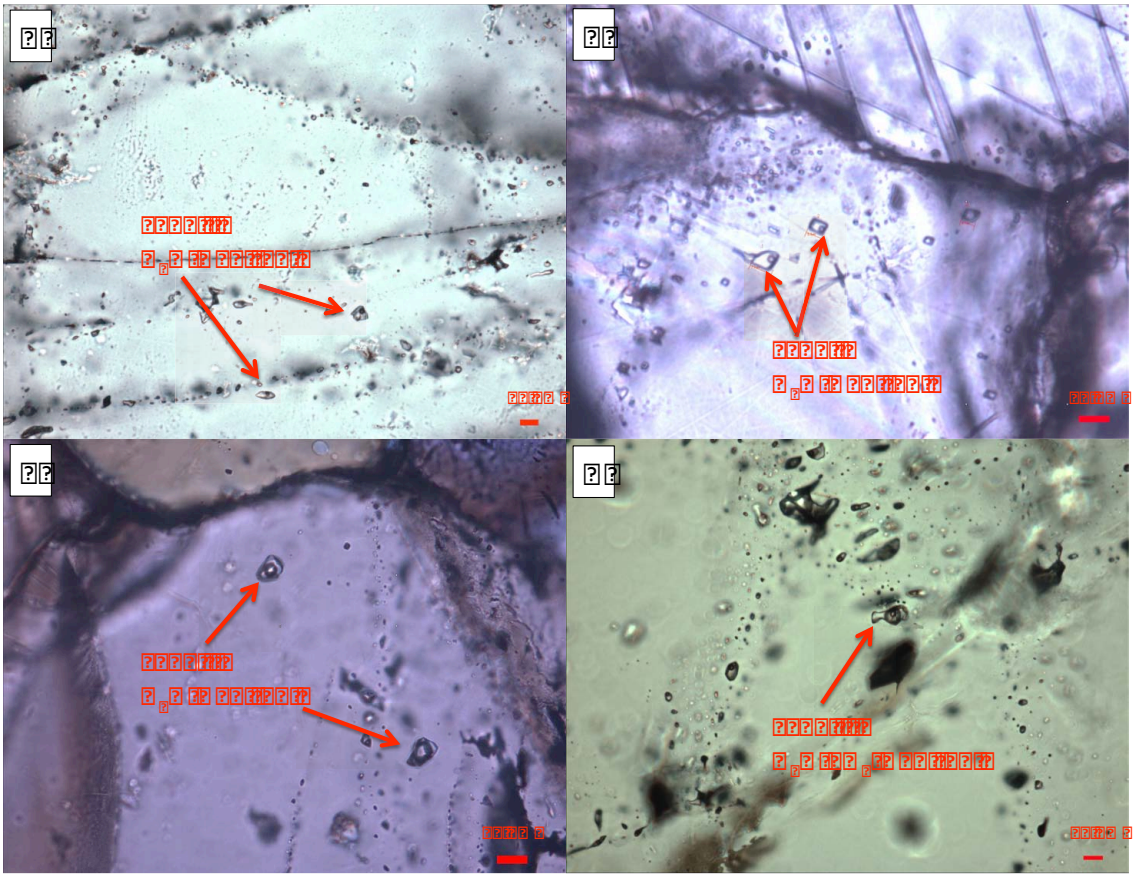

Figure 4.4: Photomicrographs at room temperature of typical A) Type I, H_2O-NaCl-KCl secondary inclusions in a quartz grain. Notice the secondary fluid inclusions crosscutting the quartz grain (HPP-14: quartz vein *within*). B) Type I, H_2O-NaCl-KCl, primary inclusions in a host calcite grain (HPP-42: Type B calcite vein *on*). C) Type II, H_2O-NaCl-KCl, vapor rich, primary inclusions in a host quartz grain (HPP-115: quartz vein *away*). D) Type III, H_2O-CO_2-NaCl-KCl, primary inclusion in a quartz grain in a miarolitic cavity *within* the contact (HPP-24).

Type I (on)

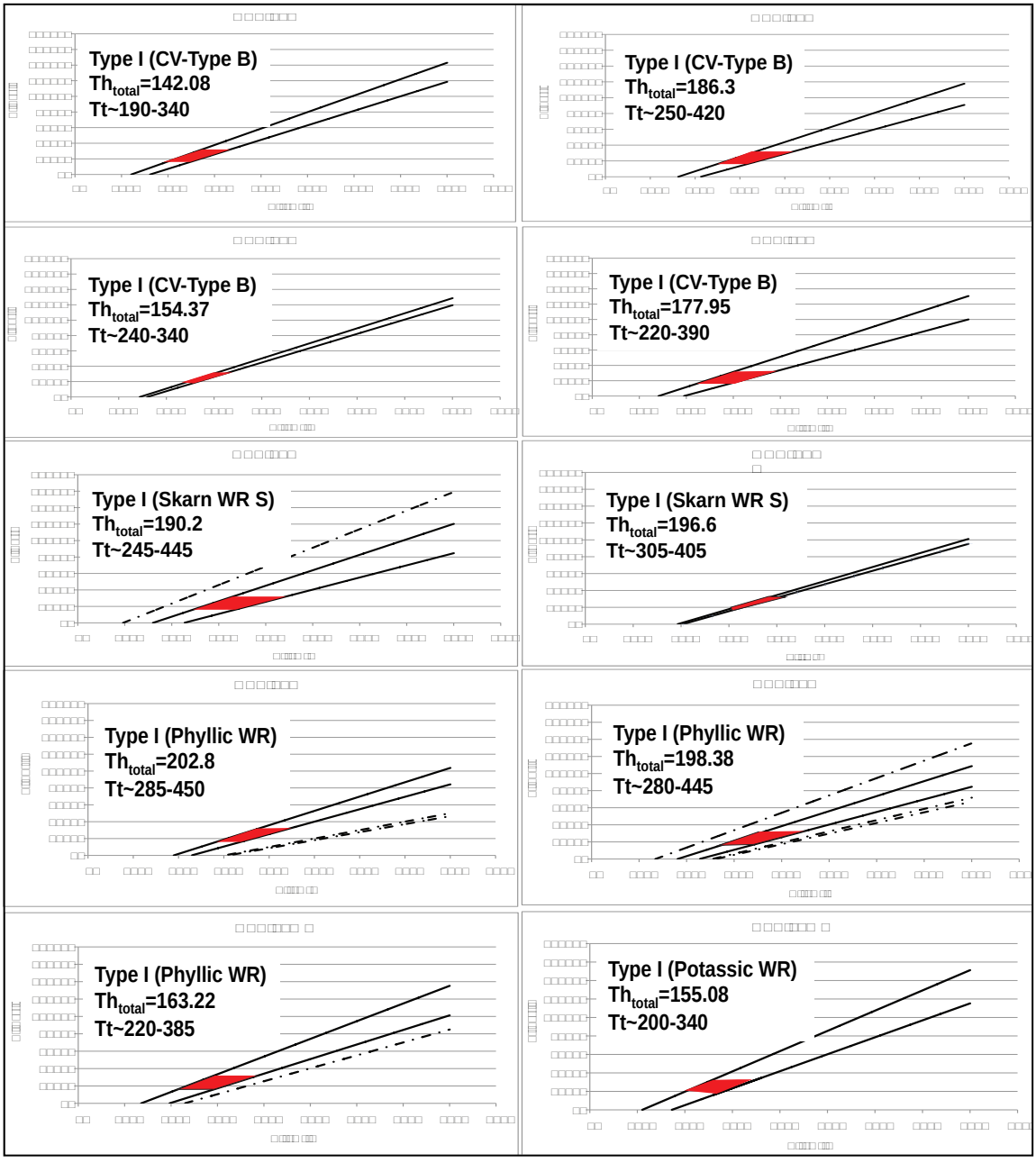
Type I (CV-Type B)
Th$_{total}$=142.08
Tt~190-340
Type I (CV-Type B)
Th$_{total}$=186.3
Tt~250-420
Type I (CV-Type B)
Th$_{total}$=154.37
Tt~240-340
Type I (CV-Type B)
Th$_{total}$=177.95
Tt~220-390
Type I (Skarn WR S)
Th$_{total}$=190.2
Tt~245-445
Type I (Skarn WR S)
Th$_{total}$=196.6
Tt~305-405
Type I (Phyllic WR)
Th$_{total}$=202.8
Tt~285-450
Type I (Phyllic WR)
Th$_{total}$=198.38
Tt~280-445
Type I (Phyllic WR)
Th$_{total}$=163.22
Tt~220-385
Type I (Potassic WR)
Th$_{total}$=155.08
Tt~200-340

Type I (away)

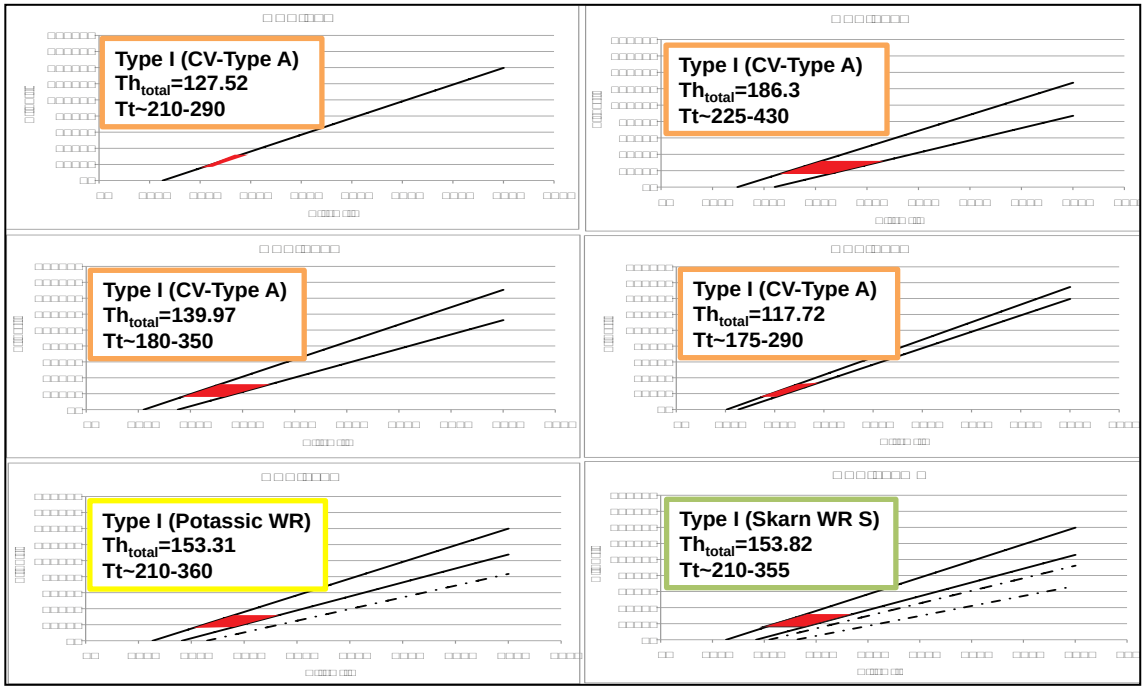

Type I (within)

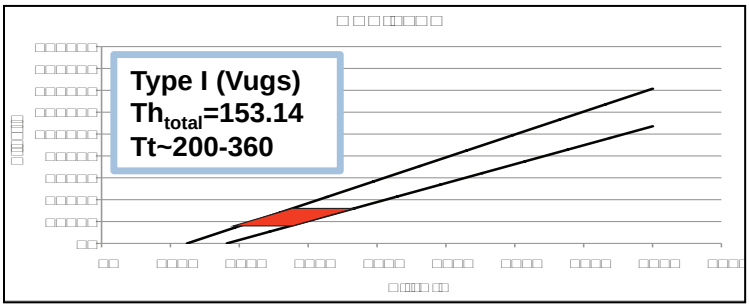

Type II (on)

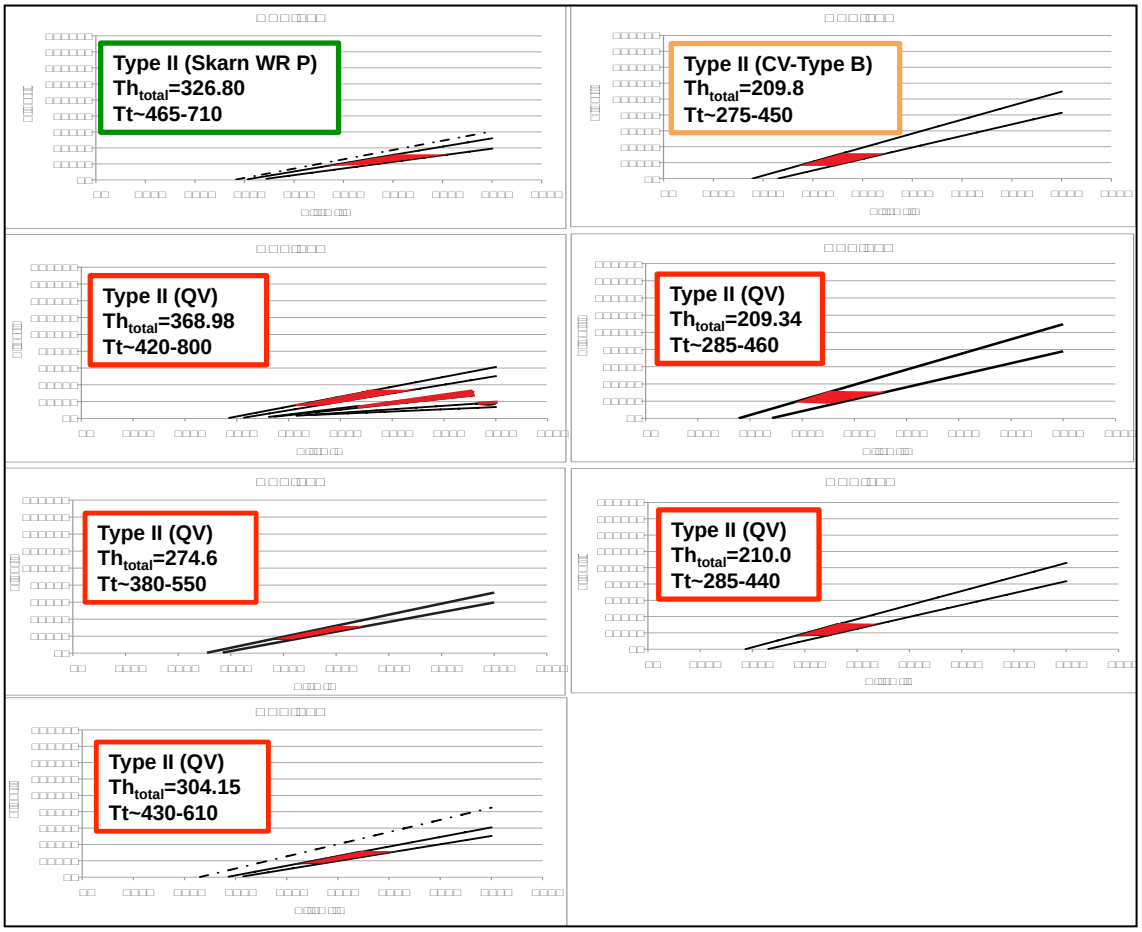

Type II (away)

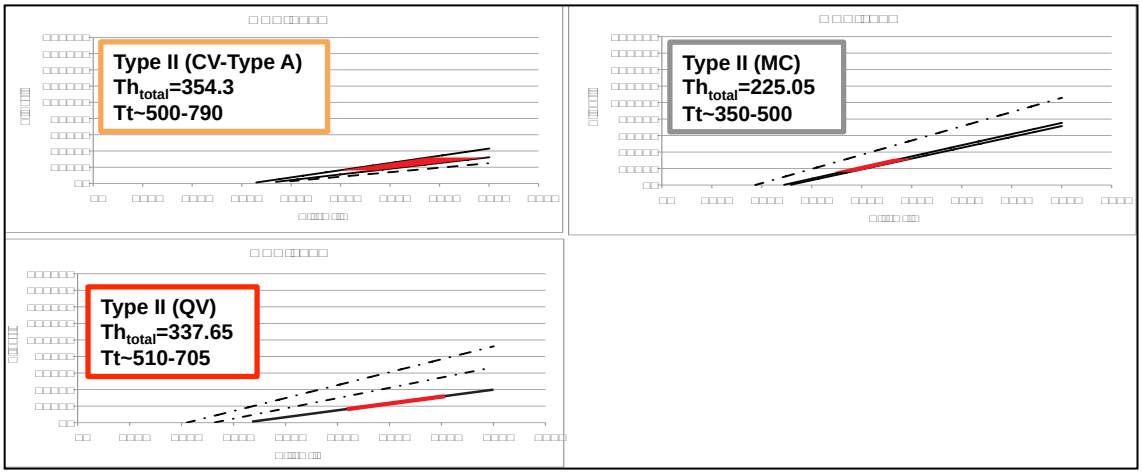

Type II (within)

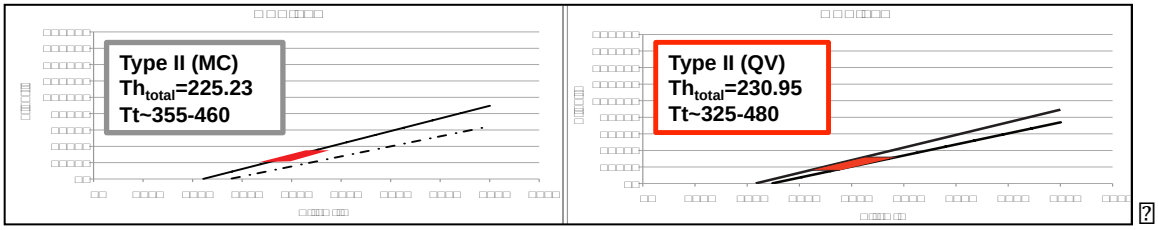

Type III (within) **Type III (away)**

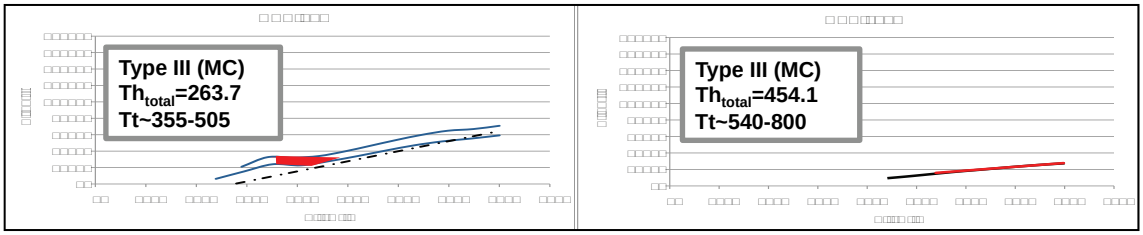

Figure 4.5: Isochore plots of Type I, Type II and Type III fluid inclusions *within* the HPP and *on* and *away* from the contact. Type I: H_2O-NaCl-KCl; Th_{total}~90 to 200°C, Type II: H_2O-NaCl-KCl; Th_{total}~ 200 to 445°C, and Type III: H_2O-CO_2-NaCl-KCl; Th_{total}~240 to 480°C. These homogenization temperature differences are reflected in the isochore slopes. Dashed lines represent measured fluid inclusions that are not consistent with other fluid inclusions measured within the same sample and are considered outliers. Isochore plots also display colored boxes around minimum homogenization (Th_{total}) and pressure corrected values (Tt). These colored boxes represent various fluid inclusion settings; red: Quartz veins; dark green: Skarn WR (P); orange: Calcite veins; brown: Phyllic WR; yellow: Potassic WR; light green: Skarn WR (S); grey: Miarolitic cavities; light blue: Quartz vugs. All isochore plots for each *inclusion type* display similar isochore slopes and narrow temperature and pressure ranges indicating homogeneous conditions during fluid entrapment besides HPP-24 (see text). Note: CV = Calcite Vein, MC = Miarolitic Cavity, QV = Quartz Vein.

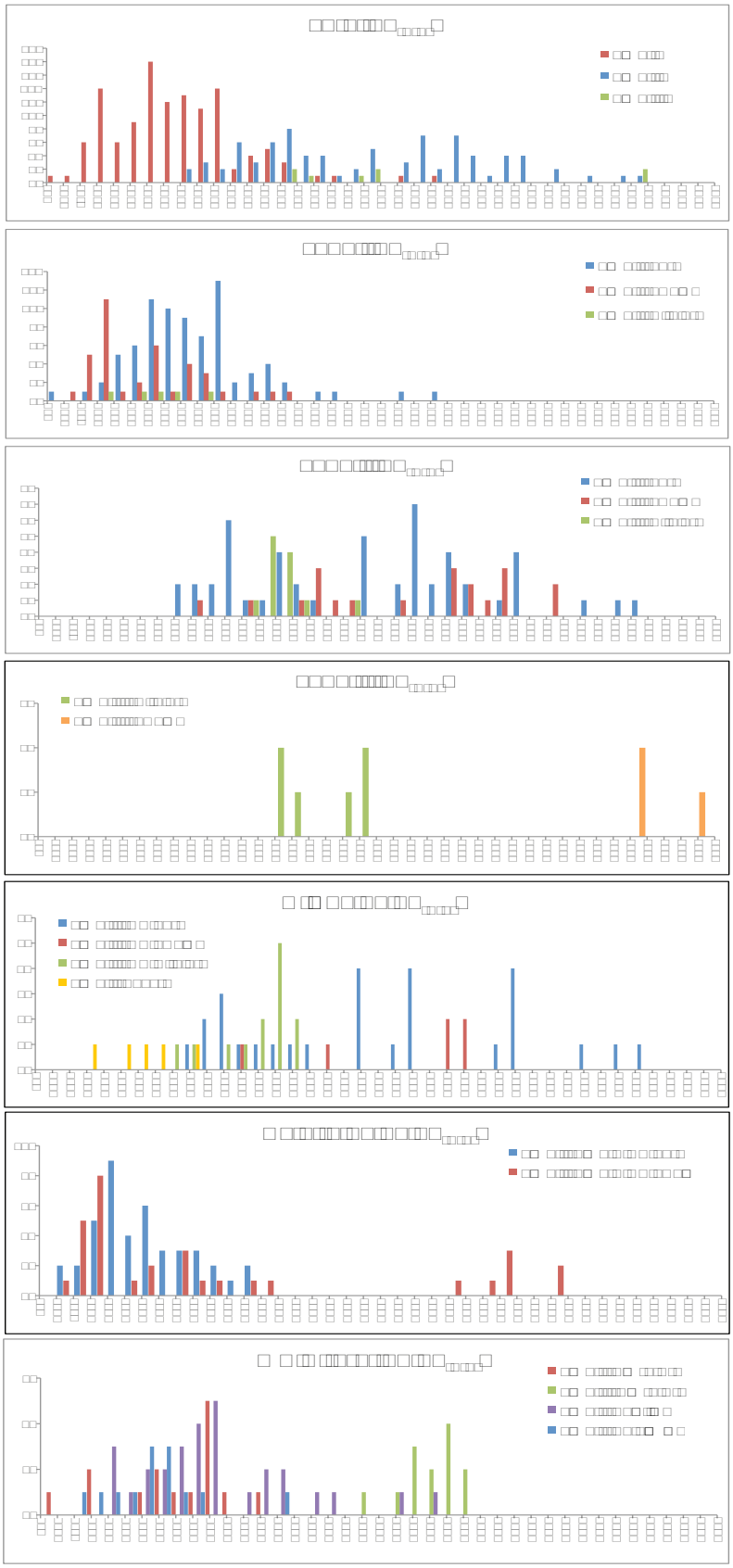

Figure 4.6: Histogram plots of fluid inclusion microthermometric results classified by: *Total Data, Inclusion Type, Quartz Veins, Calcite Veins,* and *Wall Rock Alteration*. Groups are further subdivided by location (within, on, away). Miarolitic cavities are represented by Type III inclusions. Note that the type of inclusion for each setting is listed first in the key description.

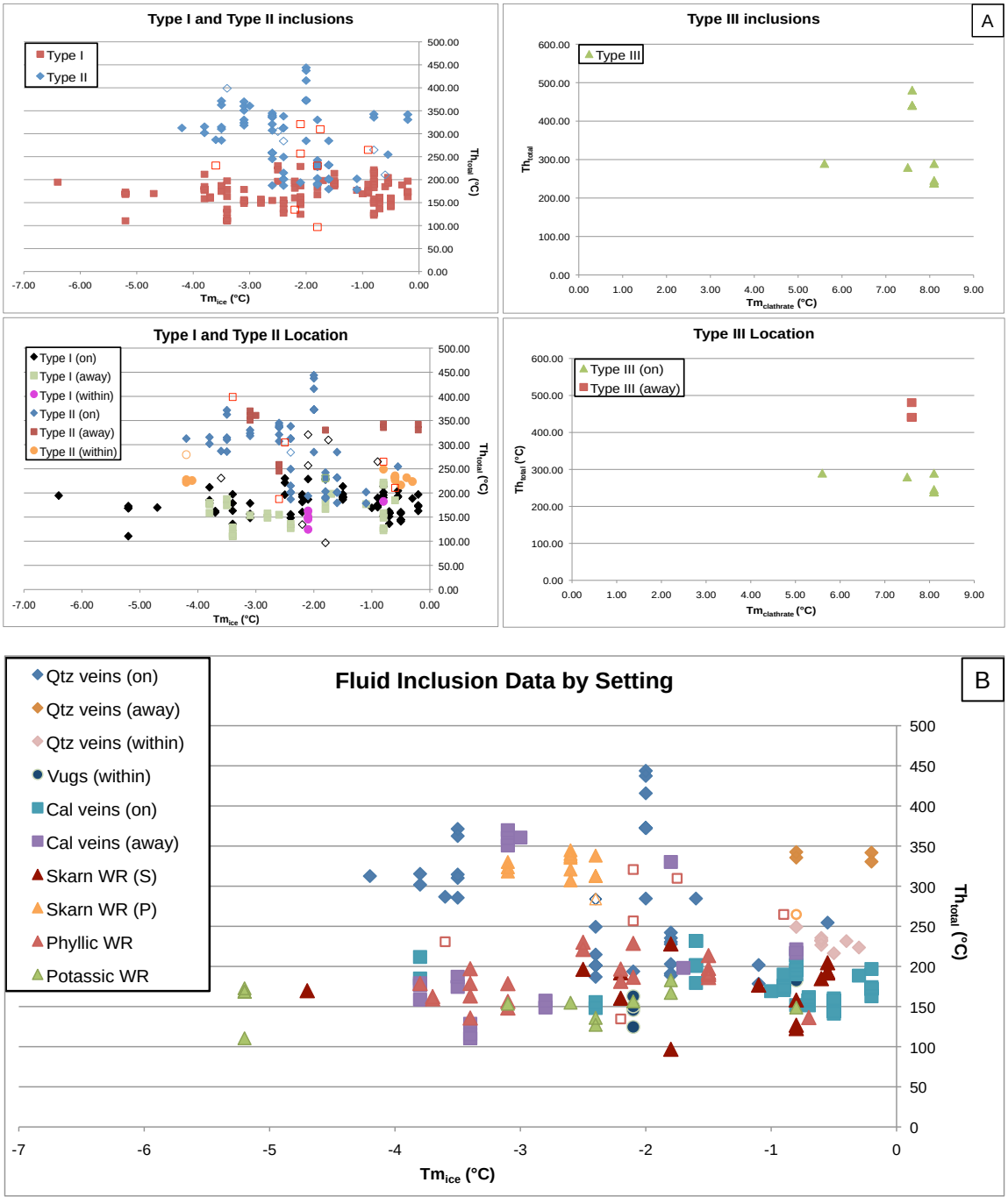

Figure 4.7: Th_{total} vs. Tm_{ice} ($Tm_{clathrate}$ for Type III inclusions) plots for fluid inclusion types (A) and fluid inclusion settings (B). It is evident that a marked separation occurs ~200°C, which is the transition from Type I inclusions to Type II and III inclusions. Note that open filled polygons represent outliers determined from fluid inclusion isochore plots.

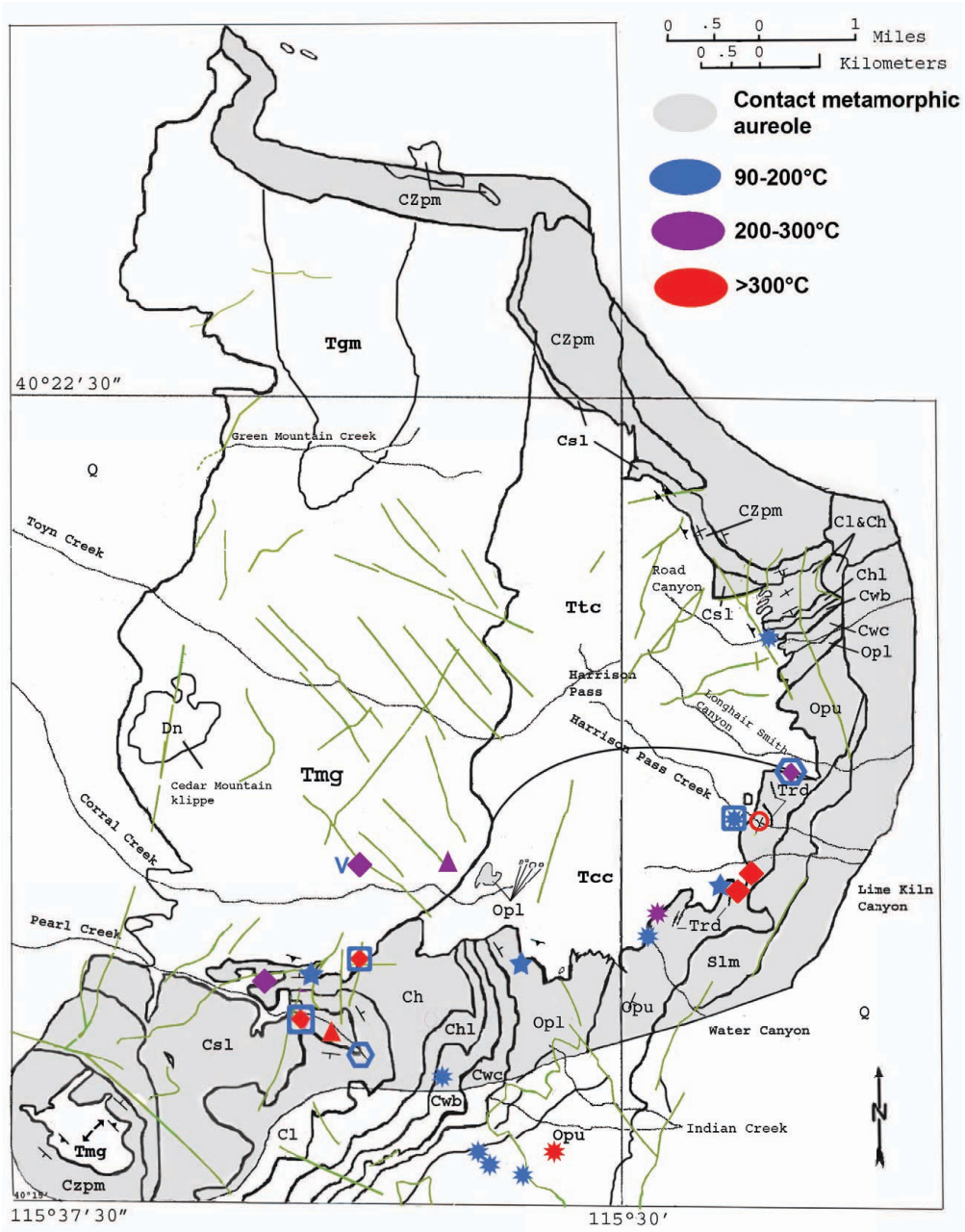

Figure 4.8: Map showing the distribution of average Th_{total} values around the HPP. It is clear that a complex fluid history exist *within* the HPP and *on* and *away* from the contact suggested by a variation in fluid inclusion homogenization temperatures. Type I fluid inclusions are represented by the 90 to 200°C group, which include calcite veins (asterisk); quartz vugs (V), Skarn WR (S) (square), Phyllic WR (star), and Potassic WR (hexagon). Type II inclusions are represented by both 200 to 300°C and >300°C groups and consist of quartz veins (diamond), one calcite vein (HPP-43), and Skarn WR (P) (open circle). Type III inclusions consist of both 200 to 300°C and >300°C groups and are only found in miarolitic cavities (triangle). It is also clear that most quartz veins are >300°C, and a temperature gradient is broadly preserved away from the contact.

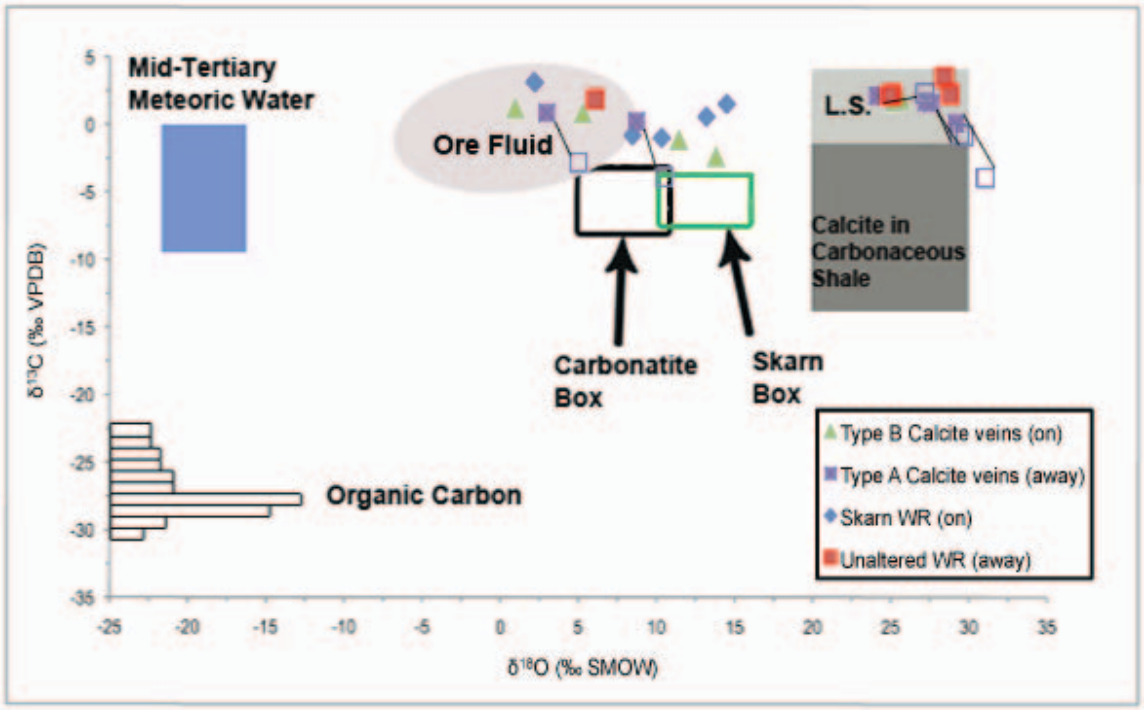

Figure 4.9: $\delta^{13}C$ versus $\delta^{18}O$ plot of fluids in equilibrium with Type B calcite veins *on*, Type A calcite veins *away*, Skarn WR *on*, and unaltered metasedimentary wall rocks *away*. Theoretical fluid field boxes include: c*arbonatite* (magmatic waters)*, skarn* (magmatic waters interacted with limestone), *L.S./calcite in carbonaceous shale* (connate waters*), and Mid-Tertiary Meteoric Water* (meteoric). The *Ore Fluid* region, from Hofstra and Cline (2000), represents the carbon and oxygen isotope composition of fluids measured in late stage calcite veins in Carlin-type gold deposits. Note its position represents a mixed origin between meteoric and connate fluids. Organic matter compositions are shown for reference. Distinct clusters are evident within certain fluid fields, however a general linear trend extends from the *L.S.* box to the *Mid-Tertiary Meteoric Water* box indicating fluid mixing, most likely from a meteoric source. However, a magmatic source could be interpreted for some Type B calcite veins *on* the contact and Skarn WR *on* values due to their positioning and trend towards *carbonatite*/*skarn* boxes. The figure also shows uncertainty for Type A calcite veins *away* from the contact. Filled squares represent pressure corrected (Tt) values used for carbon and oxygen isotope recalculations whereas non-filled squares represent Th_{total} values used for carbon and oxygen isotope recalculations. The line connecting both scenarios represents possible carbon and oxygen isotope values for Type A calcite veins *away* from the contact. Figure is adapted from Hofstra and Cline (2000).

□

□□

5. DISCUSSION

Interpreted pressure corrected fluid inclusion trapping temperatures (Tt) will be discussed in the following sections. Th_{total} values will be provided for reference.

5.1 ALTERATION

Mapping veins of all types, and alteration styles *within* the HPP and *on* and *away* from the contact has provided a regional perspective on the distribution of alteration, and insight into migration pathways of hot, circulating fluids around the HPP during intrusion. Three types of alteration observed *within* the HPP and *on* and *away* from the contact include skarn, phyllic, and potassic alteration styles. A summary of each alteration is discussed below.

5.1.1 Skarn wall rock alteration

Skarn wall rock alteration is ubiquitously found as a narrow thin band (~m's wide) along the eastern and southern margins of the HPP and in metasedimentary enclaves *within* the HPP. Where observed, skarn metasomatism is intense and found as (~0.5 to 3 m) haloes around minor quartz/calcite veins and fractures. It is also commonly interlayered within metasedimentary carbonate wall rocks. Major minerals include tremolite+diopside+quartz+calcite, and minor minerals include hydrogrossular+sphalerite+epidote+pyrite+magnetite+iron oxides. Where skarn alteration is evident, a distinct mineral progression from tremolite to

diopside+calcite+quartz exists away from veins into the adjacent altered wall rock. Interpreted Tt values of Type I secondary inclusions are ~250 to 400°C (Th_{total}~180°C). Type II, primary, fluid inclusions within hydrogrossular in skarn wall rocks have a Tt~465 to 710°C (Th_{total}~315°C).

5.1.2 Phyllic wall rock alteration

Phyllic alteration is found as pervasive host rock replacement within granodiorite and monzogranite units *on* and *away* from the HPP contact. This type of alteration has been observed as far as ~1 km away from the main body of the HPP within apophyses of the intrusion. Major alteration minerals include quartz+sericite+pyrite, and minor minerals include biotite+magnetite. Fine-grained sericite is observed ubiquitously throughout the wall rock as veins and fracture fills, and often replaces plagioclase feldspar. Associated pyrite is subhedral to euhedral and almost always has been partially to fully replaced by hematite. One quartz vein (HPP-98W) is sharp against adjacent phyllically altered wall rock, and contains medium to coarse-grained quartz, and is unaffected by secondary alteration.

Phyllic alteration is dominated by Type I secondary inclusions in the wall rock, however some Type II inclusions have been observed with slightly higher Th_{total} values. Microthermometric data suggest that the fluids responsible for this type of alteration were trapped at a Tt~260 to 425°C (Th_{total}~180°C).

5.1.3 Potassic wall rock alteration

This type of alteration is sparse throughout the region and only locally observed within granodiorite host rocks *on* and *away* from the HPP contact. Alteration mineralogy was difficult to discern in hand sample, however petrological analysis revealed the addition of massive, aggregates of dark brown biotite, and granular, subhedral K-feldspar to the granodiorite wall rock. Type I secondary fluid inclusions in wall rock quartz suggest that fluids responsible for this type of metasomatism were trapped at a Tt~205 to 350°C (Th_{total}~170°C).

5.1.4 Alteration discussion and interpretation

It is evident from the alteration facies map (Figure 4.1) that hydrothermal alteration recorded in the early granodioritic magmatic episode of the HPP (Ttc and Tcc), and the metasedimentary rocks to the east and south-east (Opu and Opl) occur mainly *on* the contact. However, some skarn alteration is located *within* the HPP in minor metasedimentary enclaves. Major sedimentary enclaves (Opu) exposed along the southern margins of the contact near Corral Creek were mapped by Burton (1997), and were described as highly thermally metamorphosed and mineralized often containing tungsten and low-grade silver ore bodies. Within this region, faults are sparse and thicknesses of skarn alteration zones (0.5 to 3 m) are uniform and narrow *on* the contact within Opu and Opl Fms. These formations are relatively pure (do not contain significant amounts of shale or silt), thus metasomatic fluids do not migrate as easily. Because these formations contain pure lithologies and narrow skarn alteration

zones, it is interpreted that metasomatic fluid migration was contained proximal to the pluton-wall rock contact. Fluids likely migrated by percolation through pore space, and/or migration along bedding planes and fractures during the early intrusive stages of the HPP.

There are a wide range of processes and parameters involved in hydrothermal fluid flow around plutonic centers, but most studies agree that fracturing and strain of wall rocks during pluton emplacement are dominant processes critical in affecting porosity and permeability (e.g. mineral solution and deposition, metamorphic reactions) (Furlong et al., 1991). Narrow skarn thickness around the HPP is consistent with other deep (5 to 10 km) intrusive environments including the skarns of Pine Creek, California and of the Osgood Mountains of Nevada. In these deposits, skarn metasomatism is also confined to narrow zones typically less than 10 m wide (Meinert, 1992). In shallow intrusive environments skarn bodies are much thicker because host wall rocks deform more by hydrofracturing and faulting, which increases the porosity and permeability allowing altering fluids to travel further distances and greater influx of later circulating meteoric waters (Meinert, 1992).

Skarn and phyllic alteration occurring *on* the southern contact is fairly concentrated, and occurs in an approximate 2.5 km X 2.5 km region. These alteration styles are associated with the later intrusive monzogranite magmatic episode of the HPP (Tmg, Tgm), and the metasedimentary rocks along the southern contact (Csl, Cl, Ch). Major faults do occur within this area, which may have served as conduits for fluids responsible for wall rock metasomatism *on* and

away from the HPP contact. However, many of these faults show no evidence of alteration or mineralization, and most host thick quartz veins with open-space filling textures suggesting fluid migration was only at low temperatures. The high concentration of skarn alteration in this area is likely attributed to the southern contact lithologies (Csl, Cl, Ch Fms.). These units are mostly mixed silty and shaly carbonate-siliciclastic sedimentary rocks with frequent argillaceous laminae and interbeds (Burton, 1997). Because these formations are 'impure', metasomatic fluids can easily penetrate and migrate through the wall rock, which might be the reason why there is abundant skarn/phyllic alteration and associated mineralization in this area.

Skarn and phyllic alteration also occur in contact metamorphosed rocks *away* (~0.5 to 1 km) from the exposed HPP contact, which may suggest a shallow magmatic altering source, such as roof dikes (Trd) or apophyses of the intrusion stemming from the initial pluton emplacement. Although plutonic rocks/outcrops were not documented in this area, mapping by Burton (1997) shows dikes and detached granitic bodies of both early and late magmatic episodes as far as 3 km *away* from the HPP contact. Further corroboration is provided by high Tt~540 to 800°C values (Th_{total}~>440°C) measured within Type III inclusions in miarolitic cavities within detached monzogranitic host rocks locally *away* from the contact.

5.2 VEINS

Quartz, calcite, and calcite-polymetallic sulfide veins are the dominant veins observed *within* the HPP and *on* and *away* from the contact. These veins were

studied to better understand what types of fluids were present during and after the HPP intrusion and where fluids might have migrated. This can provide insight into what fluids were responsible for Carlin-type deposits along the Carlin trend. A short summary of each vein type is discussed below.

5.2.1 Quartz veins

Two main types of quartz veins exist *within* the HPP and *on* and *away* from the contact including: i) Thick (~4 to 8 m), white, fault hosted quartz veins that crosscut the HPP and metasedimentary rocks along the contact, and; ii) Minor (~mm to >20 cm), coarse-grained quartz veins. Thick, milky-white, quartz veins are hosted within faults and joints within the central, western interior, and flanks of the HPP, and can continuously or irregularly be exposed for 100's of meters. Vein quartz is extremely hard and often contains varying quartz habits including massive, comb, and vuggy. Fluid inclusion evidence within HPP-28 suggests that quartz veins *within* formed at intermediate temperatures, and contain primary Type II inclusions that have Tt~325 to 480°C (Th_{total}~230°C). Quartz vugs *within* however, display much lower Type I temperatures, Tt~200 to 360°C (Th_{total}~150°C).

Minor quartz veins *on* and *away* from the HPP contact occur mostly in fractured and brecciated mixed siliciclastic-carbonate skarn limestone and phyllically altered granodioritic host rocks *on* and locally *away* from the contact. Typically, contacts with both rock types are sharp. Fluid inclusions indicate that all quartz veins contain Type II primary fluid inclusions, and quartz veins *on* the contact

contain Tt~360 to 572°C (Th_{total}~372°C) values, and quartz veins *away* from the contact contain Tt~510 to 705°C (Th_{total}~340°C) values.

5.2.2 Calcite veins

Two types of calcite veins are observed around the HPP: Type B calcite veins *on* the contact and Type A calcite veins *away* from the contact. Type B calcite veins *on* the contact (~mm's to 40 to 50 mm) are often massive and sugary and exude a pungent sulfur odor indicating the presence of sulfides, which commonly include pockets and/or veins of galena, sphalerite, pyrite, and magnetite. These veins are typically adjacent to skarn wall rock alteration where contacts are generally sharp. Fluid inclusion petrography and microthermometry show that these veins contain primary Type I fluid inclusions that have a Tt~235 to 388°C (Th_{total}~160°C).

Type A calcite veins *away* from the contact are ~cm's to 15 to 20 cm across, and contain medium to coarse-grained calcite with trace quartz±pyrite±iron oxides. Contacts with adjacent metasedimentary rocks are sharp and show no sign of alteration. Fluid inclusion microthermometry show that these veins contain Type I inclusions that have a Tt~200 to 340°C (Th_{total}~125°C).

5.3 ORIGIN OF FLUIDS

5.3.1 Fluid inclusion clues

Fluids play a significant role in intrusive environments and fluid inclusion petrography and microthermometry are important tools in characterizing the

geochemistry of fluids around an intrusive center. Type I, II, and III inclusions were observed *within* the HPP and *on* and *away* from the contact.

5.3.1.1 Overall characteristics of Type I, II, and III inclusions

Of the >200 fluid inclusions measured within veins and wall rocks, Type I and II inclusions are chemically comprised of H_2O-NaCl-KCl, interpreted from the modal distribution (~-21°C) and range (-10 to -30°C) of Type I and II fluid inclusion $T_{eutectic}$ values. Type III inclusions, only observed in miarolitic cavities, are characterized by the H_2O-CO_2-NaCl-KCl system, and are the only type that contain a carbonic (XCO_2) phase. XCO_2 and methane (XCH_4) species within the carbonic phase respectively range from 0.952 to 0.987 and 0.013 to 0.018. Type I, II, and III inclusions are generally low salinity (<5% Mass eq. NaCl), and are divided based on fluid phases, fv, and homogenization temperatures; **Type I** inclusions: Tt~245 to 380°C (Th_{total}~<200°C); **Type II** inclusions: Tt~390 to 590°C (Th_{total}>200°C); and **Type III** inclusions: Tt~450 to 650°C (Th_{total}~350°C). The marked difference between Type I and Type II inclusions is evident in the histogram plots in Figure 4.6 and the Th_{total} versus Tm_{ice} plot in Figure 4.7A. Type III inclusions are comparable to Type II inclusions with respect to homogenization temperatures. However, the presence of a carbonic phase within Type III inclusions makes them distinct. It is also evident within these plots that no consistent difference exists in Mass% eq. NaCl between fluid types. Differences in temperatures of homogenization between fluid inclusion types suggest a complex history of fluid interaction most likely between connate waters, cooler

circulating meteoric fluids and hotter exsolved magmatic fluids expelled during crystallization processes at depth.

5.3.1.2 Type I, II and III inclusions by locality

By comparing fluid inclusion data by locality, it is possible to see where chemical and thermal variations exist around the HPP. No significant statistical differences in $T_{eutectic}$ Tm_{ice}, $Tm_{clathrate}$, and Mass% eq. NaCl values exist between Type I, II and III inclusions *within, on* or *away* from the contact. All types display consistent low salinities and uniform composition within each type. However, some Type I and Type III inclusions respectively *on* and *within* the contact display slightly higher Mass% eq. NaCl ranging between ~7 to 10%.

Thermally, by spatially comparing Type I, II, and III Th_{total} and Tt values separately around the HPP, it is apparent that a complex temperature history occurred *within* the HPP and *on* and locally *away* from the contact. Typically in an intrusive environment hotter fluids occur around and near the contact whereas cooler fluids are found away from the center of intrusion as heat provided by the intrusion dissipates. Quantitatively this is expressed in Table 4.1 and in Th_{total} Type I, II, and III histograms *on, away,* and *within* the contact. Visually, this is expressed in the Th_{total} versus Tm_{ice} plots in Figure 4.7A, and in map view in Figures 4.8 and 5.1. The Th_{total} versus Tm_{ice} plot for Type I and II inclusions shows a marked distinction between Type I and II Th_{total} values, which may indicate the difference between cooler meteoric versus hotter magmatic fluids, or is a function of fluid mixing between different fluid types (connate, meteoric,

magmatic). Type III inclusions are likely to be of magmatic origin because they are only found in granodioritic hosted quartz miarolitic cavities inferred to be a derivative of the crystallizing HPP. These inclusions also show high Tt ~450 to 650°C (Th_{total}~240°C) values further suggesting a magmatic origin. Since the Tt and Th_{total} values of Type III inclusions overlap with Type II Tt and Th_{total} values, it is likely that Type II inclusions are also magmatically derived. Further evidence for a complex fluid history around the HPP is shown on the regional Tt map (Figure 5.1), which displays the average Tt values for different settings around the HPP. From this map it can be broadly interpreted that cooler fluids (Tt~200 to 400°C) are mostly *away* from contact and hotter fluids (Tt~>400°C) are *on*, locally *away* and *within* the contact. This thermal gradient is physically preserved in the 1 to 1.5 km contact metamorphosed aureole adjacent to the main plutonic body. As described in chapter two, the rocks around the HPP contact zones have been highly metamorphosed, recrystallized, strained and folded, and as distance increases *away* from the HPP, the thermal, chemical, and physical imprints on the country rock dissipate. It is evident however, that cooler fluids also exist in the metamorphic contact aureole and *within* the intrusion, which is a likely indication of late synplutonic or post plutonic meteoric water infiltration and mixing. It is known that one of the main mechanisms for pluton cooling is provided by meteoric water convection around a pluton during and after intrusion (see reviews by Cathles, 1977; Norton and Knight, 1977). A brief description of the different Tt settings in Figure 5.1 is discussed below.

The Tt~200 to 400°C range is represented mostly by Type I, primary fluid inclusions within Type A and B calcite veins *on* and *away* from the contact besides HPP-43 and HPP-100, as secondary inclusions within skarn, potassic and phyllic altered wall rocks, and in quartz vugs (V) *within* the contact. Type II primary inclusions in quartz veins *on*, HPP-40, HPP-89 are also contained with this range. However, in section *4.7.3.1* it was determined that fluid inclusions within these veins had reequilibrated with later stage fluids after entrapment.

The Tt~400 to 600°C temperature range is represented by Type II primary inclusions in quartz veins *on* and *within* the contact, and also by Type III inclusions in a miarolitic cavity *within* the contact. Also shown within this range are Type II primary inclusions in hydrogrossular and quartz within a skarn wall rock (HPP-16) *on* the contact.

The Tt~>600°C range is represented by Type II primary inclusions in quartz veins *on* and locally *away* from the contact. Type III inclusions in a miarolitic cavity are also included. Also, anomalously high temperature primary Type II inclusions in a calcite vein (HPP-100) are observed within unaltered metasedimentary rocks *away* from the contact. Many different crosscutting secondary trails exist within the calcite vein, so it is possible that the fluid inclusions measured are not representative of the original fluids responsible for vein formation. The fluid could be a result of a hot circulating fluid that was initiated by increased heat flow from Basin and Range extension (Ilchik and Barton, 1997) or from a buried, unexposed apophysis of the intrusion.

It is not geologically unusual to have a complex history of fluids within and around a plutonic center involving mixtures of connate, meteoric, and magmatic waters. It is hypothesized that fluids around intrusive centers evolve from an early magmatic stage to a later meteoric stage (Nabelek, 1991). Connate fluids are also present and can have an impact on the bulk fluid chemistry. Other known upper crust aureoles from single peraluminous intrusive centers that display contact metamorphic aureoles and a complex fluid history similar to the HPP include: Birch Creek, McCullough Butte, and Tungstonia (California, USA), Land's End, Dartmoor, St. Austell (Cornwall-Devon, SW England), Seward Peninsula (Western Alaska), and Notch Peak, Utah, USA (Barton et al., 1991).

5.3.1.3 Fluid inclusions in quartz veins

Type I and Type II fluid inclusions measured in quartz veins and vugs *within*, *on*, and *away* from the HPP contact display only minor differences in terms of $T_{eutectic}$, and Mass% eq. NaCl, which suggest all fluids are dominantly low salinity (~<4 Mass% eq. NaCl) and composed of H_2O-NaCl-KCl. Thermally, Tt and Th_{total} values vary spatially around the HPP contact revealed by the histogram and Th_{total} versus Tm_{ice} plots in Figures 4.6 and 4.7B as well as on the average Tt and Th_{total} maps. The one investigated quartz vein (HPP-115) *away* from the contact is consistent with quartz veins *on* values, and thus is interpreted to be from the same origin. Fault hosted quartz veins *within* (HPP-28) contain open filled Vugs *within* (HPP-28V), and respectively have Tt~325 to 480°C (Th_{total}~230°C) and Tt~200 to 360°C (Th_{total}~150°C) values.

The above thermal and chemical similarities and differences suggest:

i) Quartz veins *on* and *away* are related. Similarities in Tt and Th_{total} values, salinities and H2O-NaCl-KCl systems, and the distribution and mineralogy of quartz veins and adjacent wall rock skarn alteration corroborate this. Both settings display a uniform, gradational skarn wall rock mineralogy consisting of tremolite+diopside+quartz+calcite. Further evidence is provided by spatial relationships. HPP-115 is <0.5 km *away* from the contact within the contact metamorphic aureole and contains Tt and Th_{total} values similar to those from quartz veins *on* the contact. It is possible that the same hot, low salinity fluid responsible for quartz veins *on* migrated a distance through observed fractures and faults and formed quartz veins locally *away* from the HPP contact as well as the same skarn wall rock mineralogy. It is also possible that a buried apophysis of the intrusion, of the type mapped away from the HPP by Burton (1997), provided compositional fluid similar to that forming quartz veins *on* the contact. In regards to the origin of the fluid, quartz *on* and *away* microthermometric data is comparable to that of primary fluids measured in quartz and hydrogrossular (Skarn WR (P)) in skarn wall rocks *on* the contact, which presumably was derived from exsolved magmatic fluids of the HPP. However, retrograde alteration through cooling by meteoric waters can also stabilize skarn minerals, but most fluid inclusion and isotope studies have shown that exsolved magmatic fluids are most commonly responsible (Meinert, 1992). Compositionally, Skarn WR (P) and quartz veins *on* and *away* are low salinity, comprised of the same chemical system (H_2O-NaCl-KCl), and share a similar range in Tt and Th_{total}

values. The Tt range (~410 to 650°C) is slightly lower, but comparable to the ~720°C temperature estimated for the HPP during intrusion, which also infers a magmatic derivation (Deans, 2010). Given the chemical and thermal similarities of Skarn WR (P*)* values and the temperature of the HPP, it is inferred that the fluid that formed quartz veins *on* and *away* are derived from a magmatic source.

ii) Quartz veins *within* were formed by later, circulating lower temperature, surface derived, meteoric fluids. This is supported by intermediate Tt~325 to 480°C (Th_{total}~230°C) values, and crosscutting relationships of the host veins in the field. The majority of these continuous, steep, major quartz veins strike along normal faults and joints that crosscut both the HPP and metasedimentary rocks along the southern and eastern margins of the HPP contact, suggesting a later, lower temperature, brittle deformation episode and subsequent fluid event.

iii) Quartz vugs *within* were found within these crosscutting, thick, and steeply dipping major quartz veins and likely represent the final crystal forming stages of these later, silica-saturated, low temperature fluids. Hence, quartz vugs *within* are interpreted to be crystallized from meteorically derived waters.

Since fault-hosted quartz veins and quartz vugs *within* are interpreted to have formed post-HPP intrusion, temperatures of entrapment likely fall between Th_{total} (minimum temperature of entrapment) and Tt values. This is because Tt values are adjusted Th_{total} values based on the pressure of the HPP during intrusion. This range will be represented throughout by the following format (example): Th_{total}~100°C to Tt~250 to 400°C.

5.3.1.4 Fluid inclusions in calcite veins

Two types of calcite veins were found *on* and *away* from the HPP contact. Type A calcite veins were observed *on* and *away* from the HPP contact, and typically are small (~mm's to cm's). However, *away* from the contact they can reach up to 15 to 20 cm across. This type typically displays sharp contacts with unaltered adjacent metasedimentary wall rocks. Type B calcite veins were only observed *on* the contact, are thicker (~mm's-40 to 50 cm's), regularly contain poly-metallic sulfide minerals, and occur adjacent to skarn wall rocks. Frequently, Type B calcite veins crosscut Type A calcite veins *on* the contact, which suggest that Type A calcite veins predate the formation of Type B calcite veins. Type B calcite veins are interpreted to have formed synchronously with quartz veins *on* the contact. This is supported by similar adjacent skarn wall rock mineralogy, and multiple crosscutting generations in the field.

Both Type A calcite veins *away* and Type B calcite veins *on* are characterized by Type I inclusions besides HPP-43 and HPP-100, which contain Type II inclusions. HPP-43 has Tt~275 to 450°C (Th_{total}~210°C), which is near the range of Type I inclusions (Tt~200 to 400°C), and HPP-100 as discussed above, may be the product of later fluid events. The distribution of Th_{total} versus Tm_{ice} in Figure 4.7B and in histogram plots in Figure 4.6 for Type A and B calcite veins is especially narrow, and a major overlap between these two groups is evident. Mass% eq. NaCl values for both vein types are low salinity (~1% Mass% eq. NaCl), however some Type A calcite veins *away* salinity values are slightly higher but not statistically significant. Tt values for Type B calcite veins *on* are

~235 to 388°C (Th_{total}~160°C) and for Type A calcite veins *away* are ~200 to 340°C (Th_{total}~125°C), excluding sample HPP-100. Although both vein settings are physically and mineralogically different, geochemical data suggests that fluids responsible for both types is low salinity and composed of H_2O-NaCl-KCl.

Thermally, Tt values for Type A calcite veins *on* range approximately 200 to 350°C lower than quartz veins *on* and *away*, however chemically they are both low salinity and comprised of H_2O-NaCl-KCl. Type A calcite veins *away* are hosted in unaltered shallow marine carbonate siliciclastic rocks and display no wall rock alteration. Because crosscutting relationships suggest these veins predate the formation of Type B calcite veins *on*, it is interpreted that the fluids responsible for vein formation are unrelated to the hydrothermal activity around the HPP, and formed before the HPP intrusion.

Type B calcite veins *on* and quartz veins *on* and *away* both display similar skarn wall rock alteration mineralogy (tremolite+diopside+quartz+calcite) although Type B calcite veins *on* do not display distinct tremolite crystals near the vein edge, suggesting that the H_2O responsible for tremolite formation was in the fluid for quartz vein precipitation. Type B calcite veins *on* the contact also are not associated with hydrogrossular crystals in the skarn wall rock. The lack of tremolite or hydrogrossular adjacent to Type B calcite veins *on* the contact may be explained by a too low of a temperature during metasomatism to stabilize these calc-silicate minerals. Type B calcite veins *on* do however contain Pb-Zn sulfide ore minerals (galena and sphalerite), which may have precipitated out from exsolved magmatic fluids as the HPP was crystallizing, which is the most

common process responsible for skarn type Pb-Zn mineralization. However, it is possible that these minerals could have been leached out from shallow marine carbonate country rocks by circulating surface derived meteoric waters during and after intrusion, which is a common process typical of seafloor/volcanogenic massive sulfide deposits (Franklin et al., 1981). Carbon and oxygen isotopic data discussed in the following section can further help determine the origin of fluids within Type A and Type B calcite veins.

5.3.1.5 Wall rock fluids

Primary and secondary fluid inclusion analyses of Type I and Type II inclusions in skarn, phyllic, and potassic altered wall rocks provide a chemical and thermal history of fluids responsible for these alteration types. Chemically, all fluid inclusions measured within altered wall rocks have similar $T_{eutectic}$ ranges, low Mass% eq. NaCl values (~<5%) and contain either Type I or Type II inclusions, which provides strong evidence that the fluids responsible for alteration were dominantly low salinity and composed of H_2O-NaCl-KCl.

5.3.1.5.1 Skarn wall rock alteration

Type I and II fluid inclusions were measured in skarn wall rocks *on* and *away* from the HPP contact. Type I, secondary fluid inclusions (Skarn WR (S)) measured in quartz grains provide intermediate Tt~250 to 400°C (Th_{total}~185°C) values. Type II, primary inclusions measured in quartz and hydrogrossular (Skarn WR (P)) yielded significantly higher Tt~465 to 710°C (Th_{total}~315°C) values. The difference in the temperature of entrapment between Skarn WR (S) and Skarn

WR (P*)* suggest a complex fluid entrapment history. Low Skarn WR (S*)* Tt and Th_{total} values are not characteristic of most skarn forming environments. In fact, fluid inclusion studies of different skarn types around the world yield overall high homogenization temperatures up to ~700°C (Meinert, 1992). Also, primary inclusions measured in hydrogrossular within skarn wall rocks provide an unambiguous determination of temperature, pressure, and composition of skarn forming fluids because high-temperature skarn minerals (e.g. hydrogrossular) are unlikely to trap later low-temperature circulating fluids (Meinert, 1992). The Tt values for Skarn WR (P) inclusions are marginally lower, however comparable to magmatic temperatures at which the HPP was emplaced (~720°C from Deans, 2010), and presumably represents the infiltration of magmatic fluids exsolved from the HPP during crystallization, which is the common fluid process that creates skarn metamorphic minerals without replacement by lower temperature skarn minerals (Meinert, 1992). These trapping temperatures are also consistent with quartz vein *on* and *away* values suggesting a similar high temperature fluid. Therefore, Skarn WR (S) fluids may be derived from a later low-temperature (Tt~250 to 400°C), low salinity (~3% Mass% eq. NaCl) meteoric event or is the result of an evolved and 'cooled' low temperature magmatic fluid. Carbon and oxygen isotope data can further help determine the origin of these fluids. Skarn WR (P) inclusions are low salinity (~4.5% Mass% eq. NaCl) and high temperature (Tt~465 to 710°C), and most likely are derived from expelled magmatic waters as the HPP was crystallizing at 6 to 12 km depth. Thus, Skarn

WR (P) will serve as the fluid responsible for skarn metasomatism and as an indicator of the nature of primitive magmatic fluids.

5.3.1.5.2 Phyllic wall rock alteration

Type I, secondary fluid inclusions measured in phyllically altered wall rocks have Tt~260 to 425°C (Th_{total}~180°C). This Tt range correlates well with that of typical phyllic metasomatism temperatures (200 to 450°C) required to form characteristic secondary minerals including quartz+sericite+pyrite (Moore and Nash, 1974). Typically, phyllic metasomatism occurs outside the potassic alteration shell, and is formed from acidic magmatic vapors (Lowell and Guilbert 1970; Hedenquist et al., 1998). However, an increasing meteoric water contribution to the wall rock increases with distance from the intrusion (Hedenquist et al., 1998). No isotopic evidence was available to support a magmatic origin for these fluids. However, a clear characteristic quartz-sericite-pyrite alteration mineralogy, and Tt values of ~260 to 425°C provides evidence of typical phyllic metasomatism. Since phyllic alteration is interpreted to be the result of infiltration of magmatic fluids (Lowell and Guilbert, 1970; Hedenquist et al., 1998), it is interpreted that the fluids responsible for this alteration are also magmatically derived, and in part had possibly been subjected to slight mixing with meteoric waters. It is possible that a juvenile primary magmatic fluid, derived from the interior of the HPP or one of the late phases (Tmg), cooled from 465 to 710°C (Skarn WR (P)) to ~200 to 450°C as it migrated away a short distance from the plutonic source to phyllically alter the outer margins of the HPP. In fact, Hedenquist et al. (1998) found that a primary magmatic fluid (450 to 550°C)

responsible for K-metasomatism cooled to a phyllically altering fluid of ~350°C over a vertical interval as small as 100 m.

Therefore, from the above geochemical data it is interpreted that during cooling and degassing of the HPP, a primary low salinity magmatic fluid migrated a distance and cooled to ~260 to 425°C, which resulted in phyllic alteration. Possible contributions of convecting meteoric waters are also considered. These same fluids interpreted to be responsible for phyllic alteration also correlate well with other subgroups chemical characteristics including Skarn WR (S), Potassic WR, and Type B calcite veins *on*, which might indicate a similar fluid origin between subgroups.

5.3.1.5.3 Potassic wall rock alteration

Type I, secondary fluid inclusions measured in potassically altered wall rocks display low trapping temperatures, Tt~205 to 350°C (Th_{total}~170°C), and some of the highest Mass% eq. NaCl values (~8%). Typical potassic metasomatism occurs closest to the intruded pluton and is produced by high temperature fluids (450 to 600°C) (Lowell and Guilbert, 1970; Moore and Nash, 1974; Roedder, 1971). The Tt and Th_{total} values suggested by fluid inclusion microthermometry are significantly lower than the typical high temperature range needed to potassically alter wall rocks, suggesting that the measured inclusions are not representative of the true altering fluids. It is thus considered that fluids trapped within secondary fluid inclusions within quartz were not the cause of potassic metasomatism. These low trapping temperatures are consistent with Vugs *within*,

and based on the above interpretations it is determined that these fluids are likely derived from a similar later stage, cooler fluid event.

5.3.2 Stable isotope clues into fluid origin

Carbon and oxygen stable isotope analyses were conducted on Type A and B calcite veins and wall rocks *on* and *away* from the HPP contact to geochemically trace the origin of fluids around the HPP. Values are plotted along with theoretical and empirical regional fluid boxes in Figure 4.9. A summary of carbon and oxygen data is shown in Table 4.2.

It is well known in intrusive environments that $\delta^{18}O$ isotope exchanges can occur through extensive water-rock interaction in open system aureoles (Nabelek, 1991; Taylor, 1974; 1977). This is commonly but not always demonstrated by a decrease in $\delta^{18}O$ values near an intrusive center and an increase in $\delta^{18}O$ values away from the intrusion. In Figure 4.9 it is shown that the recalculated $\delta^{13}C$ values are fairly consistent, ranging from -2.17 to 3.80‰. However, recalculated $\delta^{18}O$ values are highly variable ranging from 1.09 to 29.36‰, which suggest different origins of fluids including meteoric, magmatic, metamorphic and connate. Note: this $\delta^{18}O$ range is much broader than typical $\delta^{18}O$ isotope wall rock exchange of most Carlin-type deposits (-15 to +10‰) (Hofstra and Rye, 1998), suggesting mixing between end-member fluid species (connate, meteoric, magmatic). Below is a description of each setting and interpretation of fluid origins.

5.3.2.1 Skarn wall rock on

Skarn WR *on* recalculated $\delta^{18}O$ values average 8.63‰ and range from 2.30 to 14.66‰, and recalculated $\delta^{13}C$ values average -0.75‰ and range from 1.36 to 3.45‰. The $\delta^{18}O$ average values are near the magmatic $\delta^{18}O$ value (~10‰) measured for the HPP (Burton, 1997), and are close to the *carbonatite* box of magmatic origin and *skarn* box of mixed magmatic/connate origin. Two data points do fall in or near the *ore fluid* region suggesting mixing with meteoric waters. As seen in Figure 4.9, values are spaced along a linear array extending from the unaltered *L.S.* box to either the *carbonatite/skarn* box or the *Mid-Tertiary Meteoric* field. Typically, linear trends or arrays positioned between the host rock and fluid source are the product of mixing between fluids and wall rock, and data will almost always spread from the source fluid to the original host wall rock (Hofstra and Cline, 2000). In this case, it is clear that Skarn WR *on* values have been affected by fluid/wall rock interaction indicated by the linear array. However, interpretation of the fluid source is uncertain, and can either be interpreted as i) *Mid-Tertiary Meteoric* waters interacting with *L.S.* wall rock (connate fluids) or; ii) Mixing between magmatic waters (*carbonatite* box) and connate waters from the *L.S.* wall rock. Since most $\delta^{18}O$ values are higher than the magmatic fluids field, a magmatic mixing interpretation is more likely. However, two skarn wall rocks (HPP-33, HPP-43) may have had minimal interaction with meteoric waters due to its position in the *ore fluid* field between *L.S.* and *Mid-Tertiary Meteoric* boxes.

Mixing between fluids of different origins (meteoric, magmatic, connate) is not uncommon in intrusive environments. In fact, many open aureoles are believed

to evolve from an early magmatic stage to a later meteoric stage (Nabelek, 1991). Skarn WR (P) fluid inclusion evidence supports a primary magmatic origin, however Skarn WR (S) fluid inclusions were of inconclusive origin. Skarn WR (S) Type I fluid inclusions generally contain intermediate temperatures, Tt~250 to 400°C (Th_{total}~185°C), whereas Type II primary fluid inclusions in hydrogrossular and quartz contain high temperatures Tt~465 to 710°C (Th_{total}~315°C). This marked difference in inclusion type, temperature, and style of entrapment (crosscutting secondary trails) may be explained by later stage infiltration of meteoric waters as indicated by the mixed meteoric-connate samples (HPP-33, HPP-43) located in or near the *ore fluid* region. Therefore, it is interpreted that Skarn WR (S) Type I, low salinity, fluid inclusions are the result of mixing between meteoric and connate waters yielding *ore fluid* $\delta^{18}O$ and $\delta^{13}C$ values and an overall lower bulk Tt and Th_{total} temperatures.

5.3.2.2 Type B calcite veins on

Type B calcite veins *on* recalculated $\delta^{18}O$ values average 13.89‰ and range from 1.09 to 25.85‰, and recalculated $\delta^{13}C$ values average 0.60‰ and range from -2.17 to 2.16‰. These values do not include the outlier HPP-33, located in the *L.S.* box. Two samples (HPP-42, HPP-18) cluster near the *carbonatite/skarn* boxes indicating a mixture between magmatic and connate waters. The other two samples (HPP-43, HPP-61) fall within the *ore fluid* region, which indicates mixing between meteoric and connate waters. The recalculated $\delta^{18}O$ range suggests that Type B calcite veins *on* are a product of both magmatic-connate and meteoric-connate mixing.

5.3.2.3 Unaltered wall rock away

Unaltered WR *away* values have a recalculated average $\delta^{18}O$ of 27.01‰ and range from 25.08 to 29.02‰. Recalculated $\delta^{13}C$ values average 2.81‰ and range from 2.39 to 3.80‰. (data does not include the HPP-105 outlier). The majority of the data is located within the *L.S.* box, which is typical of unaltered metasedimentary shallow marine rocks. These recalculated $\delta^{13}C$ and $\delta^{18}O$ values are also typical of connate fluids trapped within the pore space of unaltered sedimentary rocks. An obvious outlier (HPP-105) occurs within the *ore fluid* region, which may have been influenced by meteoric waters during intrusion or later Basin and Range extension as a clear trend extends between this data point and the *Mid-Tertiary Meteoric* and *L.S.* boxes. The above data suggest that there was not pervasive influx of magmatic waters > 10 m distance *away* from the pluton-wall rock contact.

5.3.2.4 Type A calcite veins away

Figure 4.9 shows two sets of data for Type A calcite veins *away* because Tt values used for the recalculation of $\delta^{18}O$ and $\delta^{13}C$ values, may not be representative of this fluid setting since Type A calcite veins *away* occur >2 km *away* from the pluton-wall rock contact. Therefore, a line connecting Th_{total} (minimum temperature) used for $\delta^{18}O$ and $\delta^{13}C$ recalculations and Tt (maximum temperature) used for $\delta^{18}O$ and $\delta^{13}C$ recalculations is shown. From Figure 4.9, it is evident that the difference between recalculated carbon and oxygen using Tt versus Th_{total} is minor for $\delta^{18}O$ (2 to 3‰) and $\delta^{13}C$ (2 to 4.5‰).

Type A calcite veins *away* display: i) A group within the *L.S.* box (HPP-100, HPP-103, HPP-78), which yields a recalculated average $\delta^{18}O$ of 29.49‰ and range between 24.32 to 31.34‰, and a recalculated $\delta^{13}C$ average of 0.77‰ and range between -4.07 to 2.40‰. The variation in this group's $\delta^{18}O$ and $\delta^{13}C$ values are minimal and most values plot within the *L.S.* box indicating that fluids responsible for these calcite veins are of connate origin. ii) The second group (HPP-105, HPP-107), yields a recalculated $\delta^{18}O$ average of 6.94‰ and range from 3.12 to 10.66‰, and a recalculated $\delta^{13}C$ average of -1.32‰ and range from -3.99 to 1.13‰. This group displays a $\delta^{18}O$ and $\delta^{13}C$ range from the *carbonatite*/skarn boxes to the *ore fluid* region. These fluids may have been influenced by magmatic waters exsolved from unexposed buried apophyses of the intrusion or be the result of mixed meteoric waters that had interacted with connate waters in limestone. The latter is more likely because no outcrops of granodiorite were observed or previously mapped in this area. Deep circulation of meteoric waters induced by Basin and Range extension was proposed by Ilchik and Barton (1997), and may have been the likely local source of meteoric water infiltration. Another source could be meteoric convection provided by heat from the HPP.

5.3.2.5 Comparison with fluids at Carlin-type deposits

It is clear that most of the measured values fall along a linear path from the *L.S.* box to either the *carbonatite/skarn* boxes or *Mid-Tertiary Meteoric Water* box indicating fluid mixing between various end member fluid sources. Other data points are positioned within end-member fluid fields. Carbon and oxygen stable isotope data measured in ore stage calcite veins from Carlin deposits along the

Carlin-trend are represented by the *ore fluid* field. This field, interpreted by Hofstra and Cline (2000), indicates that ore stage calcite veins had interacted with meteoric waters because the field 'extends' toward the *Mid-Tertiary water* box. Data collected from around the HPP follows a similar trend, however it cannot be determined whether the array is influenced by meteoric or magmatic waters or both. It is possible there are both meteoric and magmatic fluid signatures, which can result by mixing hydrothermal circulating waters and magmatic waters during and after an intrusive event. The above isotopic data suggests that Skarn WR *on* values are certainly affected by fluid-fluid interaction, most likely between magmatic and connate fluids. However, meteoric-connate mixing is apparent for some samples. Values for Type B calcite veins *on* show a similar pattern where some values fall within or near *carbonatite*/*skarn* boxes indicating a magmatic mixed connate origin. However, some fall within the *ore fluid* region suggesting meteoric water input is also possible. Isotope values for Type A calcite veins *away* display a dominant group within the *L.S.* box inferring a connate fluid origin. However, another anomalous group extending from the *carbonatite*/*skarn* boxes to the *ore fluid* region field is most likely the product of meteoric-connate mixing as no plutonic rocks were observed or mapped within this area. Unaltered WR *away* values are dominantly of connate origin except HPP-105, which displays an isotopic shift towards meteoric values. Overall, it is clear that the isotopic values preserve a complex fluid history around the HPP, and there exist mixtures of fluids of different origins.

5.4 INTERPRETATION OF FLUID HISTORY

From field evidence, fluid inclusion, and $\delta^{18}O$ and $\delta^{13}C$ isotope data a reconstruction of fluid flow around the HPP can be made. Schematic diagrams depicting fluids of early and late stages of the HPP are shown in Figure 5.2. Fluid events organized by before the HPP intrusion and early and late stage events are discussed below.

5.4.1 Before the HPP intrusion

A thick succession of Paleozoic siliciclastic and carbonate rocks were deposited on a broad shallow carbonate platform. These sedimentary rocks form much of the country rocks that the HPP intruded into and locally contact metamorphosed. Major tectonic episodes, including the Antler (Robert's Mountain Thrust) and Sonoma orogenies, provided a series of thrust faults and deformation to the area. A later Jurassic polyphase intrusive event provided a number of plutons in the west-central Ruby Mountains including one monzogranitic pluton just north of the HPP (Burton, 1997).

Type A calcite veins *away*: These veins are found ubiquitously in Cambrian and Ordovician unaltered metasedimentary country rocks *on* and *away* from the HPP contact. Frequently, Type B calcite veins *on* and quartz veins *on* and locally *away* from the contact crosscut these veins. These veins contain dominantly Type I inclusions, are low salinity (~1%), and contain some of the lowest temperatures recorded in this study, (Th_{total}~125°C to Tt~200-340°C). $\delta^{18}O$ and $\delta^{13}C$ values suggest mainly a connate origin. However, some values range between the

carbonatite/skarn boxes and *ore fluid* field, which most likely implies local mixing with meteoric waters. This would isotopically decrease the recalculated $\delta^{18}O$ values. Based on low trapping temperatures, crosscutting relations, and recalculated $\delta^{18}O$ and $\delta^{13}C$ values, I interpret these veins to be emplaced within the unaltered sedimentary wall rocks before the HPP intrusion, and vein calcite to be precipitated from connate fluids. Some Type A calcite veins *away* were not consistent with this interpretation, and show high homogenization temperatures (HPP-100), or are isotopically classified within the *ore fluid* field implying a mixed meteoric origin (HPP-105, HPP-107). These veins are interpreted to be influenced by local circulating meteoric fluids, post HPP intrusion, that migrated during Basin and Range extension (Ilchik and Barton, 1997). Since these veins occurred near the east flank of the RMEHR it is possible that an increased geothermal gradient produced by Basin and Range extension could have caused deep circulation of surface derived meteoric fluids and overprinted earlier fluids events.

5.4.2 Early HPP stage

The ~36 Ma HPP intruded during voluminous activity that swept NE to SW across much of Utah and Nevada 40 to 32.4 Ma (Burton, 1997). Emplacement of the pluton is broadly synchronous with the first stages of core-complex related extension that is proposed to have commenced during or shortly after intrusion, however no evidence suggests a temporal or spatial relationship between emplacement and crustal extension (Burton, 1997). Geochemical and stratigraphic data suggest that the HPP was emplaced around 6 to 12 km at

depth at ~1600 to 3200 bars (Burton, 1997) at approximately 720°C (Deans, 2010). It is proposed that during cooling and crystallization of the HPP, magmatic waters were in part expelled into the country rock and are responsible for the following events. Minor meteoric infiltration and input is considered during this stage.

***Miarolitic Cavities*:** These cavities formed as volatile rich bubbles trapped in the granodioritic melt during HPP crystallization, and were found *within* the HPP and locally *away* within granodioritic apophyses of the intrusion. These cavities contain Type II inclusions (vapor-rich) and were the only setting where Type III inclusions (CO_2-rich) were found. The presence of both types suggests a volatile phase separation within the parent magma. It is known that carbonic fluids are poorly miscible with aqueous fluids within silicate melts and as the pluton (magma) rises and/or cools, the low solubility of CO_2 to H_2O causes both phases to partition preferably into any vapor phase (Lowenstern, 2001). It is interpreted that this process resulted in both Type II and Type III inclusions in miarolitic cavities.

Type III Tt and Th_{total} values varied by location. Miarolitic cavity *away* values displayed higher temperatures, Tt~540 to 800°C (Th_{total}~465°C) than miarolitic cavity *within* values, Tt~355 to 505°C (Th_{total}~240°C). These temperatures were some of the highest recorded in this study and miarolitic cavity *away* values are consistent with the 720°C crystallization temperature proposed for the HPP (Deans, 2010). This infers that fluids are most likely derived from the HPP, are predominantly magmatic in origin, and were trapped close to the source.

***Skarn WR (P)*:** Primary Type II fluid inclusions measured in quartz and hydrogrossular within skarn wall rocks reveal high homogenization and pressure corrected temperatures, Tt~465 to 710°C (Th_{total}~315°C), which are consistent with fluid inclusion temperatures of miarolitic cavities and are slightly lower than the proposed ~720°C for the HPP. These temperatures are also consistent with typical high fluid inclusion homogenization temperatures (Th_{total}~350 to 800°C) in hydrogrossular and quartz within Au and Tungsten skarns, which are interpreted to be the result of magmatic fluid infiltration (Meinert, 1992). Hydrogrossular homogenization temperatures in the well-known Au bearing skarn of Fortitude Mine in the Battle Mountain district in North-central Nevada (360 to 590°C) are also comparable to the hydrogrossular Tt and Th_{total} values measured within skarn wall rocks *on* the HPP contact (Myers and Meinert, 1991). Further, calc-silicate phase diagrams indicate that high temperatures (~450 to 500°C) at 1500 bars are required to stabilize common skarn minerals including: hydrogrossular+diopside+tremolite+quartz+calcite. In most cases, these high temperature fluids are of magmatic origin. Because of the above relationships it is interpreted that the fluids responsible for skarn metasomatism are magmatically derived. However, Skarn WR *on* recalculated $\delta^{18}O$ and $\delta^{13}C$ average values (8.63‰ and -0.75‰) are interpreted to be the result of mixing between magmatic and connate waters as a linear trend extends between the *L.S.* and *carbonatite/skarn* boxes. However, several samples fall within or near the *ore fluid* field indicating some infiltration and mixing with meteoric waters (relevance will be discussed below). Given the above fluid inclusion and

recalculated $\delta^{18}O$ and $\delta^{13}C$ data it is interpreted that magmatic waters were first expelled into the country rock during HPP crystallization and were mixed with connate fluids in unaltered limestones, which formed skarn in the country rock.

Quartz veins on, away: Type II, primary inclusions within quartz veins *on* and *away* from the contact are low salinity (<5% Mass% eq. NaCl) and contain high temperatures Tt~410 to 650°C (Th_{total}~360°C) besides HPP-40, HPP-89, which have inclusions that were interpreted to be reequilibrated by later stage fluid events. Similar to Skarn WR (P) inclusions, quartz *on* and *away* inclusions have high pressure corrected and homogenization temperatures, the same composition (H_2O-NaCl-KCl), and fluid type (Type II), which suggests a comparable fluid origin. It is not unlikely that fluids responsible for skarn wall rock metasomatism are also the same or similar to fluids responsible for adjacent quartz vein formation. In typical intrusive environments, conduits for magmatic fluids expelled during crystallization are formed through hydrofracturing of the country rock, and depending on the composition of the fluids within the magma, these fractures are often filled with quartz, calcite, and ore minerals. Other fluid migration pathways are also considered including, but not limited to, pore space migration, faults, and bedding plane migration. However, no clear evidence was available to support this. Since it is proposed that skarn wall rock metasomatism was due to the infiltration of magmatic fluids, it can be interpreted that this type of fluid was also responsible for quartz vein formation *on* and *away* from the HPP contact.

Type B calcite veins (on): Type I inclusions in Type B calcite veins *on* are low salinity (<2% Mass% eq. NaCl) and contain low to intermediate fluid inclusion temperatures, Tt~235 to 388°C (Th_{total}~160°C). These cooler homogenization temperatures could result by calcite vein formation after the outer edge of the HPP was crystallized, or from an evolved and 'cooled' magmatic fluid. Field and petrographical evidence confirm that these veins regularly contain Pb-Zn sulfides including sphalerite, galena and pyrite and both would crosscut or be crosscut by quartz veins *on* and *away* from the HPP contact, suggesting contemporaneous formation. Similar to quartz veins *on* and *away* they cut calc-silicate wall rocks, but lack the distinct tremolite-diopside zonation around the vein. Recalculated $\delta^{18}O$ and $\delta^{13}C$ data average respectively 13.89‰ and 0.60‰ and some of the values fall near the *carbonatite*/*skarn* boxes suggesting a magmatic origin. This $\delta^{18}O$ value is also close to the magmatic $\delta^{18}O$ value (~+10‰) measured for the HPP (Barnes et al., 2001). However, a group within the *ore fluid* region infers mixing of meteoric and connate waters. Most studies conclude that fluids responsible for Pb-Zn and W skarn minerals and deposits are magmatically derived (Meinert, 1992). Based on the above crosscutting relationships with quartz veins, and fluid inclusion and stable isotope data it is concluded that Type B calcite veins *on* and associated Pb-Zn minerals were precipitated out of a dominantly magmatically derived fluid. Though some meteoric-connate mixing is possible due to the range in recalculated $\delta^{18}O$ and $\delta^{13}C$ data.

Phyllic WR*:* Type I, secondary inclusions within phyllic altered wall rocks around the HPP contact are low salinity (<3% Mass% eq. NaCl), and have low to

intermediate temperatures Tt~260 to 425°C (Th_{total}~180°C). These values are consistent with typical low salinity, intermediate temperature (200 to 450°C) fluids responsible for phyllic metasomatism. As discussed above, typical phyllic alteration is primarily the result of a magmatically derived fluid with increasing input of meteoric fluids away from the intrusion (Hedenquist, 1998). Evidence is lacking to support a quantitative estimate of a meteoric input. However, based on detailed hand and petrographic identification of classic phyllic replacement mineralogy (quartz-sericite-pyrite), consistent phyllic alteration fluid inclusion temperatures, and the assumption that phyllic alteration is the result of a primary magmatic fluid; it is concluded that the fluids responsible for this type of alteration are magmatically derived.

Potassic WR: Type I, secondary inclusions within potassically altered wall rocks contained some of the highest recorded Mass% eq. NaCl values (~8.14%), but some of the lowest pressure corrected and homogenization temperatures Tt~205 to 350°C (Th_{total}~170°C). Some inclusions even homogenized to a liquid as low as ~120°C. Due to these low trapping temperatures, and from mineral stability diagrams that require potassic wall rock metasomatism to be the result of high temperature metasomatic processes, it can be ruled out that fluids trapped in Type I fluid inclusions are responsible for this type of alteration. No evidence suggest that these fluids are dominantly magmatic or meteoric, however based on low trapping temperatures it is interpreted that the secondary fluids within potassically altered wall rocks are dominantly meteoric in origin. Based on petrographic and mineralogical evidence of the addition of patchy brown biotite

and granular K-feldspar to the original granodiorite/monzogranite host rock (K-metasomatism), and that potassic alteration is the result of high temperature fluids commonly of magmatic origin, it is interpreted that Potassic WR is the result of magmatic fluids. This type of alteration is very common in intrusive environments and porphyry style deposits, and has been found around many dikes in Jurassic plutonic centers in the Basin and Range province including the Yerington Copper Mining District located on the western edge of Nevada (Einaudi, 1994). Within this district, fluid inclusions associated with this type of alteration homogenize by halite dissolution from 150 to 500°C, and whole rock K-spar have $\delta^{18}O$ values from 6.5 to 8.4‰, which is consistent with magmatic water values (Einaudi, 1994). Hence, secondary inclusions measured in quartz in potassic wall rocks around the HPP are most likely not associated with the primary altering fluid.

5.4.3 Late HPP stage

Thermochronological data suggest rapid cooling of the pluton from initial emplacement (~36 Ma) to 33.3 Ma was to 285 ± 15°C (Burton, 1997). After 33.3 Ma, temperatures were relatively stable and decreased at approximately 8.5°C/My (Burton, 1997). In most plutonic centers cooling of the pluton is partly the result of convection of cool, surface derived meteoric fluids driven by the heat of the intrusion. Also, an increased thermal gradient provided by synchronous Basin and Range extension can contribute to deep meteoric convection (Ilchik and Barton, 1997). Evidence for meteoric water infiltration comes from isotopic studies by Fricke et al. (1992) who documented low δD (-125 to -175‰) and $\delta^{18}O$

(down to -4.4‰) values in mylonites within shear zones along the eastern flank of the Ruby Mountains. Fricke et al. (1992) also suggested that meteoric waters penetrated 5 to 10 km at depth during extensional deformation. Further evidence for meteoric water infiltration within and around the HPP is the presence of large hydrothermal quartz veins hosted within crosscutting brittle fault zones, which indicates that these fault zones were once conduits for fluid flow. Steeply dipping faults along the western side of the range also contain thick, white hydrothermal quartz veins. Also, the presence of active hot springs and sinter deposits along the eastern side of the range confirms continued geothermal activity. At this stage a cool crystallized HPP has degassed, and a convecting surface derived meteoric fluid now dominates.

***Skarn WR (S)*:** Type I, secondary fluid inclusions measured in quartz within skarn wall rocks *on* the contact are low salinity (~1% Mass% eq. NaCl), are composed of H_2O-NaCl-KCl, and fluid inclusion temperatures are low, Th_{total}~185°C to Tt~250 to 400°C. As described above, some Skarn WR samples (HPP-33, HPP-43) contain $\delta^{18}O$ and $\delta^{13}C$ values within or near the *ore fluid* region suggesting meteoric-connate mixing. Because of intermediate to low Tt and Th_{total} temperatures, and evidence of a meteoric component in recalculated carbon and oxygen isotope data, it is interpreted that the secondary fluid inclusions trapped within quartz within skarn wall rocks are the result of infiltration of local meteoric waters, which had likely mixed with connate fluids after initial cooling of the HPP.

Quartz veins and vugs (within): Type II inclusions within a large, crosscutting fault hosted quartz vein are low salinity (~1% Mass% eq. NaCl) and contain intermediate fluid inclusion temperatures Th_{total}~230°C to Tt~325 to 480°C. Later stage quartz fluids were precipitated as vugs (HPP-28V) within these quartz veins, and are also low salinity (~3.5% Mass% eq. NaCl), and contain some of the lowest trapping temperatures recorded within this study Th_{total}~155°C to Tt~200 to 360°C. Based on crosscutting relationships, open space filling textures, and low to intermediate homogenization temperatures, it is interpreted that these quartz veins and vugs hosted within steeply dipping faults are dominantly meteoric in origin.

5.5 MODEL FOR LINKAGES TO FLUIDS RESPONSIBLE FOR GOLD IN THE CARLIN TREND

The origin and source of fluids responsible for gold in Carlin-type deposits remains enigmatic and has been highly debated, and in view of the spatial and temporal association of gold mineralization with a distinct phase of plutonic magmatism has been narrowed down to two contrasting genetic models:

(1) Ore fluids were predominantly of magmatic origin derived from felsic magmas that crystallized at depth (10 to 15 km), which provided the ore components and thermal energy to drive fluid migration beyond the emplacement of the intruded plutons (Henry and Ressel, 2000; Ressel and Henry, 2006; Sillitoe and Bonham, 1990).

(2) Ore fluids were of meteoric origin that had convected to 10 to 15 km depth through sedimentary and meta-sedimentary rocks below the deposits. Here, fluids scavenged gold and other base metals and deposited them along high angle faults along trends in Northeastern Nevada (Emsbo et al., 2003; 2006).

Fluid inclusions studies from Hofstra et al. (1988); Jewell and Parry (1988); Osterberg (1990); Cline et al. (1995); and Kuehn and Rose (1995) indicate that in most cases, two hydrothermal fluids were present during gold mineralization. Both fluids are relatively low salinity (<6 % wt% eq. NaCl), and homogenize from 150 to 220°C at likely pressures between ~400 to 1500 bars. However, one fluid appears to be more saline and contain significant dissolved gas (CO_2). Other species including N_2+H_2S+CH_4±SO_2±Ar± short-chain hydrocarbons have also been observed.

Inclusions of ore stage fluids in most veins within Carlin-type deposits require a pressure correction. If ore deposition occurred between shallow hydrostatic and deeper overpressured environments at 3.8±1.9 km, and most inclusions within Carlin-type deposits have homogenization temperatures between 150 to 220°C, then for an approximate pressure correction of 10°C/km, the true trapping temperature (Tt) for most late gold ore veins will range between ~170 to 280°C (Kuehn and Rose, 1995). This Tt range will be compared against calculated Tt ranges around the HPP.

δD_{H_2O} data (δD_{H_2O}<-100‰) of fluid inclusions and alteration phases suggest ore fluids were isotopically light and likely to be derived from Later Cretaceous or

Tertiary meteoric water (Rye et al., 1974; Radtke et al., 1980; Ilchik, 1990b; Hofstra, 1994). $\delta^{18}O$ values measured from fluids inclusions within jasperoid range between -10 to +4% (Rye, 1985; Hofstra et al., 1988; Holland et al., 1988; Ilchik, 1990a). Positive values have been interpreted to indicate that ore fluids likely interacted with sedimentary rocks, prior to gold deposition. $\delta^{13}C$ and $\delta^{18}O$ isotope data from mostly calcite and dolomite in host unaltered carbonate rocks, in Carlin-type deposits generally have $\delta^{18}O$ and $\delta^{13}C$ values of +18 to +24‰ and -2 to +1‰ respectively, which is consistent with the unaltered wall rock isotope compositions in this study. In most deposits, a broad $\delta^{18}O$ decrease is observed with increasing hydrothermal alteration, which is also observed in this study in skarn wall rocks and calcite veins *on* the contact. Also, $\delta^{13}C$ values generally increase and $\delta^{18}O$ decrease adjacent to fractures and veins which might be the result of reequilibration of the rock with the fluids at higher temperatures or input of magmatically or meteorically sourced CO_2, but this is yet to be determined (Arehart, 1996).

Gold is interpreted to have been transported as a bisuflide complex ($Au(HS)_2^-$) and gold deposition is believed to have occurred by more than one mechanism including fluid mixing between a reduced, gold bisulfide-bearing solution at relatively high temperatures with a cooler, oxidized, less saline meteoric fluid. This would result in oxidation, dilution, and cooling of the ore fluid (Arehart, 1996). Recent hydrogen and oxygen, and LA-ICP-MS data on Cu and Au in silicate glasses from Muntean et al. (2011) support this mixing theory suggesting that the ore fluids responsible for Carlin-type deposits were a product of meteoric

and magmatic fluid mixing at ~<10 km depths. They propose that the initial primitive Au ore fluid was separated out into an immiscible high salinity and low salinity (~3 to 5 wt% NaCl) vapor fluid as it ascended away from the magmatic fluid source. Au, Cu, As, Sb, and S are preferentially transported in the vapor phase and subsequently focused along high-angle faults away from the source magma. Upon cooling and further fluid ascent, increasing density differences between the high salinity and vapor fluids, would have promoted the vapor phase leaving behind the high salinity fluid at depth (Muntean et al., 2011). As the fluids continued to ascend through the crust, they were subjected to meteoric water infiltration, which increased the cooling rate of the ascending fluids. At this point, the ore fluid would have been ~250°C and 2 to 3 wt% NaCl, which is consistent with fluid inclusion chemistry in most Carlin-type gold deposits (Muntean et al., 2011). These mixed fluids where then transported, and focused into high angle faults along the Carlin trend containing reactive carbonate wall rocks where gold was precipitated and adsorbed onto pyrite and arsenopyrite (Muntean et al., 2011).

Much of this meteoric-mixing model proposed by Muntean et al. (2011) is consistent with the fluid inclusion and stable isotope data recorded around the HPP, besides evidence for a high salinity fluid during early stages of primitive Au ore fluid separation. It is demonstrated that both meteoric and magmatic fluid signatures are present *within* the HPP and *on* and *away* from the HPP contact. It is also shown that there exist a dominant low salinity (~3% Mass% eq. NaCl) vapor-rich (Type II) magmatic phase that has trapping temperatures Tt~390 to

590°C. These Type II vapor-rich inclusions found within early HPP stage quartz veins, miarolitic cavities, and Skarn WR (P) could represent the vapor rich magmatic phase in which Au and other base metals were transported. As the vapor rich fluid rose through the crust, it would have evolved and most likely become immiscible with Type III, CO_2-rich inclusions. The fluid would also have cooled and may represent the less vapor rich, early HPP stage, magmatically derived Type I inclusions within Type B calcite veins *on*, and Phyllic WR. Further cooling and ascent of this fluid would have interacted with convecting meteoric waters at shallower depths. At this point, both meteoric and magmatic phases are mixed. The range of recalculated $\delta^{18}O$ values broadly supports evidence of mixing of end member meteoric and magmatic fluid components. As the magmatic phase becomes more diluted by the circulating meteoric convection cell (Later HPP stage) low salinity (~3% Mass% eq. NaCl) and low temperature (Tt~200 to 480°C) inclusions in Potassic WR, Skarn WR (S) and major fault hosted quartz veins/vugs *within* are trapped, which overlaps with the temperatures and salinity of fluid inclusions in gold ore stage quartz veins (Tt~170 to 280°C; <6 % wt% eq. NaCl). There was likely mixing above the HPP (Figure 5.2D), but now the country rock has either been eroded or downthrown below the Ruby Valley graben. The above relationships are interpreted to be consistent with the mixed meteoric/magmatic fluid Carlin-type gold deposit model proposed by Muntean et al. (2011).

Fluid inclusion and isotope data display an intimate relationship between meteoric and magmatic fluid signatures. Therefore, it is concluded that the fluid

responsible for gold deposition is of mixed origin between magmatic and meteoric fluids (Muntean et al., 2011; Kuehn and Rose, 1995) and connate waters. The convergence of these processes is not geologically unusual, and not necessarily unique to the Great Basin. Many other ore deposits are proposed to be derived from similar major thermal and hydrothermal events including the giant Bingham Canyon porphyry Cu-Au-Mo deposit and Mount Hope porphyry Mo deposits, and the Neoarchean orogenic gold deposits in the Superior craton of eastern Canada and the Yilgarn craton of Western Australia (Muntean et al., 2011).

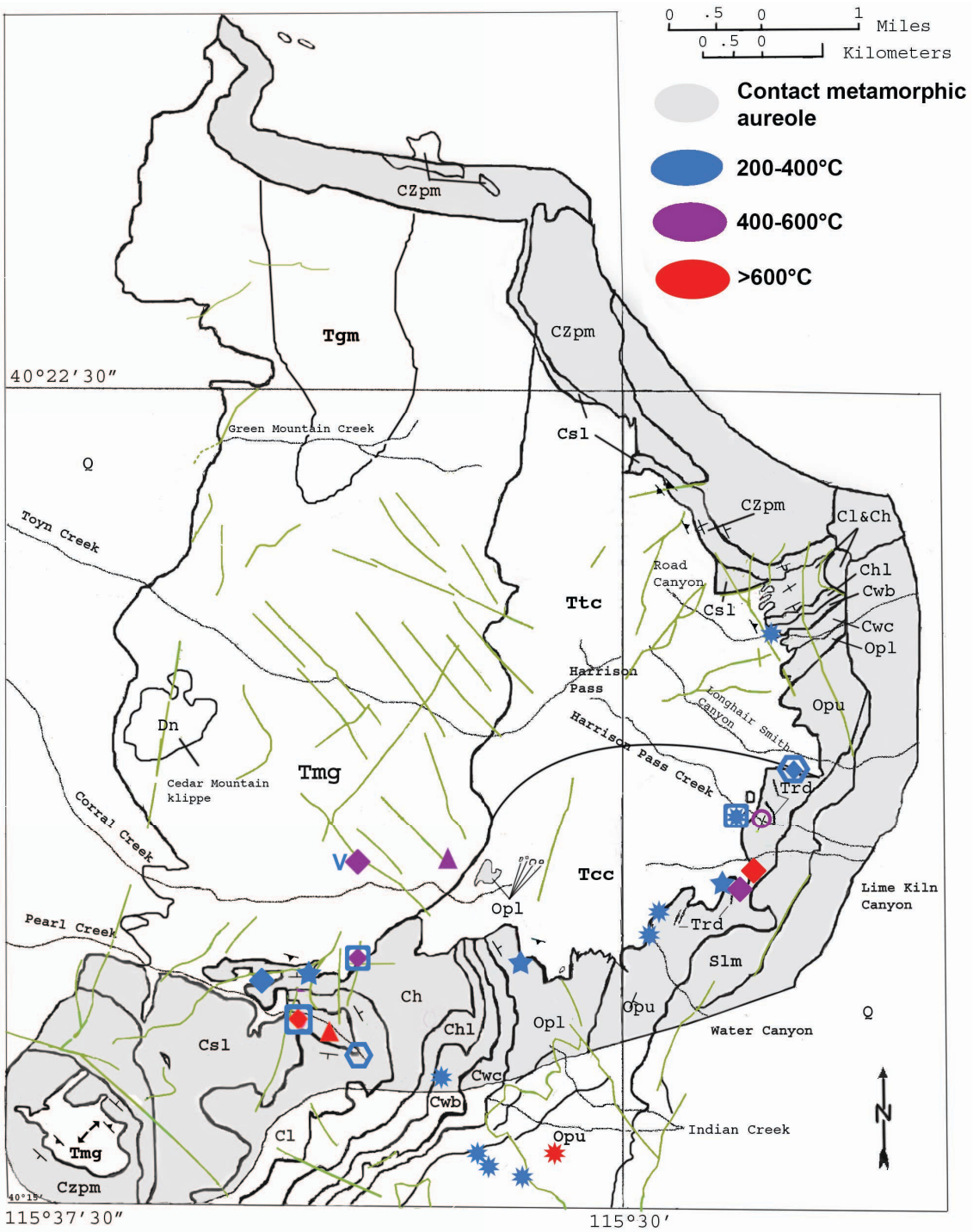

Figure 5.1: Map showing the distribution of average Tt values around the HPP. On average, Th_{total} values are adjusted 90 to 275°C based on the range of HPP emplacement pressures of ~1600 to 3200 bars. Type I fluid inclusions are represented by the 200 to 400°C group, besides HPP-43 (Type B calcite vein *on*). Type II and III inclusions are represented by both 200 to 400°C and >600°C groups. The same symbols used in Figure 4.8, are also used in this figure.

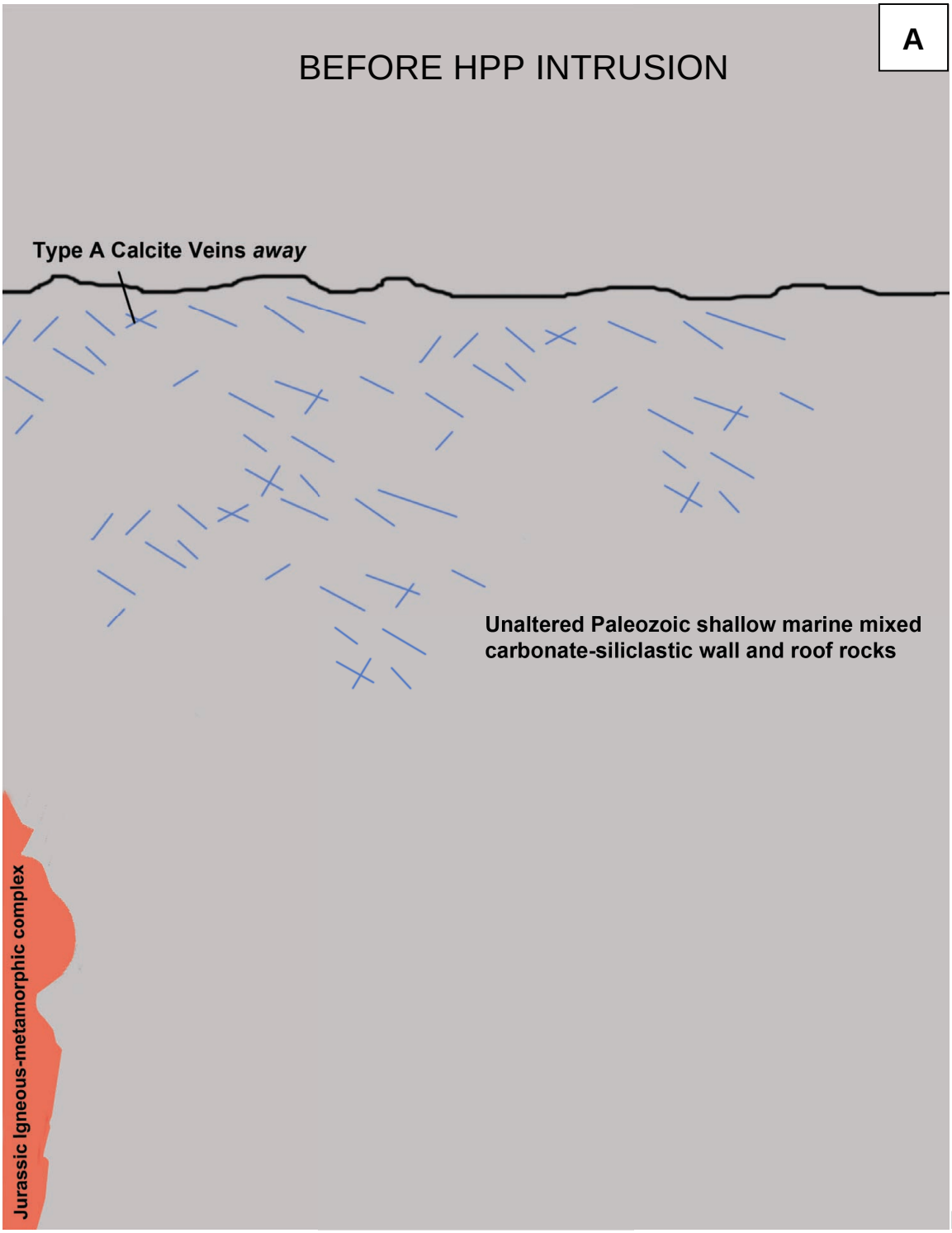
A
BEFORE HPP INTRUSION
Type A Calcite Veins *away*
Unaltered Paleozoic shallow marine mixed carbonate-siliclastic wall and roof rocks
Jurassic Igneous-metamorphic complex

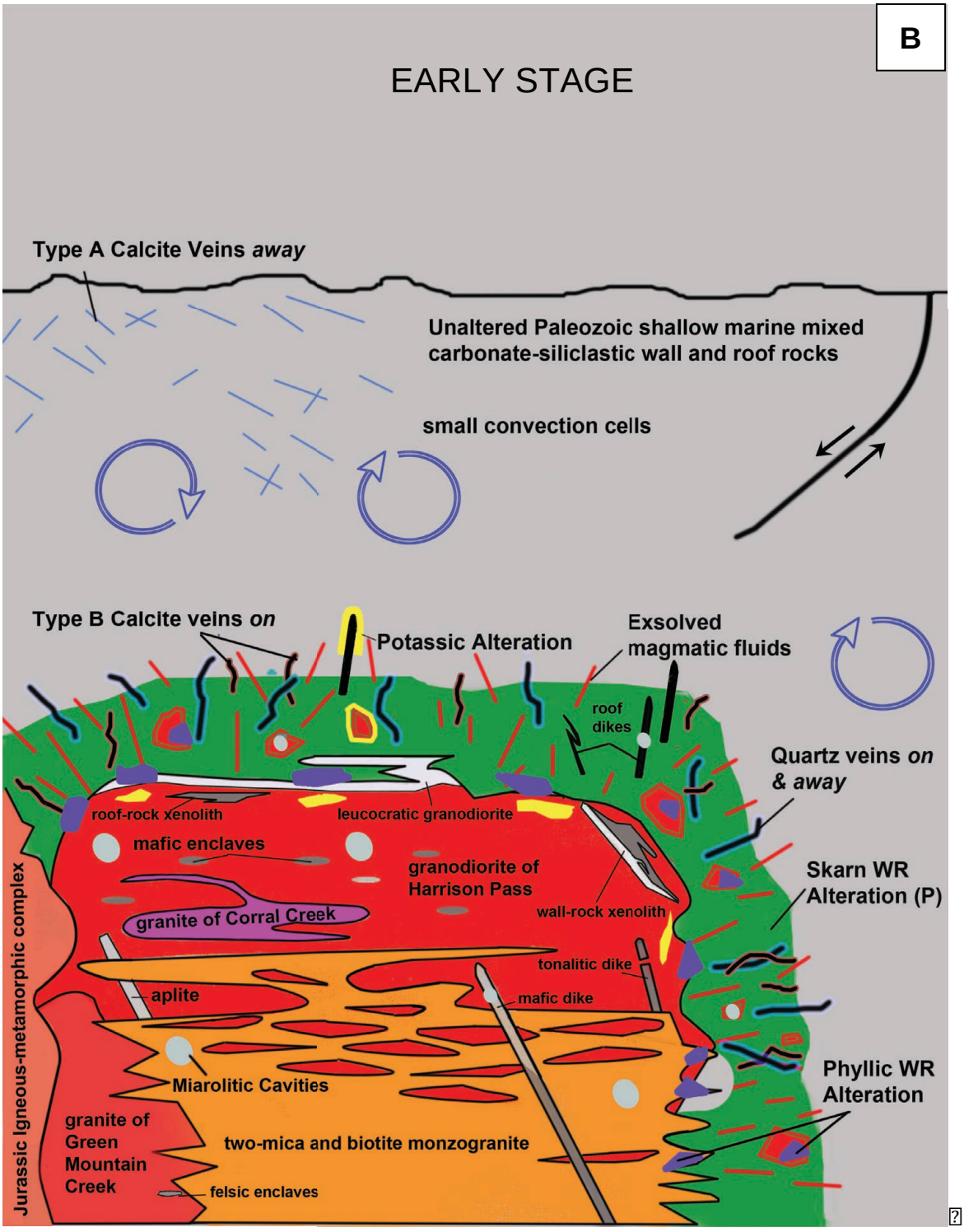
B
EARLY STAGE
Type A Calcite Veins *away*
Unaltered Paleozoic shallow marine mixed carbonate-siliclastic wall and roof rocks
small convection cells
Type B Calcite veins *on*
Potassic Alteration
Exsolved magmatic fluids
roof dikes
Quartz veins *on* & *away*
roof-rock xenolith
leucocratic granodiorite
mafic enclaves
granodiorite of Harrison Pass
Skarn WR Alteration (P)
granite of Corral Creek
wall-rock xenolith
tonalitic dike
aplite
mafic dike
Miarolitic Cavities
Phyllic WR Alteration
granite of Green Mountain Creek
two-mica and biotite monzogranite
felsic enclaves
Jurassic Igneous-metamorphic complex

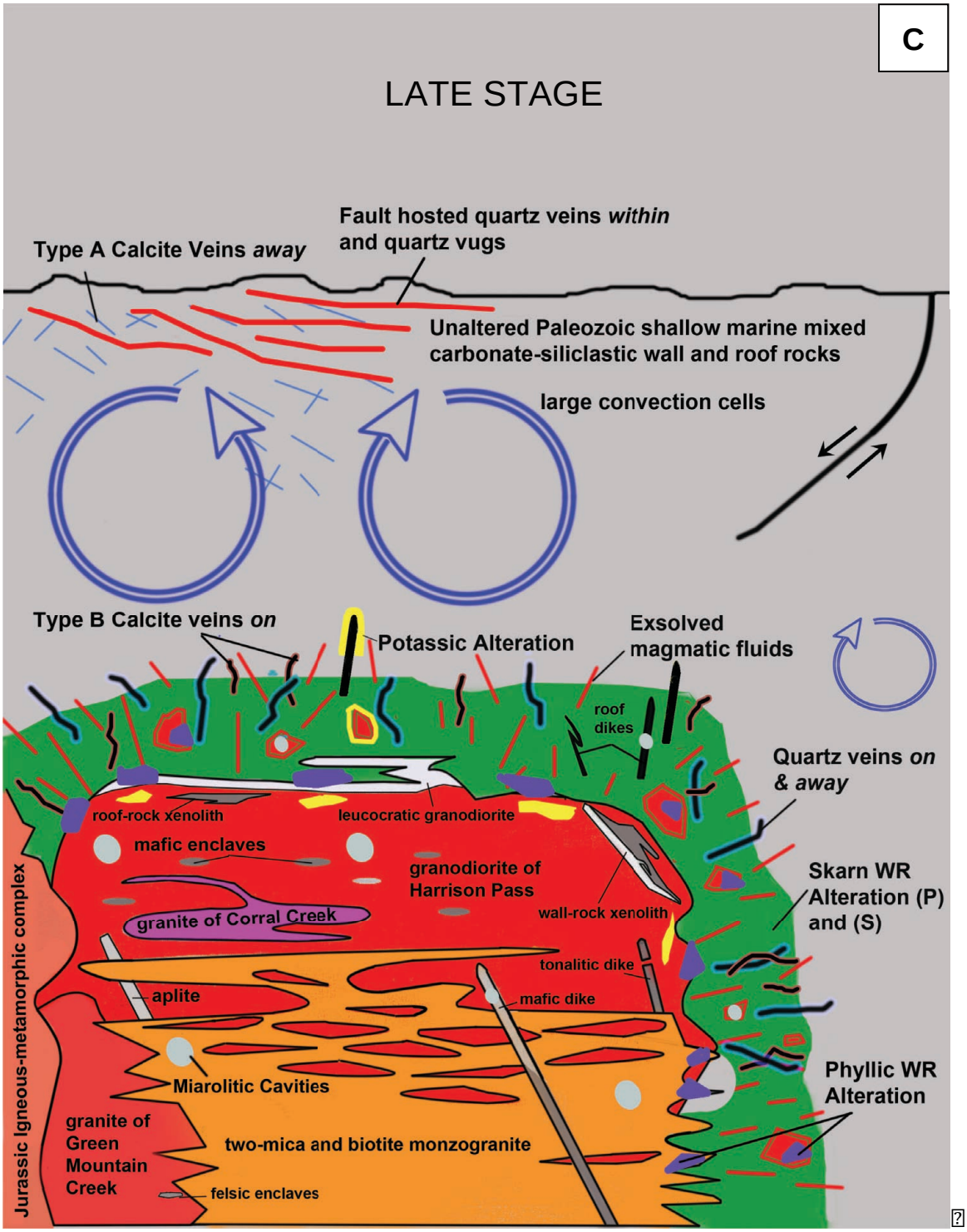
C
LATE STAGE
Type A Calcite Veins *away*
Fault hosted quartz veins *within* and quartz vugs
Unaltered Paleozoic shallow marine mixed carbonate-siliclastic wall and roof rocks
large convection cells
Type B Calcite veins *on*
Potassic Alteration
Exsolved magmatic fluids
roof dikes
Quartz veins *on* & *away*
roof-rock xenolith
leucocratic granodiorite
mafic enclaves
granodiorite of Harrison Pass
granite of Corral Creek
wall-rock xenolith
Skarn WR Alteration (P) and (S)
tonalitic dike
aplite
mafic dike
Miarolitic Cavities
Phyllic WR Alteration
granite of Green Mountain Creek
two-mica and biotite monzogranite
felsic enclaves
Jurassic Igneous-metamorphic complex

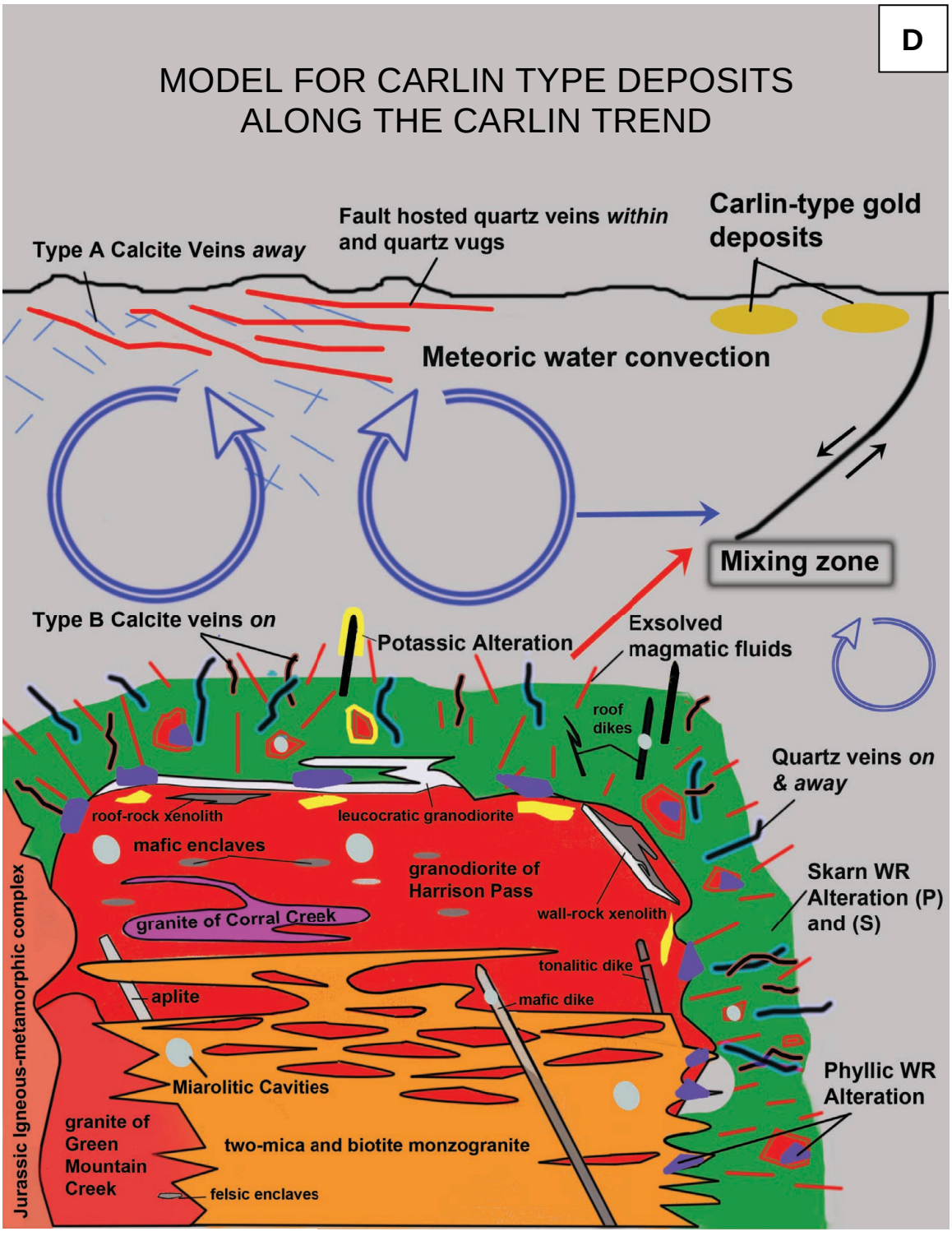

Figure 5.2: Figures showing the evolution of fluid circulation around the HPP; Before HPP intrusion (A), Early HPP Stage (B), and Late HPP Stage (C). A model for the source of fluids responsible for transporting gold in the Carlin trend is also shown (D) after Muntean et al. 2011.

6. CONCLUSION

6.1 SUMMARY

The HPP is a ~36 Ma 110 km^2 multiphase, granodiorite to monzogranite, high-K calc-alkaline pluton that intruded into the transition zone of the RMEHR core complex. It was emplaced during ‘inland’ arc-style magmatism that swept NE-SW across western Utah and much of Nevada between 40 and 32.6 Ma, and was broadly contemporaneous with the onset of Basin and Range extension that commenced during or shortly after intrusion. This timing of magmatism and extension also corresponds to the regional hydrothermal event responsible for Carlin-type gold mineralization. Field, petrological, fluid inclusion microthermometry, and stable isotope investigations were carried out on early magmatic and later meteoric fluid circulation phases around the HPP, which has provided insight into what type(s) of fluids are responsible for Carlin-type gold deposits.

Skarn, phyllic and potassic wall rock alteration styles are recorded around the HPP. Skarn mineralogy is uniform in most locations and consists of diopside+tremolite+calcite+quartz±hydrogrossular±epidote. This alteration is pervasive within Ordovician and Cambrian metasedimentary siliciclastic carbonate wall rocks, and forms an approximate 0.5 to 3 m wide discontinuous zone *on* and locally *away* from the pluton-wall rock contact. Phyllic alteration is

characterized by a quartz+sericite+pyrite mineral assemblage within both Early and Late stages of the HPP, and is observed *on* the contact and within apophyses of the intrusion. Sparse potassic alteration is found *on* and locally *away* from the pluton margin near the roof zone of the HPP, and consists of patchy brown biotite and granular K-spar in granodiorite/monzogranite.

Quartz, calcite, and calcite-polymetallic sulfide veins are the dominant types of veins observed *within* the pluton and *on* and *away* from the contact. Fault-hosted major quartz veins *within* the HPP are thick (~4 to 8 m), white, and sharply crosscut the pluton-wall rock contact. Minor quartz veins *on* and *away* from the pluton contact occur mostly in fractured and brecciated mixed siliciclastic-carbonate skarn limestone and phyllically altered granodioritic host rocks. Type B calcite veins (~mm's to 40 to 50 mm) *on* the contact are sharply adjacent to skarn wall rocks, are often massive and sugary and contain pockets and/or veins of sulfides including galena, sphalerite, pyrite, and magnetite. Type A calcite veins *away* from the contact contain sharp contacts with unaltered metasedimentary rocks, are ~cm's to 15 to 20 cm across, and contains medium to coarse-grained calcite with trace quartz±pyrite±iron oxides.

Fluid inclusion microthermometry revealed Type I, II, and III fluid inclusions *within* the HPP and *on* and *away* from the contact. All fluid types contain low Mass% eq. NaCl (~<10%) values and based on $T_{eutectic}$ ranges (-10 to -30°C) are composed of H_2O-NaCl-KCl besides Type III inclusions, which contain an carbonic phase (CO_2-H_2O-NaCl-KCl). These types are divided based on their phases, fv ratio, and homogenization temperatures. Type I <200°C, Type II

>200°C and Type III >200°C + contain a carbonic phase. Further $\delta^{13}C$ and $\delta^{18}O$ isotope analyses constrain fluid sources into mostly mixed origins between connate, magmatic, and meteoric fluid end members. Combining field, petrologic, fluid inclusion microthermometry and carbon and oxygen stable isotope data allowed a reconstruction of the fluid history around the HPP.

Based on crosscutting relationships, connate fluids within unaltered sedimentary wall rocks and Type A calcite veins *away* from the contact are considered to predate the HPP intrusion. Fluids within these veins and wall rocks display typical $\delta^{18}O$ (~27‰) and $\delta^{13}C$ (~2.5‰) values of unaltered limestones, and Type I (H_2O-NaCl-KCl), primary inclusions suggest that fluids are low salinity (~1% Mass% eq. NaCl) and were trapped at low temperatures, Th_{total}~125°C to Tt~195 to 340°C. Lower $\delta^{18}O$ values (~7‰) in some samples likely indicate a mixed origin between circulating meteoric and connate fluids, driven either by Basin and Range extension or from heat from the HPP intrusion.

Early magmatic phases of the HPP expelled hot, magmatic fluids during crystallization, and are interpreted to be responsible for the formation of miarolitic cavities, skarn, potassic, and phyllically altered wall rocks, quartz veins and Type B calcite veins *within* the HPP and *on* and locally *away* from the contact. Evidence for magmatically derived fluids is supported by low salinity (~4% Mass% eq. NaCl), high trapping temperatures Tt~450 to 650°C (Th_{total}~240°C) in Type III CO_2-rich (CO_2-H_2O-NaCl-KCl) primary inclusions within miarolitic cavities, and by low salinity (~3% Mass% eq. NaCl), high trapping Tt~390 to 590°C (Th_{total}~315°C) Type II, vapor-rich (H_2O-NaCl-KCl) primary inclusions

within quartz veins, skarn wall rocks, and miarolitic cavities. Further evidence is provided by $\delta^{18}O$ and $\delta^{13}C$ values (13.89 and 0.60‰) within Pb-Zn bearing calcite veins *on* the contact, and the $\delta^{18}O$ and $\delta^{13}C$ values (8.63 and -0.75‰) within skarn wall rocks *on* the contact, which show a mixing line between connate and magmatic theoretical fluid ranges indicating a mixed magmatic-connate fluid source. Mineralogical evidence in skarn wall rocks around the HPP also confirms a primary magmatic origin. Most skarn wall rocks contain tremolite+diopside+calcite+quartz and in some wall rocks hydrogrossular+epidote, which is a typical calc-silicate mineral assemblage in metamorphic aureoles as the result of an infiltration of magmatic fluids.

A later, cooler convecting meteoric phase driven by the heat during and after intrusion is observed within low salinity (~1% Mass% eq. NaCl) major crosscutting fault hosted quartz veins and vugs. Type II fluid inclusions within these quartz veins are characterized by intermediate temperatures, Th_{total}~230°C to Tt~325-480°C, and Type I inclusions in quartz vugs are low temperatures Th_{total}~150°C to Tt~200-360°C. Secondary inclusions in skarn wall rocks are also determined to be a formed from a later stage meteoric event due to mixed meteoric-connate $\delta^{18}O$ and $\delta^{13}C$ values (4.42‰ and 2.09) in some samples and low to intermediate trapping temperatures Th_{total}~185°C to Tt~250 to 400°C.

In comparison with other end member models proposed for the origin of Carlin-type gold deposits associated with a distinct plutonic phase, this study supports much of the meteoric-mixing model proposed by Muntean et al. (2011). It is demonstrated that both meteoric and magmatic fluid signatures are present

within the HPP and *on* and *away* from the contact and commonly are mixed. It is also shown that there exists a dominant low salinity (~3% Mass% eq. NaCl) vapor-rich (Type II) magmatic phase that has Tt~390 to 590°C. These Type II vapor-rich, primary inclusions found within 'Early Stage' quartz veins, miarolitic cavities, and skarn wall rocks, could represent the immiscible vapor-rich magmatic phase from the CO_2-rich phase (Type III inclusions) in which Au and other base metals were transported. As the vapor-rich fluid rose through the crust, it would have evolved and cooled and may represent the less vapor-rich, Early Stage, magmatically derived Type I inclusions within Type B calcite veins *on* the contact and phyllically altered wall rocks. Further cooling and ascent of this fluid would have interacted with convecting meteoric waters at shallower depths, and at this point, both meteoric and magmatic phases are mixed. The range of recalculated $\delta^{18}O$ (1.09 to 29.36‰), and $\delta^{13}C$ (-2.17 to 3.80‰) values broadly supports evidence of mixing of end member meteoric and magmatic fluid components. As the magmatic phase becomes more diluted by the circulating meteoric convection cell (Late Stage), low salinity (~3% Mass% eq. NaCl) and low temperature (Th_{total}~180 to Tt~200 to 480°C) secondary inclusions in skarn wall rocks and major fault hosted quartz veins/vugs within are trapped. There was likely mixing above the pluton, but in rocks now eroded or downthrown below the Ruby Valley graben. It is interpreted that mixed fluids were then focused along high angle faults as a result of Basin and Range extension, observed along the flanks of the HPP, where a mixture of further cooling,

oxidation and fluid-rock reactions resulted in gold deposition within pyrite and arsenopyrite within sedimentary country rocks along the Carlin trend.

6.2 FUTURE RESEARCH

Further work is needed to better characterize the fluid relationships and associated mineralization around the HPP. Detailed geochemical analyses including Electron-Microprobe Analysis (EMPA) would help constrain sulfide phases that would likely have influenced ore element behavior and element fractionation into fluid phases around the HPP. To better constrain fluid composition, Laser Raman Spectroscopy and Laser Ablation Inductively Couple Plasma Mass Spectrometry (LAICPMS) techniques on fluid inclusions would help recognize the presence and concentration of minor gas components (CH_4, N_2, H_2S) and provide multi-element data, particularly Au, Cu and Pb down to a ppm level. Further geochemical work on quartz-feldspar pegmatitic segregations and abundant aplites observed within the HPP would further constrain the magmatic exsolution phases of the HPP. Also, petrographic and geochemical studies of nearby Eocene high-level stocks, such as the Railroad intrusion, could be conducted to see whether and how hydrothermal fluids at this stock differ from those of the HPP, which would provide more insight into the chemistry and composition of magmatohydrothermal fluids during the Eocene.

REFERENCES

Arehart, G.B., Eldridge, C.S., Chryssoulis, S.L., Kesler, S.E. and O'Neil, J.R., 1993b, Ion microprobe determination of gold, arsenic, and sulfur isotopes in sulfides from the Post/Betze sediment-hosted disseminated gold deposit, Nevada; Geochimica et Cosmochimica Acta, v. 57, p.1505-1520.

Arehart, G.B., 1996, Characteristics and origin of sediment-hosted disseminated gold deposits: A review, Ore Geology Reviews, v.11, p. 383-403.

Arehart, G., Coolbaugh, M.F., and Poulson, S.R., 2003, Evidence for a magmatic source of heat for the Steamboat Springs geothermal system using trace elements and gas geochemistry: Geothermal Resources Council Transactions, v. 27, p. 269–274.

Archer, D.G., 1992, Thermodynamic properties of the NaCl + H2O system: II. Thermodynamic properties of NaCl (aq), NaCl $2H_2O$(cr), and phase equilibria, J. Phys. Chem. Ref. Data, v. 28, p. 1-17.

Bakker, R.J., 2003, Package FLUIDS 1. Computer programs for analysis of fluid inclusion data and for modeling bulk fluid properties. Chemical Geology, v. 194, p. 3-23.

Barnes, C.G., Burton, B.R., Burling, T.C., Wright, J.E., and Karlsson, H.R., 2001, Petrology and geochemistry of the late Eocene Harrison Pass pluton, Ruby Mountains core complex, northeastern Nevada, Journal of Petrology, v. 42, p. 901-929.

Barton, M.D., Ilchik, R.P., and Marikos, M.A., 1991, Metasomatism: in Kerrick, D. M., Contact Metamorphism, Reviews in Mineralogy, v. 26, p. 321-350.

Bodnar, R.J., 1993, Revised equation and table for determining the freezing point depression of H2O-NaCl solutions, Geochimica et Cosmochimica Acta, v. 57, p. 683–684.

Burnham, C.W., 1979, Magmas and hydrothermal Fluids, in Geochemistry of Hydrothermal Ore Deposits, Barnes, H.L., 2nd ed., Wiley, New York, p. 63-124.

Burton, B., 1997, Structural geology and emplacement history of the Harrison Pass pluton, central Ruby Mountains, Elko County, Nevada. Ph.D. thesis, University of Wyoming, Laramie, Wyoming, p. 295.

Candela, P.A,, Holland, H.D., 1984, The partitioning of copper and molybdenum between silicate melts and aqueous fluids, Geochimica et Cosmochimica Acta, v. 48, p. 373-380.

Cathles, L. M., 1977, An analysis of the cooling of intrusives by ground-water convection which includes boiling: Economic Geology, v. 72, 804-826.

Chacko T., Mayeda T.K., Clayton R.N., and Goldsmith J.R., 1991, Oxygen and carbon isotope fractionations between CO_2 and calcite, Geochimica et Cosmochimica Acta, v. 55, p. 2867-2882.

Cline, J.S., Hofstra, A.H., Landis, G.P., Allerton, S.B., Gent, C.A., and Eastoe, C.J., 1995, Stable isotope and gas compositions of ore fluids at Getchell Mine, Nevada: Evidence for contrasting ore fluids. Geol. Soc. Am. Abstr. Prog. 27: A66.

Cline, J.S., Hofstra, A.H., Muntean, J.L., Tosdal, R.M., and Hickey, K.A., 2005, Carlin-type gold deposits in Nevada: Critical geologic characteristics and viable models: Economic Geology 100th Anniversary Volume, p. 451−484.

Craig H., 1957, Isotopic standards for carbon and oxygen and correction factors for mass spectrometer analysis of carbon dioxide, Geochimica et Cosmochimica Acta, v.12, p. 133-149.

Deans, R.L.J., 2010, Trace element and calculated temperature variation in quartz and titanite in the 36 Ma Harrison Pass pluton, Ruby Mountains NE Nevada, M.S. Thesis, Texas Tech University, p. 88.

Dickinson, W. R., 2006, Geotectonic evolution of the Great Basin, Geosphere, v. 2, p. 353-368.

Duan, Z., M∅ller, N., and Weare, J. H., 1992a, An equation of state for the CH_4-CO_2-H_2O system: I. Pure systems from 0 to 1000°C and 0 to 8000 bar, Geochimica et Cosmochimica Acta, v. 56, no. 7, p. 2605-2617.

Duan, Z., M∅ller, N., and Weare, J.H., 1992b, An equation of state for the CH_4-CO_2- H_2O system: II. Mixtures from 50 to 1000°C and 0 to 1000 bar, Geochimica et Cosmochimica Acta, v. 56, p. 2619-2631.

Einaudi, M.T., 1994, 6-km vertical cross section through porphyry copper deposits, Yerington District, Nevada: multiple intrusions, fluids, and metal sources: SEG International Exchange Lecture, June.

Emsbo, P. Hofstra, A.H., Lauha, E.A., Griffin, G.L., and Hutchinson, R.W., 2003, Origin of high-grade gold ore, source of ore fluid components, and genesis of

the Meikle and neighboring Carlin-type deposits, northern Carlin Trend, Nevada, Economic Geology, v. 98, p. 1069-1105.

Emsbo, P., Groves, D.I., Hofstra, A.H., and Bierlein, F.P., 2006, The giant Carlin gold province; A protracted interplay of orogenic, basinal, and hydrothermal processes above a lithospheric boundary, Mineralium Deposita, v. 41, p. 517-525.

Florindo, F., Roberts, A. P., and Palmer, M. R.. 2003, Magnetite dissolution in siliceous sediments, Geochem. Geophys. Geosystems, v. 4, no. 7, p. 13.

Fricke, H.C., Wickham, S.M., and O'Neil, J.R., 1992, Oxygen and hydrogen isotope evidence for meteoric water infiltration during mylonitisation and uplift in the Ruby mountains-East Humboldt Range core complex, Nevada. Contributions to Mineralogy and Petrology, v. 111, p. 203-221.

Franklin, J.M., Sangster, D.M., Lydon, J.W., 1981, Volcanic Associated Massive Sulphide Deposits, Economic Geology 75th Anniversary Volume, p. 485 627.

Furlong, K.P., Hanson, R.B., and Bowers, J.R., 1991, Modeling thermal regimes, in Kerrick, D.A., ed., Contact metamorphism: Reviews in Mineralogy, v. 26, p. 437-505.

Grauch, V.J.S., Rodriguez B.D., and Wooden J.L., 2003, Geophysical and isotopic constraints on crustal structure related to mineral trends in north-central Nevada and implications for tectonic history, Economic Geology, v. 98, p. 269-286.

Hedenquist, J.W., Arribas, A., Jr., and Reynolds, T.J., 1998, Evolution of an intrusion-centered hydrothermal system: Far Southeast-Lepanto porphyry and epithermal Cu-Au deposits, Philippines, Economic Geology, v. 93, p. 373–404.

Henry, C.D., and Boden, D.R., 1998, Eocene magmatism: the heat source for Carlin-type gold deposits of northern Nevada, Geology, v. 26, p. 1067-1070.

Henry, C. D., and Ressel M.W., 2000, Eocene magmatism of northeastern Nevada: The smoking gun for Carlin-type gold deposits, Geological Society of Nevada Symposium 2000 Proceedings, p. 365-388.

Hofstra. A.H., Northrop, H.R., Rye, R.O., Landis, G.P. and Birak, D.J., 1988, Origin of sediment-hosted disseminated gold deposits by fluid mixing - Evidence from jasperoids in the Jerritt Canyon gold district, Nevada, USA, Proceedings of Bicentennial Gold '88, p. 284-289.

Hofstra, A.H., 1994, Geology and genesis of the Carlin-type gold deposits in the Jerritt Canyon district, Nevada, Ph.D. dissertation, University of Colorado, Boulder, Colorado, p. 719.

Hofstra, A.H., and Rye, R.O., 1998, δD and $\delta^{18}O$ data from Carlin-type gold deposits-Implications for genetic models, in Tosdal, R. M., ed., Contributions to the gold metallogeny of northern Nevada, U. S. Geological Survey Open File Report 98-338, p. 202-210.

Hofstra, A.H., Snee, L.W., Rye, R.O., Folger, H.W., Phinisey, J.D., Loranger, R.J., Dahl, A.R., Naeser, C.W., Stein, H.J., and Lewchuk, M., 1999, Age constraints on Jerritt Canyon and other Carlin-type gold deposits in the western United States—Relationship to mid-Tertiary extension and magmatism, Economic Geology, v. 94, p. 769-802.

Hofstra, A.H., and Cline, J.S., 2000, Characteristics and models for Carlin-type gold deposits, SEG Reviews in Economic Geology, v. 13, p. 163-220.

Holland, P.T., Beaty, D.W. and Snow, G.G., 1988, Comparative elemental and oxygen isotope geochemistry of jasperoid in the northern Great Basin: Evidence for distinctive fluid evolution in gold-producing hydrothermal systems, Economic Geology, v. 83, p. 1401-1423.

Howard, K. A., 2003, Crustal structure in the Elko-Carlin region, Nevada during Eocene gold mineralization: Ruby-East Humboldt metamorphic core complex as a guide to the deep crust. Economic Geology, v. 98, p. 249-268.

Hudec, M.R., 1990, The structural and thermal evolution of the Central Ruby Mountains, Elko County, Nevada, Laramie, Wyoming, Ph.D. dissertation, University of Wyoming, p. 272.

Ilchik, R.P., 1990a, Geology and geochemistry of the Vantage gold deposits, Alligator Ridge-Bald Mountain mining district, Nevada, Economic Geology, v. 85, p. 50-75.

Ilchik, R.P., 1990b, Geology and genesis of the Vantage gold deposits, Alligator Ridge-Bald Mountain mining district, Nevada, Unpublished Ph.D. dissertation, University of California at Los Angeles, Los Angeles, California, p. 138.

Ilchik, R.P., and Barton, M.D., 1997, An amagmatic origin of Carlin-type gold deposits, Economic Geology, v. 92, p. 269-288.

Jewell, P.W. and Parry, W.T., 1987, Geology and hydrothermal alteration of the Mercur gold deposit, Utah, Economic Geology, v. 82,1958-1966.

Kamenetsky, V.S., Wolfe, R.C., Eggins, S.M., Mernagh, T.P. and Bastrakov, E. 1999, Volatile exsolution at the Dinkidi Cu-Au porphyry deposit, Philippines: A

melt-inclusion record of the initial ore-forming process, Geology, v. 27, p. 691-694.

Kamenetsky, V.S., Naumov, V.B., Davidson, P., Van Achterbergh, E. and Ryan, C.G. 2004, Immiscibility between silicate magmas and aqueous fluids: a melt inclusion pursuit into the magmatic-hydrothermal transition in the Omsukchan Granite (NE Russia), Chem. Geol., v. 210, p. 73-90.

Kistler, R.W., Ghent, E.D., and O'Neil, J.R., 1981. Petrogenesis of gamet two mica granites in the Ruby Mountains, Nevada. Jour. Geophys. Res., v. 86, p. 10,591-10,606.

Kuehn, C. A., and Rose, A. W., 1995, Carlin gold deposits, Nevada: Origin in a deep zone of mixing between normally pressured and over pressured fluids: Economic Geology, v. 90, p. 17–36.

Labotka, T.C., 1991, Chemical and physical properties of fluids, Rev. Mineral. v. 26, p. 43-104.

Lapointe, D.D., Tingley, J.V., and Jones, R.B., 1991, Mineral Resources of Elko County, Nevada. Nevada Bureau of Mines and Geology Bulletin 106, p. 236.

Lowell, J.D., and Guilbert, J.M., 1970, Lateral and vertical alteration mineralization zoning in porphyry ore deposits, Economic Geology, v. 65, p. 373-408.

Lowenstern, J.B., 2001, Carbon dioxide in magmas and implications for hydrothermal systems, Mineralium Deposita, v. 36, p. 490-502.

MacCready, T., Snoke, A. W., Wright J. E., and Howard, K. A., 1997, Mid-crustal flow during Tertiary extension in the Ruby Mountains core complex, Nevada, Geological Society of America Bulletin, v. 109, p. 1576-1594.

Meinert, L.D., 1992, Skarns and skarn deposits: Geoscience Canada, v. 19, p. 145-162.

Moore, W.J., and Nash, J.T., 1974, Alteration and fluid inclusion studies of the porphyry copper orebody at Bingham, Utah, Econ. Geol. v. 69, p. 631-645.

Myers, G. L., and Meinert, L.D., 1991, Alteration, mineralization, and gold distribution in the Fortitude gold skarn: in Raines, G.L., Lisle, R.E., Schafer, R.W., and Wilkinson, W.H. (eds.), Geology and Ore Deposits of the Great Basin, Geol. Soc. Nevada, Reno, v. 1, p. 407-418.

Muntean, J., Cline, J., Simon, A., and Long, A., 2011, Magmatic-hydrothermal origin of Nevada's Carlin-type gold deposits: Nature Geoscience, v. 4, p. 122-127.

Nabelek, P.I., 1991, Stable Isotope Monitors, Reviews in Mineralogy, v. 25, p. 395-435.

Norton, D., and J. E. Knight., 1977, Transport phenomena in hydrothermal systems: Cooling plutons, Am. J. Sci., v. 277, p. 937-981.

Osterberg, M.W., 1990, Geology and geochemistry of the Chimney Creek Gold Deposit, Humboldt County, Nevada: University of Arizona, Tucson, Ph. D. dissertation, p. 173.

Radtke, A.S., Rye, R.O., and Dickson, F.W., 1980, Geology and stable isotopes of the Carlin gold deposit, Nevada: Economic Geology, v. 75, p. 641-672.

Reese, N.M., 1986, Cenozoic tectonic history of the Ruby Mountains and adjacent areas, northeastern Nevada: Constraints from radiometric dating and seismic reflection profiles, M.S. thesis, Southern Methodist University, Dallas, p. 88.

Ressel, M.W., Noble, D.C., Henry, C.D., and Trudel, W.S., 2000a, Dike-hosted ores of the Beast deposit and the importance of Eocene magmatism in gold mineralization of the Carlin trend, Nevada: Economic Geology, v. 95, p. 1417-1444.

Ressel, M.W., and Henry, C.D., 2006, Igneous geology of the Carlin Trend, Nevada: development of the Eocene plutonic complex and significance for Carlin-type gold deposits. Economic Geology, v. 101, p. 347-383.

Ridley, J., and Hagemann, S.G., 1999, Interpretation of post-entrapment fluid-inclusion re-equilibration at the Three Mile Hill, Marvel Loch and Griffins find high-temperature lode-gold deposits, Yilgarn Craton, Western Australia, Chemical Geology, v.154, p. 257-278.

Roedder, E., 1971, Fluid inclusion studies on the porphyry-type ore deposits at Bingham, Utah, Butte, Montana, and Climax, Colorado, Economic Geology, v. 66, p. 98-120.

Roedder, E., and Bodnar, R. J., 1980, Geologic pressure determinations from fluid inclusion studies. Annual Review of Earth and Planetary Sciences, v. 8, p. 263-301.

Roedder, E., 1984, Fluid Inclusions, Min. Soc. Am. Rev. in Min. v. 12, p. 644

Rye, R.O., Doe B.R., and Wells J.D., 1973, Stable isotope and lead isotope study of the Cortez, Nevada gold deposit and surrounding area: U.S. Geol. Survey Jour. Research, v. 2, p. 13-23.

Rye, R.O., 1985, A model for the formation of carbonate-hosted disseminated gold deposits based on geologic, fluid inclusion, geo-chemical, and stable isotope studies of the Carlin and Cortez deposits, Nevada. USGS Bull. v. 1646, p. 35-42.

Sharp, Z., 2006, Principles of Stable Isotope Geochemistry, Prentice-Hall, Upper Saddle River, N. J., p. 344.

Shepherd, T.J., Rankin, A.H., and Alderton, D.H.M., 1985, A Practical Guide to Fluid Inclusion Studies, Blackie, Glasgow, p. 239.

Sheppard, S.M.F., 1977, Identification of the origin of ore-forming solutions by the use of stable isotopes. Volcanic Processes in Ore Genesis. Geological Society, London, Special Publication, v. 7, p. 25-41.

Shinohara, H., 1994, Exsolution of immiscible vapor and liquid phases from a crystallizing silicate melt; implications for chlorine and metal transport, Geochimica et Cosmochimica Acta, v. 58, p. 5215-5221.

Sillitoe, R.H., and Bonham, H.F. Jr., 1990, Sediment-hosted gold deposits; distal products of magmatic-hydrothermal systems, Geology, v. 18, p. 157-161.

Taylor, H.P. Jr. 1974, An application of oxygen and hydrogen isotope studies to problems of hydrothermal alteration and ore deposition, Economic Geology, v. 69, p. 843-883.

Taylor, H.P. Jr., 1977, Water/rock interactions and the origin of H_2O in granitic batholiths, J. Geol. Soc. Lond. v. 133, p. 509-558.

Tingley, J. V., 1981a, Results of geochemical sampling within the Wells Resource Area, Elko County, Nevada (portions of Wells, and Elko, 20 sheets), Nevada Bureau of Mines and Geology Open-File Report 81-3, p. 79.

Vityk, M.O., and Bodnar, R.J., 1995, Do fluid inclusions in high-grade metamorphic terranes preserve peak metamorphic density during retrograde decompression?, American Mineralogist, v. 80, p. 641-644.

Webster, J.D., 1997. Chloride solubility in felsic melts and the role of chloride in magmatic degassing, J. Petrol. v. 38, p. 1793-1807.

Wilden, R., and Kistler, R. W., 1967, Ordovician tectonism in the Ruby Mountains, Elko County, Nevada, in Geological Survey Research 1967: U.S.

Geological Society Survey Professional Paper 575-D, p. D64-D75.

Wilden, R., and Kistler, R.W., 1969, Geology of the Jiggs quadrangle, Elko County, Nevada, U.S. Geological Survey Map GQ-859, scale 1:62,500.

Woitsekhowskaya, M.B., and Peters, S.G., 1998, Geochemical modeling of alteration and gold deposition at the Betzte deposit, Eureka County, Nevada. US Geological Survey Open-File Report, 98-338, p. 211-222.

Wright, J.E., and Snoke, A.W., 1993, Tertiary magmatism and mylonitization in the Ruby-East Humboldt metamorphic core complex, northeastern Nevada: U-Pb geochronology and Sr, Nd, Pb isotope geochemistry. Geol. Soc. Amer. Bull. v. 105, p. 935-952.

Zhang, Y.G., and Frantz, J.D., 1987, Determination of the homogenization temperatures and densities of supercritical fluids in the system NaCl – KCl – $CaCl_2$ – H_2O using synthetic fluid inclusions, Chem. Geol. v. 64, p. 335-350.

APPENDIX 1: HPP INTRUSIVE AND SEDIMENTARY-METASEDIMENTARY ROCKS OF THE SOUTHERN RUBY MOUNTAINS

Intrusive rocks of the HPP (Paleogene)

Tmg Monzogranite, undivided: includes biotite-and two mica monzogranite in tabular and massive units, and granodiorite units that are pervasively intruded by monzogranite.

Tgm Muscovite-biotite monzogranite of Green Mountain Creek.

Trd Porphyritic rhyodacite and granodiorite dikes.

Tcc Porphyritic-biotite monzogranite of Corral Creek.

Thp Porphyritic megacrystic biotite±hornblende granodiorite of Harrison Pass.

Sedimentary-metasedimentary rocks of the southern Ruby Mountains

Slm Silurian Lone Mountain Dolomite. Thick bedded (.2-1.5 m) gray, bioclastic, arenaceous dolostone and dolomite marble.

Opu Ordovician Pogonip Group, upper unit. Yellow-orange to dark yellow-brown interbeds of calc-silicate rock and black chert.

Opl Pogonip Group, lower unit. Unit is composed of dark grey, thin-to-medium bedded limestone with minor argillaceous laminae. Where metamorphosed, the unit contains pale-blue calcite marble and contains minor argillite, calc-silicate, or siliceous laminae.

Cwb Upper Cambrian Windfall Formation, Bullwacker Member. The unit consists of alternating beds of light brown, shaly-to-silty limestone, and light gray limestone. Where thermally metamorphosed, it consists of interlayered marble and calc-silicate rock in unequal proportions.

Cwc Upper Cambrian Windfall Formation, Catlin Member. Grey limestone in thin beds with thin dark grey chert and argillite layers. Where thermally metamorphosed, the unit consists of calcite marble with calc-silicate interlayers.

Chl Upper Cambrian hornfelsic limestone unit. Interbeds of limestone and argillite, with infrequent siltstone and silty limestone layers. Where

thermally metamorphosed, it consists of calcite and dolomite marble with argillite and calc-silicate rock.

Ch Upper Cambrian limestone unit. Mixed carbonate-siliciclastic sedimentary rocks, predominantly silty limestone with infrequent mudstone and carbonaceous shale. Where thermally metamorphosed, it consists of layered siliceous marble, argillite, and calc-silicate rocks.

Cl Middle Cambrian shaly limestone unit. Light brown to light-grey, thin to medium bedded (1-25 cm) recyrstallized limestone and massive calcite marble with frequent argillaceous interbeds and laminae.

Csl Lower Cambrian shaly limestone unit. Thin (1-10 cm) to thick (1 cm) bedded recyrstallized limestone and recyrstallized argillaceous limestone with thin sandy to silty limestone and argillite interlaminae. A complete gradation to calcite marble, impure argillite-marble, and phyllite were thermally metamorphosed.

Cp Cambrian Pioche Formation. Consist of micaceous and nonmicaceous shale, siltstone, sandstone, and bioclastic and nonbioclastic limestone, arranged in cyclic siliclastic-carbonate successions.

CZpm Neoproterozoic Prospect Mountain Quartzite Light-brown, thin to medium bedded (10-100 cm), planar and trough cross-laminated quartzite with occasional interbeds of brown phyllite or schist.

Descriptions from Burton (1997)

APPENDIX 2: THIN SECTION DESCRIPTIONS OF SAMPLES

*(Latitude, Longitude)

HPP-14 *(40.30475, -115.48850)**:** Sample is from a 10-14 cm thick quartz vein within monzogranite (Tcc) ~900 m *within* the HPP contact. The vein is 99% coarse-grained quartz ranging from approximately 2800-13,500 μm. Some quartz grains exhibit undulose extinction suggesting a deformation event. The monzogranite wallrock contact with the quartz vein is sharp, and no alteration is present. The monzogranite consist of quartz (35%)+plagioclase (35%)+K-feldspar (15%)+biotite (5%)±sericite ±pyrite ±hematite. Quartz is coarse-grained (~1500 μm), subhedral, and displays undulose extinction. Plagioclase is euhedral and most have been replaced partially by biotite and sericite. K-feldspar grains are phenocrysts and are typically coarse grained and subhedral. Pyrites are disseminated throughout the wallrock, are subhedral to euhedral, and are only a couple microns across. Three large (~400 μm), subhedral hematite grains are observed within fractures of the granodiorite wallrock.

HPP-15 (40.31092, -115.47608)**:** Sample is a deformed monzogranite (Tcc) directly adjacent to a skarn from the Star Mine *on* the HPP contact. The mineralogy consists of quartz (35%)+K-feldspar (25%)+plagioclase (25%)+biotite (5%)+sericite (10%)±sphene±epidote. Quartz is subhedral, coarse-grained, and forms sheared, ribbon like laths that are heavily fractured and have been minimally replaced by sericite. Quartz also displays undulose extinction suggesting a period of deformation, and grain sizes range from 200 to 350 μm. Potassium feldspar is coarse-grained, subhedral, and occurs as large as 2500 μm. Plagioclase is subhedral and has been partially to fully replaced by sericite±biotite. Locally, a few large (1400 μm) sphenes are present displaying characteristic diamond shaped habit.

HPP-16 (40.31092, -115.47608): This sample is from a skarn within Star Mine *on* the HPP contact within the Opu formation. The skarn metasedimentary hostrock consist of hydrogrossular (40%)+sericite (20%)+quartz (15%)+calcite (5%)+biotite/chlorite (15%)+diopside (5%)±plagioclase. Quartz is euhedral, coarse grained, has been partially replaced by calcite+biotite+chlorite, and is approximately 600 μm in size. Some quartz shows undulose extinction suggesting a deformation event. Calcite, biotite and chlorite are ubiquitous throughout and are found in fine-grained masses, and in veinlets typically replacing plagioclase. Hydrogrossular is ubiquitous throughout giving the sample a reddish tint and is primarily subhedral, and ranges in size from 100-500 μm. Characteristic growth banding is evident in some. Diopside is sparse and is coarse grained, subhedral, and ~300 μm in size.

HPP-18 (40.31092, -115.47608)**:** This sample is from a calcite vein (4.5 cm) in Star Mine *on* the HPP contact within the Opu formation. In this sample a first-generation calcite vein (5 mm) crosscuts a second-generation calcite vein (1.5 cm). The first-generationcalcite vein is composed of calcite (70%)+diopside (20%)+biotite (10%)±quartz±sericite. Diopside is subhedral to euhedral columnar blocks approximately 100 µm in size. Calcite is bladed, fine to medium grained, and has been replaced by sericite. The second-generation calcite vein is comprised of calcite (90%)+diopside (10%)±quartz±biotite. Calcite is coarse grained, subhedral-euhedral, and is approximately 500-800 µm in size. Locally, some calcite has experienced some recrystallization by quartz. Diopside is subhedral-euhedral, columnar and blocky, and is 100-200 µm in size.

HPP-21 (40.30208, -115.47247)**:** This sample is from a 1.2-1.7 cm quartz vein adjacent to a skarned wallrock *on* the HPP contact within the Opu fm. The vein is composed of quartz (99%)±plagioclase±sericite. Quartz is subhedral, fine to coarse grained, and ranges in size from 50-500 µm. Close to the vein, the wallrock is a skarn assemblage consisting of fine-grained calcite (60%)+quartz (20%)+tremolite (10%)+diopside (10%)± plagioclase±apatite. Plagioclase has completely been altered by biotite. Progressing further away from the vein the wall-rock composition is quartz/calcite (60%)+diopside (15%)+tremolite (15%)+biotite (10%)±plagioclase±pyrite± magnetite. Diopside grains are coarse-grained, subhedral, and blocky. Tremolite grains (~500 µm) are highly fractured, and appear as massive, bladed, crystal aggregates. Most biotites have been replaced by chlorite and also serve as replacement products in plagioclase. Pyrite is subhedral to euhedral, displays hematite oxidation and are approximately 70 µm. Magnetite grains (30-80 µm) are subhedral to euhedral, contain pyrite inclusions, and show hematite oxidation and illmenite exsolution.

HPP-24 (40.30403, -115.53511)**:** This sample is from a miarolitic cavity within an enclave (Opl fm) within the later stage monzogranite unit (Tmg) ~1600 m *within* the HPP contact. The sample consists of three coarse, subhedral, moderately fractured quartz (99%) grains approximately 11,750 µm, 17,500 µm, and 24,100 µm in size. 1-3 µm, anhedral to subhedral pyrites can be found disseminated throughout the sample.

HPP-26 (40.30133, -115.53058)**:** This sample is from a 4-6 mm quartz vein from a limestone enclave (Opl fm) within the earlier stage monzogranite (Tcc) unit ~1400 m *within* the HPP contact. 100-9300 µm chaotic veining crosscuts the sample, which is comprised of quartz (99%)±biotite. Growing inward towards the vein, quartz is subhedral to euhedral, mostly coarse grained, and ranges from approximately 25-650 µm. The wallrock consist of calcite (99%)±quartz±biotite±hematite. Calcite is fine to coarse-grained, subhedral to euhedral, and appears cloudy, which is most likely the result of fine-grained clays and micas. Locally, along vein edges, biotite is replaced by chlorite. Disseminated throughout the wallrock are irregular, subhedral polygons of hematite.

HPP-28 (40.30383, -115.55486)**:** This sample is from a hydrothermal quartz vein hosted within a fault within the later stage monzogranite (Tmg) unit ~1300 m *within* the contact. The sample consists of 3 generations of quartz. The first generation consists of quartz (99%)±magnetite±pyrite. Quartz is fine to coarse grained, subhedral-euhedral, brecciated, and ranges in size from 80 to 100 µm. Magnetites (~113 µm) are euhedral cubes, and display hematite oxidation and illmenite exsolution. Pyrites (66-115 µm) are euhedral to subhedral cubes, and have been fully oxidized by hematite. Locally, some pyrites show a twinned habit. The second generation consists of several vugs infilled by euhedral, coarse-grained quartz crystals as large as 1300 µm. The third generation is a 1.3-1.4 cm quartz vein, which crosscuts the second-generation vugs. This vein consists of 99% coarse-grained, euhedral, cone quartz, which grows inward towards the vein. Grains are as large as 8250 µm in size, and some display Brazil twinning.

HPP-30a (40.29036, -115.55367)**:** This sample is from a phyllic-altered monzogranite (Tmg) ~30 meters *within* the HPP contact. The main monzogranite consist of quartz (40%)+plagioclase (40%)+K-feldspar (10%)+biotite (10%)±hornblende. Quartz (200-1800 µm) is coarse grained, subhedral, and has been hydrothermally brecciated/fractured. Plagioclase (>3500µm) is subhedral and displays minor replacement by sericite. K-feldpsar is coarse grained and subhedral and biotites are large subhedral masses that have been partially to fully replaced by chlorite. Minor deformation is evident by undulose extinction and kink banding in quartz. Phyllic alteration is found in large and small veins (180-4000 µm) and within fractures and consists of mainly quartz (45%)+ sericite (50%)+ pyrite (5%)±biotite±hematite. Pyrites occur as euhedral cubes, range from 20-2500 µm and in some instances display a twinned habit. Pyrite has also been fully oxidized by hematite. A third generation, euhedral quartz vein (350 µm) crosscuts the secondary phyllic alteration.

HPP-33 (40.33836, -115.46928)**:** This sample is a 1-2 cm calcite vein from a Pb-Zn prospect *on* the HPP contact within the Cwb fm. The vein is comprised of calcite (99%)±pyrite±magnetite±sphalerite±hematite. Calcite is coarse grained, subhedral-euhedral, and ranges in size from 900-5000 µm. Subhedral-to-euhedral pyrites (~45 µm) are disseminated throughout the sample, and some have been oxidized by partially to fully oxidized by hematite. Magnetite grains (~420 µm) are euhedral, have pyrite inclusions, and display oxidized rims of hematite and illmenite exsolution. Sphalerite forms irregular masses and subhedral cubes approximately 40-130 µm in size. The wallrock is comprised of calcite (85%)+quartz (15%)±biotite±rutile. Calcite crystals (170-1000 µm) are subhedral to euhedral, have been slightly deformed and are aligned in the same direction producing a banded appearance. In between these crystals are recyrstallized fine grained, bladed calcite cement. Quartz within the wallrock is euhedral, coarse grained, and is ~200 µm. Small (10-20 µm) subhedral grains of rutile can be found disseminated in the wallrock.

HPP-35 (40.33953, -115.47158)**:** This sample is a quartz/plagioclase miarolitic cavity within a leucotonalite/granodiorite (Ttc) from a scheelite mine *on* the HPP

contact. The miarolitic cavity consists of quartz (70%)+plagioclase (30%). Quartz is subhedral, coarse grained, moderately brecciated and ranges in size from 1200-5800 μm. Quartz displays an elongated ribbon like shape, which provides evidence of a deformation event. Plagioclase is coarse grained, moderately brecciated, and is approximately 1500 μm. The wallrock consist of three large (~10,000 μm) plagioclase grains±K-spar±biotite±quartz±sericite. Myrmekitic texture between plagioclase and quartz is evident, and wallrock biotite is crosscut by later generation sericite veins.

HPP-40 (40.31822, -115.46447)**:** This sample is a 3.5 cm quartz vein crosscutting a potassically altered leucogranite/tonalite *on* the HPP contact. The vein is composed of quartz (99%)±plagioclase. Quartz is coarse-grained, subhedral, and ranges from 1200-5300 μm. Locally, some quartz shows undulose extinction indicative of a deformation event. The wallrock is a classic leucogranite composed of quartz (45%)+plagioclase (40%)+K-feldspar (10%)+ biotite (5%)±pyrite. Quartz is subhedral to euhedral, coarse-grained, and ranges from ~140-800 μm. Plagioclase is coarse grained, subhedral to euhedral, and locally has been partially replaced by biotite. Biotite occurs in localized masses, and replaces surrounding quartz+plagioclase grains. K-feldspar is interstial, subhedral and locally can be seen overprinting sections of the quartz vein. Pyrites are subhedral to euhedral cubes, and are approximately 35 μm. Locally, some graphitic granitic texture is observed between plagioclase and quartz.

HPP-42 (40.29261, -115.49364)**:** This sample is a first generation quartz vein (2 cm) crosscutting a second-generation calcite+quartz vein (1 cm) within a skarn wallrock within the Opu fm. *on* the HPP contact. The first generation vein is composed of calcite (90%)+quartz (10%)±pyrite. Calcite is euhedral, medium-coarse grained, and is approximately 100 μm in size. Away from the vein, quartz and calcite grains become progressively finer grained. This vein generation also contains one grain of subhedral pyrite (206 μm). The second-generation vein is perpendicular to the first generation vein and consists of quartz (95%)+calcite (5%). Quartz is coarse grained, euhedral, and ranges in size from approximately 1600-3600 μm. The adjacent wallrock is a skarn assemblage, comprised of diopside (30%)+epidote (30%)+tremolite (20%)+quartz/calcite (20%). Diopside crystals are subhedral to euhedral, ~660 μm, and have been partially to fully replaced by tremolite. Epidote (~180 μm) occurs as subhedral to euhedral crystals and brecciated masses.

HPP-43 (40.29261, -115.49364)**:** This sample is from a 1.4 cm quartz+calcite vein within a skarn within the Opu fm. *on* the HPP contact. The vein is composed of quartz (40%)+calcite (50%)+diopside (5%)+sericite (5%)±biotite±plagioclase. Quartz is subhedral to euhedral, fine to coarse grained, brecciated and ranges in size from 100-2200 μm. Calcite is euhedral, fine to coarse grained, brecciated, and ranges from 150-1400 μm. Diopside is subhedral to euhedral and ranges from 150 to 300 μm. Biotite is sparse, but locally has been altered to chlorite. Few subhedral pyrites are disseminated, subhedral, and are approximately 2-6 μm.

HPP-51 (40.28436, -115.50011)**:** This sample is from a ~4 cm quartz vein crosscut by a ~2.5 cm calcite vein *on* the HPP contact between the Opu and Tcc fms. The quartz vein is quartz (99%)±sericite. Quartz is subhedral, fine-grained, and ranges in size from 40 to 450 µm. Crosscutting this quartz vein, are 50 to 1300 µm calcite veins comprised of calcite (95%)+pyrite (5%)±quartz. Calcite is extremely fine-grained, brown and cloudy, due to the addition of clays+micas. Pyrites are disseminated euhedral cubes, that have been fully oxidized by hematite, and range in size from approximately 20 to 40 µm. Crosscutting these calcite veins, is a 1000 µm quartz vein. Quartz is comb textured, 500 to 800 µm in size, and grows inward from the adjacent calcite wall rock. Within the vein are euhedral, hematite hexagons approximately 120 µm in size.

HPP-52 (40.28747, -115.52006)**:** This sample is from a hydrothermally, phyllic altered, megacrystic granodiorite (Tcc) *on* the contact. Alteration is ubiquitous throughout and consists of sericite (70%)+quartz (20%)+pyrite (5%)+plagioclase (5%)±biotite. Quartz (400-4600 µm) is subhedral, fine to coarse grained, and has been hydrothermally brecciated. Pyrite cubes (800-1100 µm) are disseminated, subhedral to euhedral, and have been fully oxidized by hematite. Plagioclase is coarse-grained, subhedral, and is approximately 2500 µm. Plagioclase grains have also been partially to fully replaced by sericite.

HPP-56 (40.28906, -115.55328)**:** This sample is from 2-3 cm calcite vein within a prospect mine within the Ch fm. *on* the HPP contact. The sample consists of diopside (60%)+tremolite (40%)±calcite±biotite±sericite. Diopside occurs as subhedral, highly fragmented, columnar blocks that have been partially to fully replaced by tremolite, biotite and sericite. Predominantly, diopside is coarse grained and ranges from 4000 to 9300 µm. Tremolite occurs as masses of bladed aggregates, partially to fully replacing diopside and calcite. Sericite veins are observed crosscutting earlier diopside+tremolite mineralogy.

HPP-57 (40.28906, -115.55328)**:** The sample is from a skarn alteration zone within a prospect mine within the Ch fm. *on* the HPP contact. The sample consists of quartz (99%)±biotite vein being crosscut by later stage calcite veins. Quartz is coarse-grained, subhedral, and ranges between 100 to 1000 µm. Quartz also displays elongated like grains and minor undulose extinction, which suggests a deformation episode. Crosscutting, 300 µm-1 cm, calcite veins display both a bladed and crystalline subhedral habits. Calcite grains are coarse grained and range from approximately 50 to 400 µm in size. Subhedral pyrite (~1-3 µm) can also be found disseminated throughout the sample.

HPP-59 (40.28906, -115.55328)**:** This sample is a .8 cm quartz vein crosscutting a skarn wallrock within the Ch fm. *on* the HPP contact. The vein is 99% coarse-grained, subhedral, 400-6200 µm quartz. Quartz grains display undulose extinction, indicative of a deformation/metamorphic event. The wallrock is composed of diopside (50%)+tremolite (30%)+quartz/calcite (20%)±biotite. Near the vein edge, tremolite is replacing diopside and calcite. Tremolite needles are euhedral, and can be as large as 560 µm long. Also, vein edges contain minor biotite and diopside (~100-300 µm). Progressing further away from the vein larger diopside grains (300-

2700 μm), and quartz grains (~7000 μm) are situated in coarse-grained, brecciated calc-silicate groundmass. Diopside is fine to coarse-grained, subhedral, and intensely fractured and shows partial replacement by tremolite. Quartz is fine to coarse grained, subhedral-euhedral, and is heavily fractured.

HPP-61 (40.28906, -115.55328)**:** This sample is from a sphalerite vein crosscutting a calc-silicate wallrock within a Pb-Zn prospect within the Ch fm. *on* the HPP contact. The 1.1 cm sphalerite vein is composed of 99% coarse grained, subhedral, 45 to 1300 μm moderately brecciated sphalerite. The calc-silicate wallrock consist calcite (70%)+diopside (25%)+quartz (5%). Calcite is coarse-grained, subhedral to euhedral, and ranges from 20 to 1350 μm. Diopside is coarse grained, subhedral, and ranges from 200 to 1000 μm. Diopside is seen along the edge of the sphalerite vein, and locally is found intruding into the vein.

HPP-71 (40.27922, -115.54683)**:** This sample is from a hydrothermally phyllic altered granite ~120 m *away* from the HPP contact found within the Ch fm. Alteration is ubiquitous throughout the sample and consists of sericite (50%)+quartz (25%)+biotite (20%)+pyrite (5%)±plagioclase±magnetite. Quartz is coarse grained, subhedral, hydrothermally brecciated and ranges ~200 to 1200 μm. Pyrites are euhedral, range from 340 to 1540 μm, and have completely been oxidized by hematite. Locally, some pyrites show a contact twinned habit.

HPP-74 (40.27922, -115.54683)**:** This sample is from a 10 X 10 cm miarolitic cavity in an aplite/roof-dike within the Ch formation *away* from the contact. The miarolitic cavity is predominantly all quartz (99%). Quartz is coarse grained, subhedral to euhedral, and ranges in size from 1200 to 6300 μm. The adjacent aplite/roof dike consists of quartz (60%)+plagioclase (30%)±biotite±pyrite±hematite. Quartz grains are large (~8800 μm), subhedral to euhedral, and display myrmekitic integrowth textures with subhedral plagioclase grains. Locally, some plagioclase grains have been partially replaced by biotite. A few large (480-950 μm) grains of subhedral pyrite are disseminated throughout and have been completely oxidized by hematite.

HPP-78 (40.27122, -115.53664)**:** This sample is a 1 cm, subhedral calcite (60%)+quartz (40%)±biotite vein that crosscuts a hornsfelic limestone wallrock ~2250 m within the Cwb fm *away* from the HPP contact. The contact is sharp between the vein and the wall-rock, and no alteration is observed. Quartz (200-3000 μm) ranges from fine to coarse grained, is subhedral, and displays kink-banding and undulose extinction suggesting a period of deformation. Calcite (200-3000 μm), is mostly coarse grained and euhedral. 2-20 μm, subhedral to euhedral pyrite grains are also disseminated throughout the vein. The hornsfelic wallrock is very fine grained, clay/mica rich, and contains minor magnetite+pyrite. Magnetite grains (~35 μm) are disseminated, contain inclusions of pyrite, and display hematite oxidation around grain rims. Pyrite grains (~12 μm) are disseminated, fine-grained, and have been partially oxidized by hematite.

HPP-81 (40.28464, -115.56283)**:** This sample is a phyllic altered monzogranite (Tmg) *on* the HPP contact. Alteration is ubiquitous throughout and consists of sericite (60%)+quartz (30%)+biotite (6%)+magnetite (4%)+plagioclase±rutile.

Quartz is coarse grained, subhedral, and ranges from 500-1100 µm. Euhedral cubes of magnetite are disseminated, range in size from 130 to 550 µm, and have been partially to fully oxidized by hematite/goethite and shows minor illmenite exsolution.

HPP-84 (40.28453, -115.56683)**:** This sample is from a set of recrystallized calcite veins crosscutting a monzogranite (Tmg) *on* the HPP contact. The wallrock is a classic granodiorite composed of quartz (45%)+plagioclase (45%)+biotite (10%)±K-feldpsar±hornblende. Quartz is subhedral to euhedral, coarse grained, and ranges from 100 to 2300 µm. Minor deformation is visible from undulose extinction is quartz. Plagioclase is subhedral, coarse grained, and has been partially to fully replaced by sericite. Biotites range from aggregate masses to euhedral blades, and locally has been replaced by chlorite. Crosscutting recrystallized veins are ubiquitous throughout, and infills voids and spaces throughout the monzogranitic wallrock. Veins are composed of calcite (80%)+ sericite (10%)+quartz (5%)+biotite (5%)±pyrite. Calcite displays mainly a euhedral bladed habit and ranges from approximately 50-160 µm. Minor, euhedral, disseminated cubic pyrite (~365 µm) can be found throughout.

HPP-86 (40.28344, -115.56767)**:** This sample is from a hydrothermal 2.5-3 m quartz vein within the Cl fm. crosscutting the HPP *on* contact. Two generations of veining is observed. The first generation is composed of coarse-grained (250 to 3100 µm), subhedral, 99% quartz. The second generation is composed of fine-grained (10-100 µm), subhedral to euhedral quartz (99%)±biotite±sericite. Quartz within this generation is found between fractures and spaces between the first generation quartz. A later crosscutting styolite contains subhedral magnetites (30-100 µm), which have been partially to fully oxidized by hematite.

HPP-89 (40.28564, -115.57292)**:** Sample is from a quartz pocket within a finely laminated, shaley/sandy, fractured limestone *on* the HPP contact between the Tmg and Cl fms. This sample contains quartz (85%)+biotite (5%)+sericite (10%)±pyrite±magnetite±rutile±hematite. Quartz is fine to coarse grained, subhedral-euhedral, and locally fills vugs. Euhedral quartz grains can grow as large as 1400 µm. Some quartz grains display minor undulose extinction and Brazil twinning. Localized pyrite (3-11 µm) and magnetite (15-50 µm) are subhedral to euhedral and have been partially oxidized by hematite. Rutile occurs as subhedral columnar like crystals disseminated throughout the sample.

HPP-98 (40.29928, -115.47536)**:** This sample is a 2-3 cm quartz vein cross-cutting a phyllic altered granodiorite (Tcc), taken from tailings from an abandoned Pb-Zn mine *on* the HPP contact. The quartz vein is coarse grained, subhedral, and ranges in size from 150 to 980 µm. The wall-rock has been altered (phyllic) and is comprised of a granodiorite assemblage consisting of quartz (35%)+plagioclase (30%)+biotite (20%)+sericite (10%)+K-feldspar (2-5%)±pyrite±magnetite±hematite. Quartz grains are subhedral, and are more fine grained (230-450 µm) than the adjacent quartz vein. Plagioclase grains are subhedral and have been partially replaced by biotite and sericite. One magnetite grain is large (1345 µm) and displays partial pyrite replacement, and hematite oxidation. Euhedral pyrites are

also large and range from 117 to 1600 μm. Most show partial to full hematite oxidation and illmenite exsolution. Locally, some pyrites have been replaced by laths of diagenite.

HPP-100 (40.25889, -115.51303)**:** This sample is a 5 mm calcite+quartz vein crosscutting a coarse grained limestone 3000 m *away* from the HPP contact within the Opu fm. The vein is composed of calcite (90%)+quartz (10%). Calcite within the vein is coarse-grained, subhedral-euhedral, and ranges in size from 130-1100μm. Quartz within the vein is coarse-grained, subhedral, and is approximately 560μm in size. Locally, some grains show undulose extinction suggesting a deformation event. The wall-rock consist of fine grained, subhedral-euhedral calcite (99%)±quartz±hematite.

HPP-103 (40.25592, -115.51978)**:** This sample is from a 4-5 mm calcite vein within a limestone ~3500 m *away* from the HPP contact metamorphic aureole within the Opu fm. The wall-rock is composed of calcite (98%)+quartz (2%)±pyrite±hematite. Calcite is fine to coarse grained and ranges in size from 60 to 230 μm. Most calcite is clay/mica rich, which makes it appear brown and cloudy. Pyrite grains (2-17 μm) are disseminated, subhedral to euhedral, and most have been completely oxidized by hematite.

HPP-105 (40.25769, -115.52750)**:** This sample is a ~3 cm calcite veins crosscutting a limestone wallrock 3520 m *away* from the HPP contact within the Opu fm. The vein is 99% calcite±quartz. Calcite is coarse grained, subhedral-euhedral calcite ranging in size from 850-2200 μm. The wallrock consist of very fine-grained, subhedral-euhedral calcite (99%)±quartz grains. Subhedral to euhedral, ~50 μm hematite grains can be found disseminated throughout the wallrock displaying illmenite/goethite exsolution.

HPP-107 (40.25892, -115.52900)**:** This sample is from a 30-50 cm calcite vein 3500 m *away* from the HPP contact within the Opu fm. The sample consists of calcite (99%)±pyrite±hematite. Calcite is coarse grained (1100-6250 μm), subhedral, and is heavily fractured in one distinct direction. Pyrite grains (5-17 μm) are disseminated, euhedral, and have completely been oxidized by hematite.

HPP-109 (40.26972, -115.54756)**:** Sample is a pocket of calcite ~2150 meters *away* from the HPP contact within the Ch fm. The pocket is ~2.5X3 cm wide, and contains 95% calcite and 5% quartz. Calcite within the pocket is subhedral, fractured, coarse grained and ranges in size from 950 to 3200 μm. The wall-rock displays sheared and fragmented coarse, calcite (99%) grains±clays/micas. The edge of the calcite pocket contains a slightly different mineralogy consisting of sericite+biotite±hematite±pyrite. Anhedral pyrite (~75 μm) is disseminated and found along fractures within the wall-rock.

HPP-111 (40.27414, -115.55472)**:** This sample is a .8-1 cm quartz+plagioclase vein crosscutting a potassic altered leucogranite (Tmg) found *away* from the HPP contact within the Ch fm. Quartz is subhedral, coarse grained, and ranges from 1100-3500 μm. Plagioclase is coarse-grained, subhedral, and is approximately

3600 μm. The leucogranitic wall-rock is comprised of plagioclase (50%)+quartz (40%)+biotite (5%)+sericite (5%)±pyrite. Quartz is fine to coarse grained, and is subhedral. Plagioclase is subhedral to euhedral, and locally has been replaced by biotite and sericite. Disseminated pyrite grains (~260 μm) are euhedral, and have been fully oxidized by hematite.

HPP-113 (40.27761, -115.55908)**:** This sample is a miarolitic cavity of quartz adjacent to a slightly phyllically altered granodiorite ~800 m detached from the HPP *away* from the contact within the Csl fm. The cavity is 99%, subhedral, coarse-grained quartz ranging from 4200-12,000 μm. The wall-rock is a slightly altered granodiorite consisting of sericite (30%)+quartz (25%)+plagioclase (25%)+biotite (20%)±pyrite±magnetite±hematite. Quartz is subhedral and coarse grained. Plagioclase and biotite are subhedral and have been partially replaced by sericite. Pyrite (~100μm) is disseminated, subhedral to euhedral, and displays hematite oxidation around the rims. Magnetite (~100 μm) is disseminated, anhedral to subhedral irregular polygons and displays hematite oxidation and illmenite exsolution.

HPP-115 (40.27972, -115.56533)**:** This sample is a skarned limestone ~120 meters *away* from the contact metamorphic aureole, and contains a crosscutting 1.5-1.6 cm quartz (99%)±calcite vein. Vein quartz is subhedral, coarse-grained, and ranges in size from 800 to 4000 μm. This vein is also crosscut by later capillary calcite veins. The wall rock contains a calc-silicate mineral assemblage, which shows a distinct mineral progression away from the vein. Near the quartz±calcite vein edge the mineralogy is tremolite (85%)+diopside (5%)+quartz (5%)+calcite (5%)±plagioclase±hematite+magnetite±pyrite. Tremolite is predominantly acicular and partially to fully replaces diopside. Diopside is typically subhedral, fragmented, and blocky. Magnetite is subhedral irregular shaped polygons (20-1050 μm), has been partially oxidized by hematite, and shows some inclusions of pyrite and goethite. Hematite is ubiquitous around the vein edges and is found as blocky, irregular polygons. Anhedral to subhedral quartz+calcite is mostly coarse to fine grained. Locally, euhedral plagioclase displaying carlsbad twinning can be found along the vein edge. Progressing outward from vein exists a quartz (35%)+calcite (35%)+diopside (20%)+tremolite (10%)±epidote±pyrite mineral assemblage. Quartz and calcite is finer grained than near the edge of the vein, and calcite displays both bladed and crystalline habits. Diopside displays a highly fractured, and blocky habit and is set in a fine-grained calc-silicate+quartz+calcite groundmass. Pyrite (~280 μm) is disseminated, subhedral, and has been completely to partially oxidized by hematite. Crosscutting the wallrock are medium-grained subhedral to euhedral, brown calcite veins (~1925 μm) that contain secondary hematite±goethite oxidation.

APPENDIX 3: FLUID INCLUSION DATA

The following tables represent the results of microthermometric data measured *within*, *on*, and *away* from the HPP. Table 1 represents fluid inclusion microthermometric data collected over the whole sample suite. Table 2 represents consolidated fluid inclusion microthermometric data organized by sample. Table 3 represents fluid inclusion microthermometric statistics organized by fluid inclusion setting.

Table 1: Raw fluid inclusion data for each sample

Sample #	P/PS/S	Host	VN/WR/MC	Location	F.I. #	Outlier	Tm_{CO_2}	$T_{eutectic}$	Tm_{ice}	Tm_{clath}	Th_{CO_2}	Th_{total}	Mass% eq. NaCl	Ph_{total}	Density (g/cc)
HPP-15	S	Qtz	WR		1			-22.10	-4.70			169.80	7.45	6.60	0.95
	S	Qtz	WR		2			-17.20	-6.40			194.60	9.73	11.12	0.95
	S	Qtz	WR	chip 2	3			-21.20	-1.80			228.00	3.06	23.17	0.86
	S	Qtz	WR		4			-21.20	-2.20			192.00	3.71	10.54	0.91
	S	Qtz	WR		5			-21.20	-2.50			196.40	4.18	11.63	0.90
	S	Qtz	WR		6			-28.80	-2.20			160.40	3.71	5.61	0.94
	S	Qtz	WR		7	X		-26.00	-1.80			96.80	3.06	5.31	0.98
HPP-16	P	Hydgr	Skarned WR		1			-10.70	-2.60			340.30	4.34	140.21	0.67
	P	Hydgr	Skarned WR		2			-10.70	-2.60			337.30	4.34	135.09	0.68
	P	Hydgr	Skarned WR		3			-10.70	-2.40			338.10	4.03	136.44	0.67
	P	Hydgr	Skarned WR		4			-14.60	-2.60			320.80	4.34	109.15	0.71
	P	Hydgr	Skarned WR		5			-14.60	-2.60			344.80	4.34	148.15	0.66
	P	Hydgr	Skarned WR		6			-14.60	-2.60			335.40	4.34	131.91	0.68
	P	Hydgr	Skarned WR		7			-14.60	-2.60			307.20	4.34	90.50	0.74
	P	Hydgr	Skarned WR		8				-2.40			312.60	4.03	97.62	0.72
	P	Hydgr	Skarned WR		9	X			-2.40			284.00	4.03		0.78
	P	Hydgr	Skarned WR		10				-2.40			312.60	4.03	63.96	0.72
	P	Qtz	Skarned WR		11			-10.20	-3.10			330.20	5.11	123.46	0.71
	P	Qtz	Skarned WR		12			-10.20	-3.10			323.60	5.11	113.29	0.72
	P	Qtz	Skarned WR		13			-10.20	-3.10			318.30	5.11	105.54	0.73

XCO_2	XCH_4	VCAR	fv	Phase	Comments
			0.25	L-V	3-phase with accidental solid (irregular shaped), negative crystal slightly elongated,
			0.25	L-V	oblate, regular shaped
			0.30	L-V	oblate, regular shaped
			0.30	L-V	negative crystal, slightly irregular
			0.30	L-V	slightly irregular, elongated shape
			0.25	L-V	irregular shaped, secondary
			0.20	L-V	negative crystal, slightly elongated
			0.30	L-V	large, vapor rich inclusions (10-15μm), somewhat irregular shaped to negative crystal
			0.30	L-V	large, vapor rich inclusions (10-15μm), somewhat irregular shaped to negative crystal
			0.30	L-V	large, vapor rich inclusions (10-15μm), somewhat irregular shaped to negative crystal
			0.30	L-V	large, vapor rich inclusions (10-15μm), somewhat irregular shaped to negative crystal
			0.30	L-V	large, vapor rich inclusions (10-15μm), somewhat irregular shaped to negative crystal
			0.30	L-V	large, vapor rich inclusions (10-15μm), somewhat irregular shaped to negative crystal
			0.30	L-V	large, vapor rich inclusions (10-15μm), somewhat irregular shaped to negative crystal
			0.30	L-V	large, vapor rich inclusions (10-15μm), somewhat irregular shaped to negative crystal
			0.30	L-V	vapor rich, elongate, negative crystal, large vapor bubble
			0.30	L-V	vapor rich, elongate, negative crystal, large vapor bubble
			0.30	L-V	vapor rich, elongate, negative crystal, large vapor bubble
			0.30	L-V	vapor rich, elongate, negative crystal, large vapor bubble
			0.30	L-V	vapor rich, elongate, negative crystal, large vapor bubble

HPP-18	PS	Cal	CV		1						128.80	1.00	4.49	0.95
	PS	Cal	CV		2						136.40	1.00	4.51	0.94
	PS	Cal	CV		3						148.20	1.00	4.83	0.93
	PS	Cal	CV		4						136.40	1.00	4.51	0.94
	P	Cal	CV	chip 2	5			-21.60			121.20	1.00	4.58	0.95
	P	Cal	CV		6			-21.60					5.74	
	P	Cal	CV		7			-21.60						
	P	Cal	CV		8			-21.60						
	P	Cal	CV	chip 3	9			-18.60	-0.70		161.80	1.22	5.74	0.92
	P	Cal	CV		10			-15.50	-2.40		155.60	4.03	5.24	0.94
	P	Cal	CV		11			-15.50	-2.40		148.20	4.03	4.83	0.95
HPP-21	P/PS	Qtz	QV		1				-2.00		443.80	3.39	407.85	0.34
	P/PS	Qtz	QV		2				-2.00		437.40	3.39	385.57	0.36
	P/PS	Qtz	QV		3				-2.00		415.80	3.39	316.40	0.44
	P/PS	Qtz	QV		4				-2.00		372.50	3.39	203.78	0.57
	P/PS	Qtz	QV		5				-2.00		372.50	3.39	203.78	0.57
	P/PS	Qtz	QV		6				-2.00		372.50	3.39	203.78	0.57
	P/PS	Qtz	QV	chip 2	7			-21.00	-3.50		310.20	5.71	94.41	0.76
	P/PS	Qtz	QV		8			-21.00	-3.50		314.60	5.71	100.35	0.75
	P/PS	Qtz	QV		9			-21.00	-3.50		362.50	5.71	182.31	0.64
	P/PS	Qtz	QV		10			-21.00	-3.50		285.60	5.71	65.60	0.80
	P/PS	Qtz	QV		11			-21.00	-3.50		371.40	5.71	201.34	0.62
	P/PS	Qtz	QV		12						405.80			
	P/PS	Qtz	QV		13						410.80			
HPP-24	P	Qtz	MC		1		-57.10	-26.50	-4.20	5.60	28.10	289.80	9.46	2100.47	0.85
	P	Qtz	MC		2		-57.10	-26.50		7.50	30.80	269.80	5.92	17411.78	0.83
	P	Qtz	MC		3		-57.10	-26.50		7.50	30.80	279.40	5.92	1630.06	0.83
	P	Qtz	MC		4	X		-26.50	-4.20			279.40	6.83	59.44	0.74
	P	Qtz	MC		5			-29.60	-4.20			222.10	6.83	20.48	0.66
	P	Qtz	MC		6			-29.60	-4.20			227.60	6.83	22.97	0.66
	PS	Qtz	MC		7			-24.10		8.40		238.60			
	PS	Qtz	MC		8			-24.10		8.40		231.80			
	PS	Qtz	MC		9			-24.10		8.40		238.60			

			0.25	L-V	negative crystal, high density of inclusions surrounding
			0.25	L-V	negative crystal, high density of inclusions surrounding
			0.25	L-V	negative crystal, high density of inclusions surrounding
			0.25	L-V	negative crystal, high density of inclusions surrounding
			0.25	L-V	negative crystal, slightly irregular
			0.25	L-V	negative crystal, slightly irregular
			0.25	L-V	negative crystal, slightly irregular
			0.25	L-V	negative crystal, slightly irregular
			0.25	L-V	negative crystal, slightly irregular
			0.25	L-V	negative crystal, slightly irregular
			0.25	L-V	negative crystal, slightly irregular
			0.25	L-V	elongated in shape, slightly irregular
			0.25	L-V	elongated in shape, slightly irregular
			0.25	L-V	elongated in shape, slightly irregular
			0.25	L-V	elongated in shape, slightly irregular
			0.25	L-V	elongated in shape, slightly irregular
			0.25	L-V	elongated in shape, slightly irregular
			0.25	L-V	elongated in shape, slightly irregular
			0.25	L-V	elongated in shape, slightly irregular
			0.25	L-V	elongated in shape, slightly irregular
			0.45	L-V	elongated in shape, slightly irregular
			0.25	L-V	elongated in shape, slightly irregular
			0.95	L-V	elongated in shape, blocky, slightly irregular
			0.25	L-V	elongated in shape, blocky, slightly irregular
0.98	0.03	87.00	0.25	L-V-CO2	CO2 rich, regular shaped, a bit elongated
0.98	0.03	94.00	0.25	L-V-CO2	CO2 rich, regular shaped, a bit elongated
0.98	0.03	94.00	0.25	L-V-CO2	CO2 rich, regular shaped, a bit elongated
			0.25	L-V	Vapor rich, regular shaped, a bit elongated, some necking down
			0.30	L-V	Vapor rich, regular shaped, a bit elongated, some necking down
			0.30	L-V	Vapor rich, regular shaped, a bit elongated, some necking down
			0.30	L-V	oblate, regular, large inclusions in trail
			0.30	L-V	oblate, regular, large inclusions in trail
			0.30	L-V	oblate, regular, large inclusions in trail

	PS	Qtz	MC	10		-29.80	-4.10			225.80	6.68	22.22	0.66
	P	Qtz	MC	11	-56.70	-23.80		8.10	30.40	238.80	4.14	628.63	0.80
	P	Qtz	MC	12	-56.70	-23.80		8.10	30.40	238.80	4.14	628.63	0.80
	P	Qtz	MC	13	-56.70	-23.80		8.10	30.40	245.80	4.14	731.18	0.80
	P	Qtz	MC	14	-56.70	-23.80		8.10	28.40	289.60	4.17	1767.02	0.83
HPP-28	P	Qtz	QV	1		-13.60	-0.80			249.20	1.40	35.16	0.81
	P	Qtz	QV	2		-12.40	-0.40			231.60	0.70	24.94	0.83
	P	Qtz	QV	3		-10.80	-0.60			231.60	1.05	24.94	0.83
	P	Qtz	QV	4		-10.80	-0.60			226.80	1.05	22.60	0.84
	P	Qtz	QV	5		-10.80	-0.60			235.60	1.05	27.03	0.82
	P	Qtz	QV	6		-10.80	-0.60			232.80	1.05	25.55	0.83
	P	Qtz	QV	7		-18.80	-0.30			223.60	0.53	21.13	0.84
	P	Qtz	QV	8		-18.20	-0.50			216.40	0.88	18.12	0.85
	P	Qtz	WR	9		-18.60	-0.50			242.90	0.88	31.20	0.81
	P	Qtz	WR	10		-18.60	-0.50			232.80	0.88	25.55	0.83
	P	Qtz	WR	11		-17.90	-0.50			219.60	0.88	19.41	0.85
	P	Qtz	WR	12		-17.60	-0.50			215.80	0.88	17.89	0.85
	P	Qtz	WR	13		-17.60	-0.50			241.80	0.88	30.54	0.81
HPP-28V	P	Qtz	Vug	14		-11.00	-2.10			150.20	3.55	4.93	0.94
	P	Qtz	Vug	15		-11.00	-2.10			145.60	3.55	4.72	0.95
	P	Qtz	Vug	16		-11.00	-2.10			162.80	3.55	5.83	0.93
	P	Qtz	Vug	17		-11.00	-2.10			124.60	3.55	4.53	0.96
	P	Qtz	Vug	18		-3.50	-0.80			182.50	1.40	8.55	0.90
HPP-33	P	Cal	CV	1		-16.05	-3.80			211.80	6.16	16.40	0.90
	P	Cal	CV	2		-16.05	-3.80			185.00	6.16	9.02	0.90
	P	Cal	CV	3						222.80			
	P	Cal	CV	4		-17.80	-0.20			174.20	0.35	7.19	0.90
	P	Cal	CV	5			-0.20			172.20	0.35	6.91	0.90
	P	Cal	CV	6			-0.20			162.80	0.35	5.83	0.91
	P	Cal	CV	7			-1.00			169.20	1.74	6.52	0.91
	P	Cal	CV	8			-0.80			213.60	1.40	17.05	0.86
	P	Cal	CV	9			-0.80			201.60	1.40	13.07	0.88
HPP-40	PS	Qtz	QV	1		-10.50	-1.80			242.20	3.06	30.78	0.84
	PS	Qtz	QV	2		-10.50	-1.80			235.40	3.06	26.93	0.85
	PS	Qtz	QV	3		-10.50	-1.80			188.80	3.06	9.81	0.90
	S	Qtz	QV	4		-13.30	-1.10			178.50	1.91	7.85	0.91

			0.30	L-V	oblate, regular, large inclusions in trail
0.99	0.01	94.00	0.30	L-V-CO2	CO2 rich, regular shaped, a bit elongated
0.99	0.01	94.00	0.30	L-V-CO2	CO2 rich, regular shaped, a bit elongated
0.99	0.01	94.00	0.30	L-V-CO2	CO2 rich, regular shaped, a bit elongated
0.99	0.01	88.00	0.30	L-V-CO2	CO2 rich, regular shaped, a bit elongated
			0.30	L-V	elongated
			0.30	L-V	negative crystal
			0.30	L-V	negative crystal
			0.30	L-V	slightly elongated
			0.30	L-V	negative crystal
			0.30	L-V	negative crystal
			0.30	L-V	isolated inclusion, negative crystal
			0.30	L-V	isolated inclusion, negative crystal
			0.30	L-V	slightly irregular
			0.30	L-V	slightly irregular, negative crystal
			0.30	L-V	negative crystal
			0.30	L-V	oblate, regular inclusion
			0.30	L-V	oblate, regular inclusion
			0.25	L-V	slightly elongated, negative crystal
			0.25	L-V	oblate, regular
			0.25	L-V	blocky, regular
			0.25	L-V	blocky, regular
			0.25	L-V	blocky, regular
			0.25	L-V	oblate, slightly elongated
			0.25	L-V	oblate, high density of inclusions everywhere, very small, homogenization temp difficult to discern
			0.30	L-V	elongated, oblate, vapor rich, surrounded by inclusions of different shapes and sizes
			0.25	L-V	negative crystal
			0.25	L-V	elongated, slightly irregular
			0.25	L-V	elongated, slightly irregular
			0.25	L-V	elongated, regular
			0.25	L-V	elongated, regular
			0.25	L-V	elongated, regular
			0.30	L-V	slightly irregular, negative crystal
			0.30	L-V	slightly irregular, negative crystal
			0.20	L-V	slightly irregular, negative crystal
			0.25	L-V	oblate, regular

	P	Qtz	QV		5		-13.30	-1.10	201.80	1.91	13.13	0.88
HPP-40W	S	Qtz	WR		6		-11.20	-5.20	110.50	8.14	4.84	1.00
	S	Qtz	WR		7		-11.20	-5.20	168.50	8.14	6.44	0.96
	S	Qtz	WR		8		-11.20	-5.20	168.50	8.14	6.44	0.96
	S	Qtz	WR		9		-11.20	-5.20	172.80	8.14	6.70	0.95
HPP-42	P/PS	Cal	CV		1		-23.60	-0.50	160.20	0.88	5.60	0.92
	P	Cal	CV		2		-23.60	-0.50	144.60	0.88	4.69	0.93
	P	Cal	CV		3		-23.60	-0.50	144.60	0.88	4.69	0.93
	P	Cal	CV		4		-19.20	-0.80	151.80	1.40	5.01	0.93
	P	Cal	CV		5		-17.00	-0.70	151.50	1.22	4.99	0.93
	P	Cal	CV		6		-17.00	-0.70	158.20	1.22	5.43	0.92
	P	Cal	CV		7		-17.00	-0.70	158.20	1.22	5.43	0.92
	P	Cal	CV		8		-17.00	-0.70	158.20	1.22	5.43	0.92
	P	Cal	CV		9		-17.00	-0.70	158.20	1.22	5.43	0.92
	P	Cal	CV		10		-17.00	-0.70	158.20	1.22	5.43	0.92
HPP-43	P	Cal	CV		1			-1.60	201.80	2.74	13.13	0.89
	P	Cal	CV		2			-1.60	231.80	2.74	25.04	0.85
	P	Cal	CV		3			-1.60	231.80	2.74	25.04	0.85
	P	Cal	CV		4			-1.60	179.40	2.74	8.00	0.91
	P	Cal	CV		5			-1.60	200.60	2.74	12.78	0.89
	P	Qtz	CV	chip 2	6		-19.80	-0.60	367.60	1.05	193.06	0.53
	P	Qtz	CV		7		-19.80	-0.60	352.60	1.05	162.61	0.57
	P	Qtz	CV		8		-19.80	-0.60	342.60	1.05	144.23	0.60
	P	Qtz	CV		9		18.60	-0.80	378.20	1.40	216.74	0.51
HPP-52	S	Qtz	WR		1		-18.20	-1.50	213.60	2.57	17.05	0.87
	S	Qtz	WR		2		-14.30	-1.50	192.70	2.57	10.70	0.90
	S	Qtz	WR		3		-16.30	-1.50	186.20	2.57	9.26	0.90
	S	Qtz	WR		4		-16.10	-1.50	191.20	2.57	10.35	0.90
	S	Qtz	WR		5		-16.50	-1.50	197.60	2.57	11.95	0.89
	S	Qtz	WR		6		-16.10	-1.50	189.70	2.57	10.01	0.90
	S	Qtz	WR		7		-18.40	-2.50	221.20	4.18	20.09	0.88
	S	Qtz	WR		8	X	-21.20	-2.10	320.80	3.55	109.15	0.70
	S	Qtz	WR		9	X	-18.20	-1.75	309.80	2.98	93.89	0.71
	S	Qtz	WR		10		-16.80	-2.50	230.20	4.18	24.24	0.86
HPP-57W	S	Qtz	WR		1		-21.60	-0.60	162.40	1.05	5.79	0.92

0.25	L-V	oblate, regular, a bit off S trail
0.20	L-V	negative crystal
0.20	L-V	oblate, regular
0.20	L-V	oblate, regular
0.20	L-V	oblate, regular
0.25	L-V	negative crystal
0.25	L-V	negative crystal
0.25	L-V	negative crystal
0.25	L-V	negative crystal
0.25	L-V	negative crystal
0.25	L-V	negative crystal
0.25	L-V	negative crystal
0.25	L-V	negative crystal
0.25	L-V	negative crystal
0.25	L-V	negative crystal
0.25	L-V	elongated, slightly irregular
0.25	L-V	elongated, slightly irregular
0.25	L-V	elongated, slightly irregular
0.25	L-V	elongated, slightly irregular
0.25	L-V	elongated, slightly irregular
0.25	L-V	negative crystal, next to monophase inclusions
0.25	L-V	negative crystal
0.25	L-V	negative crystal
0.25	L-V	negative crystal
0.30	L-V	large inclusion, recyrstallized, in secondary trail cutting across quartz boundary
0.25	L-V	Oblate in shape, somewhat irregular
0.25	L-V	negative crystal shape
0.25	L-V	negative crystal shape
0.25	L-V	slightly elongated
0.30	L-V	(accidental solid present), somewhat irregular, oblate
0.25	L-V	negative crystal
0.30	L-V	somewhat irregular negative crystal shape, largest inclusion in trail with largest bubble
0.30	L-V	(accidental solid present), somewhat irregular, oblate
0.30	L-V	elongated inclusion, regular, oblate
0.20	L-V	highly irregular shaped, recyrstallized, uniformly distributed

	S	Qtz	WR	2	-21.00	-0.60	158.40	1.05	5.45	0.92
	S	Qtz	WR	3	-21.00	-0.60	162.40	1.05	5.79	0.92
	S	Qtz	WR	4	-21.50	-1.60	178.40	2.74	7.83	0.91
HPP-57	PS	Qtz	QV	5	-27.50	-1.60	284.60	2.74	64.57	0.76
	PS	Qtz	QV	6	-21.50	-2.00	284.60	3.39	64.57	0.77
	S	Qtz	QV	7	-15.00	-0.55	204.60	0.97	13.98	0.87
	PS	Qtz	QV	8	-15.00	-0.55	254.60	0.97	38.85	0.79
	S	Qtz	WR	9	-15.00	-0.55	191.80	0.97	10.49	0.88
	S	Qtz	WR	10	-15.00	-0.55	193.40	0.97	10.87	0.88
HPP-61	P	Cal	CV	1	-21.60	-0.50	141.20	0.88	4.60	0.94
	P	Cal	CV	2	-21.60	-0.80		1.40		0.63
	P	Cal	CV	3	-21.60	-0.50	157.60	0.88	5.39	0.92
	P	Cal	CV	4	-22.90	-0.30	188.60	0.53	9.77	0.88
	P	Cal	CV	5	-22.80	-0.80	190.20	1.40	10.12	0.89
	P	Cal	CV	6	-22.80	-0.80	195.60	1.40	11.42	0.88
	P	Cal	CV	7	-20.10	-0.20	196.80	0.35	11.74	0.87
	P	Cal	CV	8		-0.90	173.50	1.57	7.09	0.91
	P	Cal	CV	9		-0.90	189.90	1.57	10.05	0.89
	P	Cal	CV	10		-0.90	175.60	1.57	7.39	0.91
	P	Cal	CV	11		-0.90	170.50	1.57	6.68	0.91
HPP-78	P	Cal	CV	1	-19.20		126.50	1.00	4.51	0.95
	P	Cal	CV	2	-19.20		127.60	1.00	4.50	0.95
	P	Cal	CV	3	-19.20		126.50	1.00	4.51	0.95
	P	Cal	CV	4	-19.20		127.60	1.00	4.49	0.95
	P	Cal	CV	5	-19.20		129.40	1.00	4.49	0.95
	P	Qtz	WR	6	-16.00	-1.60	217.60	2.74		0.87
	P	Qtz	WR	7	-14.00	9.10	263.20			
	P	Qtz	WR	8	-14.00	9.80	278.60			
	PS	Qtz	WR	9	-14.00	-3.50	178.80	5.71		0.93
	PS	Qtz	WR	10	-14.00	-3.50	222.60	5.71		0.89

0.20	L-V	highly irregular shaped, recyrstallized, uniformly distributed
0.20	L-V	highly irregular shaped, recyrstallized, uniformly distributed
0.20	L-V	highly irregular shaped, recyrstallized, uniformly distributed
0.30	L-V	regular, oblate inclusion
0.30	L-V	regular oblate inclusion
0.30	L-V	negative crystal, slightly irregular
0.30	L-V	elongated, stretched ellipse
0.25	L-V	elongated regular
0.25	L-V	elongated regular
0.25	L-V	regular, oblate, high density of inclusions surrounding inclusion
0.25	L-V	negative crystal high density
0.25	L-V	negative crystal high density
0.25	L-V	negative crystal, high density, accidental solid present
0.25	L-V	negative crystal, high density
0.25	L-V	negative crystal, high density
0.25	L-V	negative crystal, high density
.20-.25	L-V	very elongated, stretched inclusion
.20-.25	L-V	very elongated, stretched inclusion
.20-.25	L-V	very elongated, stretched inclusion
.20-.25	L-V	very elongated, stretched inclusion
0.20	L-V	elongated, sheared in one direction, homogenous assemblage, some necking down
0.20	L-V	elongated, sheared in one direction, homogenous assemblage, some necking down
0.20	L-V	elongated, sheared in one direction, homogenous assemblage, some necking down
0.20	L-V	elongated, sheared in one direction, homogenous assemblage, some necking down
0.20	L-V	elongated, sheared in one direction, homogenous assemblage, some necking down
0.20	L-V	slightly irregular, elongated
0.30	L-V	vapor rich, oblate, next to pyrite
0.30	L-V	vapor rich, oblate, next to pyrite
0.20	L-V	oblate, homogeneous assemblage
0.20	L-V	oblate, homogeneous assemblage

	PS	Qtz	WR		11		-14.00	-3.50	195.60	5.71		0.92
	PS	Qtz	WR		12		-14.00	-3.50	198.40	5.71		0.91
HPP-81	S	Qtz	WR		1		-15.10	-2.20	196.80	3.71	11.74	0.90
	S	Qtz	WR		2		-14.50	-2.20	181.40	3.71	8.35	0.92
	S	Qtz	WR		3	X	-15.10	-2.20	134.60	3.71	4.50	0.96
	S	Qtz	WR	chip 2	4	X	-12.50	-0.90	264.80	1.57	46.57	0.78
	S	Qtz	WR	chip 1	5		-14.25	-2.10	186.50	3.55	9.33	0.91
	S	Qtz	WR		6		-14.25	-2.10	228.80	3.55	23.55	0.86
	S	Qtz	WR		7	X	-14.25	-2.10	256.80	3.55	40.43	0.82
HPP-89	P	Qtz	QV		1		-24.60	-2.40	201.20	4.03	12.95	0.90
	P	Qtz	QV		2		-24.60	-2.40	249.40	4.03	75.08	0.84
	P	Qtz	QV		3		-24.60	-2.40	187.00	4.03	9.43	0.91
	P	Qtz	QV		4		-24.60	-2.40	201.20	4.03	12.95	0.90
	P	Qtz	QV		5		-13.60	-1.80	191.20	3.06	10.35	0.90
	P	Qtz	QV		6		-13.60	-1.80	203.00	3.06	13.49	0.89
	P	Qtz	QV		7		-15.40	-1.80	227.80	3.06	23.07	0.86
	P	Qtz	QV		8		-23.60	-2.10	193.80	3.55	10.97	0.90
	P	Qtz	QV		9		-24.80	-2.40	214.80	4.03	17.51	0.88
	P	Qtz	QV		10		-22.60	-1.80	230.60	3.06	24.44	0.85
HPP-98	P	Qtz	QV		1		-15.15	-3.80	315.40	6.16	101.46	0.75
	P	Qtz	QV		2		-15.15	-4.20	312.60	6.74	97.62	0.77
	P	Qtz	QV		3		-15.15	-3.80	178.80	6.16	7.90	0.94
	P	Qtz	QV		4		-15.15	-3.80	301.80	6.16	83.75	0.78
HPP-98W	S	Qtz	WR		5		-23.50	-3.40	178.80	5.56	7.90	0.93
	S	Qtz	WR		6		-23.60	-3.40	197.20	5.56	11.84	0.91

0.20	L-V	oblate, homogeneous assemblage
0.20	L-V	oblate, homogeneous assemblage
0.25	L-V	oblate, slightly elongated, secondary
0.25	L-V	oblate, slightly elongated, secondary
0.25	L-V	oblate, slightly elongated, secondary
0.25	L-V	oblate, slightly elongated, secondary, banana shaped
0.25	L-V	oblate, slightly elongated, secondary
0.25	L-V	negative crystal, slightly elongated, secondary
0.25	L-V	negative crystal, slightly elongated, secondary
0.30	L-V	elongated, slightly irregular, negative crystal
0.25	L-V	elongated, slightly irregular, negative crystal
0.30	L-V	elongated, slightly irregular, negative crystal
0.30	L-V	blocky, larger than other inclusions surrounding
0.30	L-V	accidental solid present, round, very small bubble, solid (yellowish), irregular shape, didn't melt when heated
0.30	L-V	accidental solid present, round, very small bubble, solid (yellowish), irregular shape, didn't melt when heated
0.30	L-V	accidental solid present, round, very small bubble, solid (yellowish), irregular shape, didn't melt when heated
0.30	L-V	isolated inclusion, rather large, slightly irregular
0.30	L-V	isolated inclusion, rather large, slightly irregular
0.30	L-V	isolated inclusion, rather large, slightly irregular
0.30	L-V	large, oblate, vapor rich, some necking down
0.30	L-V	large, oblate, vapor rich
0.25	L-V	large, oblate, vapor rich
0.30	L-V	large,v-shaped, next to number 1, not in picture
0.25	L-V	smaller inclusions, oblate, round, in trail
0.25	L-V	smaller inclusions, oblate, round, in trail

	S	Qtz	WR		7		-23.70	-0.70	136.30	1.22	4.51	0.94
	S	Qtz	WR		8		-23.80	-3.40	135.80	5.56	4.51	0.97
	S	Qtz	WR		9		-23.90	-3.40	163.20	5.56	5.87	0.95
	S	Qtz	WR		10	X	-17.80	-3.60	230.80	5.86	24.54	0.88
HPP-98	P	Qtz	QV		11		-17.80	-3.60	286.80	5.86	66.84	0.80
	S	Qtz	WR	chip 2	12			-3.70	159.60	6.01	5.54	0.95
	S	Qtz	WR		13			-3.70	162.50	6.01	5.80	0.95
	S	Qtz	WR	chip 3	14		-24.10	-3.10	156.40	5.11	5.30	0.95
	S	Qtz	WR		15		-24.10	-3.10	148.20	5.11	4.83	0.95
	S	Qtz	WR		16		-24.10	-3.10	178.60	5.11	7.87	0.93
HPP-100 (remeasured)	P	Cal	CV		1				391.10			
	P	Qtz	CV		2			-1.80	330.20	3.06	123.46	0.67
	P	Qtz	CV		3	X		-3.40	398.80	5.56	268.21	0.55
	P	Qtz	CV		4			-3.00	360.60	4.96	178.41	0.63
	P	Qtz	CV		5		-15.10	-3.10	369.80	5.11	197.82	0.61
	P	Qtz	CV		6			-3.10	360.10	5.11	177.40	0.64
	P	Qtz	CV		7			-3.10	350.70	5.11	159.00	0.66
HPP-103	P	Qtz	CV		1		-11.20	-0.80	221.40	1.40	20.17	0.85
	P	Qtz	CV		2		-11.20	-0.80	216.80	1.40	18.28	0.86
	P	Qtz	CV		3			-2.80	148.80	4.65	4.86	0.95
	P	Qtz	CV		4			-2.80	157.40	4.65	5.37	0.94
	P	Qtz	CV		5			-1.70	198.20	2.90	12.11	0.89
	P	Qtz	CV		6			-3.50	174.50	5.71	7.23	0.94
	P	Qtz	CV		7			-3.50	187.20	5.71	9.47	0.93
HPP-105	P	Cal	CV		1			-3.40	115.60	5.56	4.70	0.98
	P	Cal	CV		2			-3.40	110.80	5.56	4.83	0.98
	P	Cal	CV		3			-3.40	110.60	5.56	4.84	0.98

0.25	L-V	(accidental solid), smaller inclusions, elongated negative crystal, round, in trail secondary
0.25	L-V	(accidental solid), smaller inclusions, elongated negative crystal, round, in trail secondary
0.25	L-V	(accidental solid), smaller inclusions, elongated negative crystal, round, in trail secondary
0.30	L-V	large, oblate, vapor rich
0.30	L-V	large, oblate, vapor rich
0.15	L-V	elongated, negative crystal, in trail away from pyrite
0.15	L-V	elongated, negative crystal, in trail away from pyrite
0.25	L-V	elongated, negative crystal, in trail away from pyrite
0.25	L-V	elongated, negative crystal, in trail away from pyrite
0.25	L-V	(accidental solid), smaller inclusions, elongated negative crystal, round, in trail secondary
0.25		
0.25	L-V	negative crystal, oblate
0.25	L-V	negative crystal, oblate
0.30	L-V	vapor rich, negative crystal
0.25	L-V	negative crystal, regular inclusion
0.25	L-V	negative crystal, regular inclusion
0.25	L-V	negative crystal, regular inclusion
0.25	L-V	negative crystal, regular inclusion
0.25	L-V	(accidental solid present), oblate, negative crystal
0.25	L-V	negative crystal, in shadow so not in picture upper right above FI 1
0.25	L-V	negative crystal, oblate
0.25	L-V	negative crystal, slightly irregular
0.25	L-V	oblate, regular, not in picture
0.25	L-V	elongated, regular inclusion
0.25	L-V	oblate, regular inclusion, ice melt hard to discern
0.25	L-V	negative crystal
0.25	L-V	slightly irregular, negative crystal
0.25	L-V	slightly irregular, negative crystal

	P	Cal	CV		4			-3.40	128.60	5.56	4.50	0.97
	P	Cal	CV	chip 2	5		-20.50	-3.80	179.20	6.16	7.97	0.94
	P	Cal	CV		6		-20.50	-3.80	176.40	6.16	7.51	0.94
	P	Cal	CV		7		-20.50	-3.80	158.60	6.16	5.47	0.95
HPP-107	P	Cal	CV	chip 1	1				110.60	1.00	4.84	0.96
	P	Cal	CV		2				126.80	1.00	4.50	0.95
	P	Cal	CV		3				128.40	1.00	4.49	0.95
	P	Cal	CV	chip 2	4				103.20	1.00	5.08	0.96
	P	Cal	CV		5				119.60	1.00	4.61	0.95
HPP-111	S	Qtz	WR		1		-24.60	-2.40	127.20	4.03	4.50	0.96
	S	Qtz	WR		2		-24.60	-2.40	135.90	4.03	4.50	0.96
	S	Qtz	WR		3		-24.60	-3.10	153.50	5.11	5.11	0.95
	S	Qtz	WR		4		-24.00	-2.60	154.80	4.34	5.19	0.94
	S	Qtz	WR		5		-24.10	-1.80	182.80	3.06	8.60	0.91
	S	Qtz	WR		6		-27.05	-1.80	167.00	3.06	6.27	0.93
	S	Qtz	WR		7		-24.10	-2.10	156.50	3.55	5.31	0.94
	S	Qtz	WR		8			-0.80	148.80	1.40	4.86	0.93
	S	Qtz	WR		9	X	-27.05	-1.80	230.60	3.06	24.44	0.85
		Qtz	WR									
HPP-113	P	Qtz	MC		1		-13.20		221.80			
	P	Qtz	MC		2		-13.20					
	P	Qtz	MC		3		-13.20	-2.60	245.20	4.34	32.61	0.85
	P	Qtz	MC		4	X	-10.20	-2.60	187.40	4.34	9.51	0.91
	-	Qtz	MC		5		-13.00		273.50			
	P	Qtz	MC		6			-2.60	258.60	4.34	41.76	0.83
	P	Qtz	MC		7			-2.60	257.80	4.34	41.16	0.83
	P	Qtz	MC		8			-2.60	258.60	4.34	41.76	0.83
	S	Qtz	MC	chip 2	9		-11.60	-2.90	187.20	4.80		0.92
	S	Qtz	MC		10		-10.60	-2.50	304.60	4.18		0.74
	S	Qtz	MC		11		-10.60	-1.10	145.80	1.10		0.94

0.25	L-V	slightly irregular, negative crystal
0.25	L-V	slightly elongated
0.25	L-V	slightly irregular, negative crystal
0.25	L-V	slightly irregular, negative crystal
0.25	L-V	elongated, bubble disappeared upon cooling (very low salinity)
0.25	L-V	elongated, bubble disappeared upon cooling (very low salinity)
0.25	L-V	elongated, bubble disappeared upon cooling (very low salinity)
0.25	L-V	elongated, bubble disappeared upon cooling (very low salinity)
0.25	L-V	elongated, bubble disappeared upon cooling (very low salinity)
0.25	L-V	oblate, regular shaped
0.25	L-V	negative crystal
0.25	L-V	elongated, negative crystal
0.25	L-V	elongated, negative crystal
0.30	L-V	elongated, slightly irregular, appears stretched
0.25	L-V	elongated, cylindrical
0.25	L-V	(accidental solid present), v-shaped
0.20	L-V	negative crystal,
0.25	L-V	elongated, cylindrical, oblate
0.30	L-V	vapor rich, large vapor bubble, negative crystal, oblate, decrepitates temperature
0.30	L-V	vapor rich, large vapor bubble, negative crystal, oblate, decrepitates temperature
0.30	L-V	vapor rich, large vapor bubble, negative crystal, oblate, decrepitates temperature
0.20	L-V	vapor rich, large vapor bubble, negative crystal, oblate, decrepitates temperature
0.20	L-V	vapor rich, large vapor bubble, negative crystal, oblate, decrepitates temperature
0.20	L-V	smaller inclusions that didn't decrepitates, squarish, blocky inclusion
0.20	L-V	smaller inclusions that didn't decrepitates, squarish, blocky inclusion
0.20	L-V	smaller inclusions that didn't decrepitates, squarish, blocky inclusion
0.20	L-V	slightly irregular
0.30	L-V	negative crystal
0.20	L-V	slightly irregular, negative crystal

	P	Qtz	MC	12		-57.50	-13.40	-2.60	7.80	27.80	366.00	7.53	7258.45	0.99
	P	Qtz	MC	13		-59.70	-13.10		8.00	30.40	309.80			
	P	Qtz	MC	14		-59.30	-13.10	-2.40	4.10	30.40	278.80			
	P	Qtz	MC	15		-57.50	-13.60		7.60	27.60	440.80		938.99	0.58
	P	Qtz	MC	16		-57.50	-13.60		7.60	27.60	440.90		939.49	0.58
	P	Qtz	MC	17		-57.50	-13.60		7.60	27.60	480.60		1147.63	0.58
	P	Qtz	WR	18			-11.10				330.70			
	P	Qtz	WR	19							321.80			
	P	Qtz	WR	20				-3.00			347.50	4.96		0.66
	P	Qtz	WR	21				-3.00			347.50	4.96		0.66
	P	Qtz	WR	22				-3.00			347.50	4.96		0.66
HPP-115W	S	Qtz	WR	1			-13.45	-1.10			176.70	1.91	7.56	0.91
	S	Qtz	WR	2			-13.45	-0.80			158.20	1.40	5.43	0.92
	S	Qtz	WR	3			-13.45	-0.80			126.80	1.40	4.50	0.95
	S	Qtz	WR	4			-13.45	-0.80			122.60	1.40	4.55	0.95
	S	Qtz	WR	5			-10.75	-0.60			184.80	1.05	8.98	0.89
HPP-115	P	Qtz	QV	6			-29.00	-0.20			341.80	0.35	142.83	0.59
	P	Qtz	QV	7	X		-29.00	-0.60			210.50	1.05	15.93	0.86
	P	Qtz	QV	8			-29.00	-0.20			330.60	0.35	124.10	0.62
	P/PS	Qtz	QV	9	X		-23.50	-0.80			264.80	1.40	46.57	0.78
	PS	Qtz	QV	10			-23.50	-0.80			342.60	1.40	144.23	0.61
	PS	Qtz	QV	11			-23.50	-0.80			335.60	1.40	132.24	0.63
HPP-100	P	Cal	CV	3			-25.60	-8.20		18.20				
	P	Cal	CV	4			-29.60	-17.20		5.60				
	P	Cal	CV	5		-56.80		-11.80		19.20				0.72

0.95	0.05	80.20	0.30	L-V-CO2	elongated, negative crystal shaped, bubble in bubble observed
			0.40	L-V-CO2	elongated, negative crystal shaped, bubble in bubble observed
			0.40	L-V-CO2	elongated, negative crystal shaped, bubble in bubble observed
0.95	0.05	80.00	0.95	L-V-CO2	more CO2 rich, elongated, negative crystal shaped, bubble in bubble observed
0.95	0.05	80.00	0.95	L-V-CO2	more CO2 rich, elongated, negative crystal shaped, bubble in bubble observed
0.95	0.05	80.00	0.95	L-V-CO2	more CO2 rich, elongated, negative crystal shaped, bubble in bubble observed
				L-V-CO2	
			0.25	L-V	elongated, negative crystal shaped, elongated inclusion.
			0.25	L-V	elongated inclusion, ice melt difficult to discern
			0.25	L-V	elongated inclusion, ice melt difficult to discern
			0.25	L-V	elongated inclusion, ice melt difficult to discern
			0.25	L-V	elongated, appears stretched
			0.25	L-V	elongated
			0.30	L-V	elongated, oblate
			0.25	L-V	elongated, slightly irregular
			0.25	L-V	elongated
			0.45	L-V	vapor rich, oblate, negative crystal
			0.30	L-V	(accidental solid present), vapor rich, oblate
			0.40	L-V	vapor rich, oblate, negative crystal, big vapor bubble
			0.25	L-V	negative crystal
			0.40	L-V	vapor rich, oblate, negative crystal, big vapor bubble
			0.40	L-V	vapor rich, oblate, negative crystal, big vapor bubble
			0.25	L-V	oblate, no bubbles at room temp, however appeared around 2-10 degrees
			0.20	L-V	oblate, no bubbles at room temp, however appeared around 2-10 degrees
0.97	0.03	57.10	0.25	L-CO2?	oblate, appeared there was CO2, but phase changes never happened, when heated, bubble never moved

P	Cal	CV	6	-56.80	-12.50	20.10	0.73
P	Cal	CV	7	-56.80	-12.50	20.10	0.73
P	Cal	CV	8		-9.60	12.20	
P	Cal	CV	9	-47.20	-33.40	22.10	
P	Cal	CV	10	-57.50	-35.60	2.50	0.73
P	Cal	CV	11	-57.50	-35.60	2.10	0.73

0.97	0.03	58.00	0.25	L-CO2?	oblate, appeared there was CO2, but phase changes never happened, when heated, bubble never moved
0.97	0.03	58.00	0.25	L-CO2?	oblate, appeared there was CO2, but phase changes never happened, when heated, bubble never moved
			0.25	L-CO2?	oblate, appeared there was CO2, but phase changes never happened, when heated, bubble never moved
			0.25	L-CO2?	oblate, appeared there was CO2, but phase changes never happened, when heated, bubble never moved
0.95	0.05	48.20	0.25	L-CO2?	oblate, appeared there was CO2, but phase changes never happened, when heated, bubble never moved
0.95	0.05	48.30	0.25	L-CO2?	oblate, appeared there was CO2, but phase changes never happened, when heated, bubble never moved

Table 2: Consolidated average microthermometric data for each sample

Sample #	Subgroup	Location	Alteration Style	F.I. Origin/Host Mineral	Phases	fv	Avg. Size (µm)	F.I. Type	Tm_{CO_2}	$T_{eutectic}$	Tm_{ice}
HPP-15	Skarn (S)	on	skarn	S/qtz	L-V, accidental solid present in some	.25-.30	10	Type I		-21.95	-3.30
HPP-16	Skarn (P)	on	skarn	P/hydrogrossular,qtz	L-V	0.30	15-60	Type II		-12.11	-2.68
HPP-18	Type B Cal vein (on)	on	skarn	P/cal	L-V	0.25	8	Type I		-19.43	-1.83
HPP-21	Qtz vein (on)	on	skarn	P,PS/qtz	L-V	0.25	10	Type II		-21.00	-2.68
HPP-24	MC (within)	within	none	P/qtz	L-V-CO2	.25-.30	17-25	Type III	-56.83	-24.70	-4.20
HPP-24a	MC (within)	within	none	P/qtz	L-V	0.25	8-20	Type II		-29.67	-4.17
HPP-28	Qtz vein (within)	within	none	P/qtz	L-V	0.30	13	Type II		-13.28	-0.55
HPP-28V	Vugs (within)	within	none	P/qtz	L-V	0.25	8	Type I		-9.50	-1.84
HPP-33	Type B Cal vein (on)	on	skarn	P/cal	L-V	0.25	6.5	Type I		-16.63	-1.35
HPP-40	Qtz vein (on)	on	potassic	P/qtz	L-V	.25-.30	10	Type II		-11.62	-1.52
HPP-40W	Potassic	on	potassic	S/qtz	L-V	0.20	5	Type I		-11.20	-5.20
HPP-42	Type B Cal vein (on)	on	skarn	P/cal	L-V	0.25	8	Type I		-19.20	-0.65
HPP-43	Type B Cal vein (on)	on	skarn	P/cal	L-V	0.25	3.5	Type II			-1.60
HPP-52	Phyllic	on	phyllic	S/qtz	L-V, accidental solid present in some	.25-.30	12	Type I		-16.59	-1.75
HPP-57	Qtz vein (on)	on	skarn	PS/qtz	L-V	0.30	9	Type II		-21.33	-1.38
HPP-57W	Skarn (S)	on	skarn	S/qtz	L-V	.25-.30	10	Type I		-15.00	-0.55
HPP-61	Type B Cal vein (on)	on	skarn	P/cal	L-V	.20-.25	9	Type I		-21.91	-0.68
HPP-78	Type A Cal vein (away)	away	none	P/cal	L-V	.20-.25	7	Type I		-19.20	
HPP-81	Phyllic	on	phyllic	S/qtz	L-V	0.25	7	Type I		-14.53	-2.15
HPP-89	Qtz vein (on)	on	none	P/qtz	L-V, accidental solid present in some	0.30	5-18	Type II		-21.20	-2.13
HPP-98	Qtz vein (on)	on	phyllic	P/qtz	L-V	0.30	10	Type II		-15.81	-3.85
HPP-98W	Phyllic	on	phyllic	S/qtz	L-V, accidental solid present in some	0.25	7	Type I		-22.88	-3.16

Tm_{clath}	Th_{total}	Th_{CO_2}	Ph_{total}	Tt_{total} (low)	Tt (high)	Tt (avg.)	Mass% eq. NaCl	Density (g/cc)	XCO_2	XCH_4	VCAR	Comments
	190.20		11.45	245.00	445.00	345.00	5.31	0.92				oblate, negative crystal, slightly irregular
	326.80		119.08	465.00	710.00	587.50	4.45	0.70				vapor rich, round, oblate, negative crystal
	142.08		4.84	190.00	340.00	265.00	1.78	0.94				oblate, negative crystal, slightly irregular
	368.98		215.01	420.00	800.00	610.00	4.44	0.58				elongated, slightly irregular
7.58	263.70	29.75	3556.86	355.00	505.00	430.00	5.53	0.82	0.98	0.02	91.83	Double bubble, CO2 rich, oblate, round, can be elongated
	225.23		21.89	355.00	460.00	407.50	6.78	0.66				oblate, round, vapor rich
	230.95		24.94	325.00	480.00	402.50	0.96	0.83				oblate, negative crystal, slightly irregular, some vapor rich
	153.14		5.71	200.00	360.00	280.00	3.12	0.94				oblate, negative crystal, slightly irregular
	186.30		10.25	250.00	420.00	335.00	2.24	0.90				oblate, negative crystal, slightly irregular
	209.34		17.70	285.00	460.00	372.50	2.60	0.87				oblate, negative crystal, slightly irregular
	155.08		6.18	200.00	340.00	270.00	8.14	0.97				oblate, negative crystal
	154.37		5.22	240.00	340.00	290.00	1.14	0.92				negative crystal, slightly elongated
	209.80		16.80	275.00	450.00	362.50	2.74	0.88				elongated
	202.80		14.21	285.00	450.00	367.50	2.97	0.89				oblate, negative crystal, slightly irregular, some vapor rich
	274.60		56.00	380.00	550.00	465.00	2.36	0.77				oblate, negative crystal, slightly irregular
	196.60		35.34	305.00	405.00	355.00	0.97	0.88				oblate, negative crystal, slightly irregular
	177.95		8.43	220.00	390.00	305.00	1.19	0.88				negative crystal, very elongated, slightly irregular
	127.52		4.50	210.00	290.00	250.00	1.00	0.95				oblate, negative crystal, slightly irregular, some sheared in one direction
	198.38		13.24	280.00	445.00	362.50	3.63	0.90				oblate, negative crystal, slightly irregular, some surrounding inclusions very stretched
	210.00		21.02	285.00	440.00	362.50	3.59	0.88				oblate, negative crystal, slightly irregular, elongated
	304.15		87.42	430.00	610.00	520.00	6.23	0.77				vapor rich, oblate, negative crystal, v-shaped
	163.22		6.53	220.00	385.00	302.50	5.18	0.94				oblate, negative crystal, slightly irregular

HPP-100	Type A Cal vein (away)	away	none	P/qtz	L-V	0.25	5	Type II		-15.10	-2.82
HPP-103	Type A Cal vein (away)	away	none	P/qtz	L-V, accidental solid present in some	0.25	3	Type I		-11.20	-2.27
HPP-105	Type A Cal vein (away)	away	none	P/cal	L-V	0.25	5	Type I		-20.50	-3.57
HPP-107	Type A Cal vein (away)	away	none	P/cal	L-V	0.25	3	Type I			
HPP-111	Potassic	away	potassic	S/qtz	L-V	0.25	12	Type I		-24.72	-2.13
HPP-113	MC (away)	away	none	P/qtz	L-V-CO2	.35-.95	12-30	Type III	-57.50	-13.60	
HPP-113a	MC (away)	away	none	P/qtz	L-V	.25-.30	10-60	Type II		-13.20	-2.60
HPP-115	Qtz vein (away)	away	skarn	P/qtz	L-V	0.35	25	Type II		-26.25	-0.50
HPP-115W	Skarn (S)	away	skarn	S/qtz	L-V	0.25	10	Type I		-12.91	-0.82

	354.30		167.22	500.00	790.00	645.00	4.67	0.64				oblate, negative crystal, slightly irregular
	186.30		11.07	225.00	430.00	327.50	3.77	0.91				oblate, negative crystal, slightly irregular
	139.97		5.69	180.00	350.00	265.00	5.82	0.96				oblate, negative crystal, slightly irregular
	117.72		4.70	175.00	290.00	232.50	1.00	0.95				oblate, negative crystal, slightly irregular
	153.31		5.54	210.00	360.00	285.00	3.57	0.94				oblate, negative crystal, slightly irregular, elongated
7.60	454.10	27.60	2571.14	540.00	800.00	670.00	5.53	0.58	0.95	0.05	80.00	Double bubble, CO2 rich, oblate, round
	255.05		39.32	350.00	500.00	425.00	4.34	0.83				Large, some highly elongated, some regular, vapor rich
	337.65		135.85	510.00	705.00	607.50	0.91	0.61				vapor rich, oblate, negative crystal
	153.82		6.21	210.00	355.00	282.50	1.43	0.93				oblate, negative crystal, slightly irregular, slightly elongated

Table 3: Average microthermometric statistical data organized by fluid inclusion setting

Subgroup	Statistic	Tm_{CO_2}	$T_{eutectic}$	Tm_{ice}	Tm_{clath}	Th_{CO_2}	Th_{total}	Tt_{total} (low)	Tt_{total} (high)	Tt (avg.)	Mass% eq. NaCl	Ph_{total} (bars)	Density (g/cc)	XCO_2	XCH_4	VCAR
Regional	Average	-57.50	-18.21	-2.10	7.35	29.16	221.15	300.65	472.74	386.69	3.37	88.03	0.85	0.97	0.03	87.89
	Mode	-57.50	-24.60	-0.80	8.10	30.40	158.20	210.00	340.00	275.00	1.00	4.50	0.92	0.99	0.01	94.00
	Median	-57.30	-17.80	-2.10	7.70	29.40	197.20	280.00	445.00	362.50	3.39	11.27	0.89	0.98	0.03	88.00
	Max	-56.70	-3.50	-0.20	8.10	30.80	480.60	540.00	800.00	670.00	9.73	2100.47	1.00	0.99	0.05	94.00
	Min	-59.70	-29.80	-6.40	4.10	27.60	96.80	175.00	290.00	232.50	0.35	4.49	0.34	0.95	0.01	80.00
	n	12.00	168.00	193.00	12.00	12.00	219.00	31.00	31.00	31.00	212.00	212.00	215.00	9.00	9.00	9.00
Type I	Average		-18.52	-2.01			165.28	245.56	380.28	312.92	3.02	7.80	0.92			
	Mode		-21.60	-0.80			158.20	210.00	340.00	275.00	1.00	5.43	0.92			
	Median		-18.60	-1.80			162.80	222.50	372.50	297.50	2.57	5.80	0.93			
	Max		-10.75	-0.20			230.20	510.00	450.00	480.00	9.73	24.24	1.00			
	Min		-28.80	-6.40			103.20	175.00	290.00	232.50	0.35	4.49	0.63			
	n		87.00	100.00			115.00	18.00	18.00	18.00	115.00	115.00	115.00			
Type II	Average		-17.54	-2.07			287.84	391.36	591.36	491.36	3.46	93.13	0.75			
	Mode		-21.00	-1.80			312.60	285.00	460.00	372.50	3.06	203.78	0.57			
	Median		-15.15	-2.00			304.50	380.00	550.00	465.00	3.39	75.08	0.77			
	Max		-10.20	-0.20			443.80	510.00	800.00	655.00	6.74	407.85	0.91			
	Min		-29.80	-4.20			178.50	285.00	440.00	362.50	0.35	7.85	0.34			
	n		55.00	67.00			68.00	11.00	11.00	11.00	67.00	67.00	67.00			
Type III	Average	-57.06	-21.00		7.59	29.03	327.17	447.50	652.50	550.00	5.55	1168.01	0.74	0.99	0.01	94.00
	Mode	-56.70	-23.80		8.10	30.40	238.80	-	-	-	4.14	628.63	0.80	0.98	0.03	88.00
	Median	-57.10	-23.80		7.60	28.40	289.60	447.50	652.50	550.00	5.92	939.49	0.80	0.99	0.05	94.00
	Max	-56.70	-13.60		8.10	30.80	480.60	540.00	800.00	670.00	9.46	2100.47	0.85	0.95	0.01	80.00
	Min	-57.50	-26.50		5.60	27.60	238.80	355.00	505.00	430.00	4.14	628.63	0.58	9.00	9.00	9.00
	n	9.00	9.00		9.00	9.00	9.00	2.00	2.00	2.00	9.00	9.00	9.00			
Type I (on)	Average		-18.85	-1.91			174.46	243.50	396.00	319.75	3.00	8.63	0.91			
	Mode		-21.60	-0.70			158.20	220.00	340.00	280.00	1.22	5.43	0.92			
	Median		-18.20	-1.50			172.80	242.50	397.50	320.00	1.74	6.70	0.92			
	Max		-11.20	-0.20			230.20	305.00	450.00	377.50	9.73	24.24	1.00			
	Min		-28.80	-6.40			110.50	190.00	340.00	265.00	0.35	4.49	0.63			
	n		61.00	68.00			73.00	10.00	10.00	10.00	73.00	73.00	73.00			
Type I (away)	Average		-18.98	-2.30			148.81	201.67	345.83	273.75	3.05	6.45	0.94			
	Mode		-19.20	-0.80			126.80	210.00	290.00	250.00	1.00	4.50	0.95			
	Median		-19.20	-2.40			148.80	210.00	352.50	281.25	2.90	4.86	0.95			
	Max		-10.75	-0.60			221.40	225.00	430.00	327.50	6.16	20.17	0.98			
	Min		-27.05	-3.80			103.20	175.00	290.00	232.50	1.00	4.49	0.85			
	n		22.00	27.00			37.00	6.00	6.00	6.00	37.00	37.00	37.00			

Type I (within)	Average	-9.50	-1.84	153.14	200.00	360.00	280.00	3.12	5.71	0.94
	Mode	-11.00	-2.10	-	-	-	-	3.55	-	-
	Median	-11.00	-2.10	150.20	200.00	360.00	280.00	3.55	4.93	0.94
	Max	-3.50	-0.80	182.50	200.00	360.00	280.00	3.55	8.55	0.96
	Min	-11.00	-2.10	124.60	200.00	360.00	280.00	1.40	4.53	0.90
	n	5.00	5.00	5.00	1.00	1.00	1.00	5.00	5.00	5.00
Type II (on)	Average	-16.85	-2.36	284.25	362.86	574.29	468.57	3.94	93.22	0.76
	Mode	-21.00	-2.40	312.60	285.00	-	-	3.39	203.78	0.57
	Median	-15.15	-2.40	294.30	380.00	550.00	465.00	4.03	70.96	0.77
	Max	-10.20	-0.55	443.80	465.00	800.00	632.50	6.74	407.85	0.91
	Min	-27.50	-4.20	178.50	275.00	440.00	357.50	0.97	7.85	0.34
	n	37.00	50.00	50.00	7.00	7.00	7.00	50.00	50.00	50.00
Type II (away)	Average	-20.90	-2.04	320.45	430.00	602.50	516.25	3.40	112.75	0.69
	Mode	-23.50	-2.60	258.60	-	-	-	4.34	41.76	0.83
	Median	-23.50	-2.60	335.60	430.00	602.50	516.25	4.34	128.17	0.64
	Max	-13.00	-0.20	391.10	510.00	705.00	607.50	5.11	197.82	0.85
	Min	-29.00	-3.10	245.20	350.00	500.00	425.00	0.35	32.61	0.59
	n	7.00	13.00	15.00	2.00	2.00	2.00	13.00	14.00	13.00
Type II (within)	Average	-17.75	-1.54	229.37	340.00	470.00	405.00	2.55	24.10	0.78
	Mode	-10.80	-0.60	231.60	-	-	-	1.05	24.94	-
	Median	-13.60	-0.60	227.60	340.00	470.00	405.00	1.05	22.97	0.83
	Max	-10.80	-0.30	249.20	355.00	480.00	417.50	6.83	35.16	0.85
	Min	-29.80	-4.20	216.40	325.00	460.00	392.50	0.53	18.12	0.66
	n	11.00	11.00	11.00	2.00	2.00	2.00	11.00	11.00	11.00
Qtz Vein (on)	Average	-18.61	-2.36	280.18	360.00	572.00	466.00	3.93	96.41	0.76
	Mode	-21.00	-2.00	372.50	285.00	-	-	3.39	203.78	0.57
	Median	-21.00	-2.00	284.60	380.00	550.00	465.00	3.39	64.57	0.80
	Max	-10.50	-0.55	443.80	430.00	800.00	615.00	6.74	407.85	0.91
	Min	-27.50	-4.20	178.50	285.00	440.00	362.50	0.97	7.85	0.34
	n	27.00	33.00	33.00	5.00	5.00	5.00	33.00	33.00	33.00
Qtz Vein (away)	Average	-26.25	-0.57	304.32	510.00	705.00	- 607.50	0.99	100.98	0.68
	Mode	-29.00	-0.80	-	-	-	-	1.40	-	-
	Median	-26.25	-0.70	333.10	510.00	705.00	607.50	1.22	128.17	0.62
	Max	-23.50	-0.20	342.60	510.00	705.00	607.50	1.40	144.23	0.86
	Min	-29.00	-0.80	210.50	510.00	705.00	607.50	0.35	15.93	0.59
	n	6.00	6.00	6.00	1.00	1.00	1.00	6.00	6.00	6.00
Qtz Vein (within)	Average	-13.28	-0.55	230.95	325.00	480.00	402.50	0.96	24.93	0.83
	Mode	-10.80	-0.60	231.60	-	-	-	1.05	24.94	-
	Median	-11.60	-0.60	231.60	325.00	480.00	402.50	1.05	24.94	0.83

	Max	-10.80	-0.30	249.20	325.00	480.00	402.50	1.40	35.16	0.85
	Min	-18.80	-0.80	216.40	325.00	480.00	402.50	0.53	18.12	0.81
	n	8.00	8.00	8.00	1.00	1.00	1.00	8.00	8.00	8.00
Vugs (within)	Average	-9.50	-1.84	153.14	200.00	360.00	280.00	3.12	5.71	0.94
	Mode	-11.00	-2.10	-	-	-	-	3.55	-	-
	Median	-11.00	-2.10	150.20	200.00	360.00	280.00	3.55	4.93	0.94
	Max	-3.50	-0.80	182.50	200.00	360.00	280.00	3.55	8.55	0.96
	Min	-11.00	-2.10	124.60	200.00	360.00	280.00	1.40	4.53	0.90
	n	5.00	5.00	5.00	1.00	1.00	1.00	5.00	5.00	5.00
Type B Cal vein (on)	Average	-19.68	-1.05	172.73	235.00	388.00	311.50	1.70	8.26	0.90
	Mode	-21.60	-0.70	158.20	-	340.00	-	1.22	5.43	0.92
	Median	-20.10	-0.80	169.20	240.00	390.00	315.00	1.22	5.78	0.91
	Max	-15.50	-0.20	231.80	275.00	450.00	362.50	6.16	25.04	0.95
	Min	-23.60	-3.80	121.20	190.00	340.00	265.00	0.35	4.49	0.63
	n	27.00	38.00	43.00	5.00	5.00	5.00	43.00	42.00	43.00
Type A Cal vein (away)	Average	-17.73	-2.92	195.86	258.00	430.00	344.00	3.54	42.25	0.88
	Mode	-19.20	-3.40	126.50	-	290.00	-	1.00	4.50	0.95
	Median	-19.20	-3.25	157.40	210.00	350.00	280.00	4.65	5.23	0.95
	Max	-11.20	-0.80	398.80	500.00	790.00	645.00	6.16	268.21	0.98
	Min	-20.50	-3.80	103.20	175.00	290.00	232.50	1.00	4.49	0.55
	n	11.00	20.00	31.00	5.00	5.00	5.00	30.00	30.00	30.00
Cal (away) Removed Outlier (HPP-100)	Average	-17.99	-2.92	146.26	197.50	340.00	268.75	3.21	6.81	0.94
	Mode	-19.20	-3.40	126.50	-	290.00	-	1.00	4.50	0.95
	Median	-19.20	-3.40	128.50	195.00	320.00	257.50	2.15	4.84	0.95
	Max	-11.20	-0.80	221.40	225.00	430.00	327.50	6.16	20.17	0.98
	Min	-20.50	-3.80	103.20	175.00	290.00	232.50	1.00	4.49	0.85
	n	10.00	14.00	24.00	4.00	4.00	4.00	24.00	24.00	24.00
Potassic WR	Average	-19.80	-3.15	153.90	205.00	350.00	277.50	5.09	5.73	0.95
	Mode	-11.20	-5.20	168.50	-	-	-	8.14	6.44	0.96
	Median	-24.10	-2.50	155.65	205.00	350.00	277.50	4.18	5.25	0.95
	Max	-11.20	-0.80	182.80	210.00	360.00	285.00	8.14	8.60	1.00
	Min	-27.05	-5.20	110.50	200.00	340.00	270.00	1.40	4.50	0.91
	n	11.00	12.00	12.00	2.00	2.00	2.00	12.00	12.00	12.00
Phyllic WR	Average	-18.89	-2.50	183.10	261.67	426.67	344.17	4.14	10.37	0.92
	Mode	-24.10	-1.50	178.80	-	-	-	2.57	7.90	-
	Median	-16.80	-2.50	186.20	280.00	445.00	362.50	4.18	9.26	0.91
	Max	-14.25	-0.70	230.20	285.00	450.00	367.50	6.16	24.24	0.97
	Min	-24.10	-3.80	135.80	220.00	385.00	302.50	1.22	4.51	0.86

	n		21.00	23.00			23.00	3.00	3.00	3.00	23.00	23.00	23.00				
Skarn WR (S)	Average		-17.23	-1.83			178.58	253.33	401.67	327.50	2.99	9.65	0.91				
	Mode		-13.45	-0.55			-	-	-	-	0.97	-	-				
	Median		-15.00	-0.95			188.30	245.00	405.00	325.00	1.65	9.74	0.91				
	Max		-10.75	-0.55			228.00	305.00	445.00	375.00	9.73	23.17	0.95				
	Min		-28.80	-6.40			122.60	210.00	355.00	282.50	0.97	4.50	0.86				
	n		14.00	14.00			14.00	3.00	3.00	3.00	14.00	14.00	14.00				
Skarn WR (P)	Average		-12.11	-2.65			323.48	465.00	710.00	587.50	4.42	116.28	0.71				
	Mode		-14.60	-2.60			312.60	-	-	-	4.34	-	0.72				
	Median		-10.70	-2.60			323.60	465.00	710.00	587.50	4.34	118.38	0.71				
	Max		-10.20	-2.40			344.80	465.00	710.00	587.50	5.11	148.15	0.78				
	Min		-14.60	-3.10			284.00	465.00	710.00	587.50	4.03	63.96	0.66				
	n		10.00	13.00			13.00	1.00	1.00	1.00	13.00	12.00	13.00				
MC Type III (within)	Average	-56.83	-24.70		7.58	29.75	263.70	355.00	505.00	430.00	5.32	1247.67	0.82	0.98	0.02	91.83	
	Mode	-56.70	-23.80		8.10	30.40	238.80	-	-	-	4.14	628.63	0.80	0.99	0.01	94.00	
	Median	-56.70	-23.80		8.10	30.40	262.60	355.00	505.00	430.00	4.15	1180.62	0.82	0.99	0.01	94.00	
	Max	-56.70	-23.80		8.10	30.80	289.80	355.00	505.00	430.00	9.46	2100.47	0.85	0.99	0.03	94.00	
	Min	-57.10	-26.50		5.60	28.10	238.80	355.00	505.00	430.00	4.14	628.63	0.80	0.98	0.01	87.00	
	n	6.00	6.00		6.00	6.00	6.00	1.00	1.00	1.00	6.00	6.00	6.00	6.00	6.00	6.00	
MC Type III (away)	Average	-57.50	-13.60		7.60	27.60	454.10	540.00	800.00	670.00	6.00	1008.70	0.58	0.95	0.05	80.00	
	Mode	-57.50	-13.60		7.60	27.60	-	-	-	-	6.00	-	0.58	0.95	0.05	80.00	
	Median	-57.50	-13.60		7.60	27.60	440.90	540.00	800.00	670.00	6.00	939.49	0.58	0.95	0.05	80.00	
	Max	-57.50	-13.60		7.60	27.60	480.60	540.00	800.00	670.00	6.00	1147.63	0.58	0.95	0.05	80.00	
	Min	-	-13.60		7.60	27.60	440.80	540.00	800.00	670.00	6.00	938.99	0.58	0.95	0.05	80.00	
	n	3.00	3.00		3.00	3.00	3.00	1.00	1.00	1.00	3.00	3.00	3.00	3.00	3.00	3.00	
MC Type II (within)	Average		-28.88	-4.18			238.73	355.00	460.00	407.50	6.79	31.28	0.68				
	Mode		-29.60	-4.20			-	-	-	-	6.83	-	-				
	Median		-29.60	-4.20			226.70	355.00	460.00	407.50	6.83	22.60	0.66				
	Max		-26.50	-4.10			279.40	355.00	460.00	407.50	6.83	59.44	0.74				
	Min		-29.80	-4.20			222.10	355.00	460.00	407.50	6.68	20.48	0.66				
	n		4.00	4.00			4.00	1.00	1.00	1.00	4.00	4.00	4.00				
MC Type II (away)	Average		-11.33	-2.58			255.10	350.00	500.00	425.00	4.31	34.76	0.83				
	Mode		-	-2.60			258.60	-	-	-	4.34	41.76	0.83				
	Median		-10.60	-2.60			258.60	350.00	500.00	425.00	4.34	41.46	0.83				
	Max		-10.20	-2.50			304.60	350.00	500.00	425.00	4.34	41.76	0.91				
	Min		-13.20	-2.60			187.40	350.00	500.00	425.00	4.18	9.51	0.74				
	n		3.00	6.00			7.00	1.00	1.00	1.00	6.00	6.00	6.00				

APPENDIX 4: CARBON AND OXYGEN STABLE ISOTOPE DATA

The following table represents carbon and oxygen stable isotope results from Type A and B calcite veins, Skarn WR *on*, and unaltered wallrocks *on* and *away* from the HPP contact. Samples were prepared and analyzed at the Colorado School of Mines Stable Isotope Lab.

Sample	Type	$\delta^{13}C$ (‰VPDB)	$\delta^{18}O$ (‰VPDB)	$\delta^{18}O$ (‰SMOW)	Th_{total} °C	Kelvin	Frac C	Adjusted $\delta^{13}C$ (‰VPDB)	Frac O
HPP-78	Type A Calcite Vein (away)	-1.78	-10.59	19.99	127.52	400.67	-2.29	-4.07	11.35
HPP-100	Type A Calcite Vein (away)	-1.12	-10.93	19.64	354.30	627.45	3.40	2.28	7.81
HPP-103	Type A Calcite Vein (away)	-1.32	-10.97	19.60	186.30	459.45	0.44	-0.88	10.41
HPP-103.1	Type A Calcite Vein (away)	-1.21	-11.29	19.27	186.30	459.45	0.44	-0.77	10.41
HPP-105	Type A Calcite Vein (away)	-1.20	-35.85	-6.05	139.97	413.12	-1.69	-2.89	11.18
HPP-107	Type A Calcite Vein (away)	-1.19	-30.76	-0.80	117.72	390.87	-2.80	-3.99	11.46
HPP-18	Type B Calcite Vein (on)	-4.50	-25.33	4.80					
HPP-33	Type B Calcite Vein (on)	-1.27	-13.18	17.32					
HPP-33.1	Type B Calcite Vein (on)	-1.08	-12.76	17.76					
HPP-42	Type B Calcite Vein (on)	-3.63	-27.24	2.83					
HPP-43	Type B Calcite Vein (on)	-1.98	-36.37	-6.58					

Adjusted $\delta^{18}O$ (‰SMOW)	Tt (avg) °C	Kelvin	Frac C	Adjusted $\delta^{13}C$ (‰VPDB)	Frac O	Adjusted $\delta^{18}O$ (‰SMOW)	Comments
31.34	250.00	523.15	2.10	0.32	9.37	29.36	coarse-grained calcite+qtz+bi
27.45	645.00	918.15	3.52	2.40	4.68	24.32	coarse calcite+quartz vein
30.01	327.50	600.65	3.18	1.86	8.18	27.78	coarse-grained calcite
29.68	327.50	600.65	3.18	1.97	8.18	27.45	Test Sample For 103
5.13	265.00	538.15	2.33	1.13	9.17	3.12	coarse-grained calcite
10.66	232.50	505.65	1.68	0.49	9.67	8.87	coarse grained calcite vein on cliff face near shear zone
	265.00	538.15	2.33	-2.17	9.17	13.97	calcite vein (bladed) with diopside and sericite/biotite, c.c a coarse-grained calcite vein that has replaced some qtz.
	335.00	608.15	3.24	1.97	8.09	25.41	From a Pb-Zn prospect, vein is mostly calcite with minor pyrite±magnetite±sphalerite±hematite
	335.00	608.15	3.24	2.16	8.09	25.85	Test Sample for 33
	290.00	563.15	2.73	-0.90	8.76	11.59	coarse grained calcite vein which c.c. a quartz vein
	362.50	635.65	3.45	1.48	7.67	1.09	coarse grained calcite

HPP-61	Type B Calcite Vein (on)	-1.81	-33.02	-3.13					
HPP-78	Unaltered WR (away)	0.33	-9.64	20.98					
HPP-100	Unaltered WR (away)	-0.94	-9.25	21.38					
HPP-103	Unaltered WR (away)	-1.08	-13.07	17.44					
HPP-103.1	Unaltered WR (away)	-0.94	-12.84	17.67					
HPP-105	Unaltered WR (away)	-1.33	-31.35	-1.41					
HPP-16	Skarn WR (on)	-4.39	-24.75	5.39					
HPP-33	Skarn WR (on)	-0.25	-32.63	-2.73					
HPP-33.1	Skarn WR (on)	-0.19	-32.69	-2.79					
HPP-42	Skarn WR (on)	-4.20	-26.57	3.52					
HPP-43	Skarn WR (on)	-1.85	-20.70	9.57					
HPP-61	Skarn WR (on)	-2.80	-21.96	8.27					

	305.00	578.15	2.90	1.09	8.56	5.43	Calcite occurs as large aggregate masses very coarse grained, but also a skarn assemblage exist around vein
	365.00	638.15	3.47	3.80	7.64	28.62	hornsfelic limestone
	365.00	638.15	3.47	2.53	7.64	29.02	fine grained limestone
	365.00	638.15	3.47	2.39	7.64	25.08	coarse grained limestone fine to coarse grained calcite+qtz+py
	365.00	638.15	3.47	2.53	7.64	25.31	Test Sample For 103
	365.00	638.15	3.47	2.14	7.64	6.23	fine grained calcite
	587.50	860.65	3.64	-0.75	5.09	10.48	From Star Mine, Skarned WR, has considerable amnt. of garnet; F.I. temperature taken from garnet
	587.50	860.65	3.64	3.39	5.09	2.36	deformed calc-silicate
	587.50	860.65	3.64	3.45	5.09	2.30	Test Sample for 33
	587.50	860.65	3.64	-0.56	5.09	8.61	skarn
	587.50	860.65	3.64	1.79	5.09	14.66	skarn
	587.50	860.65	3.64	0.84	5.09	13.36	skarned alteration zone